Mohammad Sohrab Hossan Monsi

Laser Radar for Precise Vehicle Velocity Measurement

kassel
university
press

This work has been accepted by the faculty of Electrical Engineering and Computer Science of the University of Kassel as a thesis for acquiring the academic degree of Doktor der Ingenieurwissenschaften (Dr.-Ing.).

Supervisor: Prof. Dr.-Ing. G. Kompa
Co-Supervisor: Prof. Dr.-Ing.A. Bangert

Defense day: 27th April 2009

Bibliographic information published by Deutsche Nationalbibliothek
The Deutsche Nationalbibliothek lists this publication in the Deutsche Nationalbibliografie; detailed bibliographic data is available in the Internet at http://dnb.d-nb.de.

Zugl.: Kassel, Univ., Diss. 2009
ISBN print: 978-3-89958-736-4
ISBN online: 978-3-89958-737-1
URN: urn:nbn:de:0002-7375

Printed in Germany

Acknowledgments

First of all, my earnest gratitude is for honourable Prof. Dr.-Ing. G. Kompa, head of the Department of High Frequency Engineering, University of Kassel, and I am very much grateful for his continuous guidance, inspiration and specially for giving me the chance for research work in this department.

I wish to express my special gratitude to the Prof. Dr.-Ing. A. Bangert, head of the Department of Microwave Electronics, University of Kassel, for giving me the intellectual stimulation and academic support through the continuation of this research work.

I am very much grateful to Prof. Dr. sc. Techn. B. Witzigmann and PD. Dr.-Ing. R. Marklein for their valuable acceptance to being the member of the examination board.

I would like to convey my sincere thanks to Dipl.-Ing. J. Weide for his millstone help and cooperation along with the technical assistance during the laboratory measurements works. My special thanks go to Mrs. H. Nauditt, secretary of the Department of High Frequency Engineering for her readiness and cooperation for most of all official support during the work of this dissertation.

My sincere thanks go to all of the colleagues Mr. A. Hussein, Mr. A. Zamudio, Mr. A. Z. Markos, Mr. B. Wittwer, Mr. R. Ma, Mr. S. Embar, Mr. S. Dahmani, and all other members of the Department of High Frequency Engineering, University of Kassel, for their friendly cooperation during my work with them and spirit of team work.

My greatest acknowledgments go certainly to Prof. Dr. Dr. H. Rolfes and Mrs. M. Rolfes for their spiritual supports during my doctoral work in the University of Kassel.

Mohammad Sohrab Hossan Monsi
Kassel, April 2009

Contents

List of Figures

List of Tables

List of Symbols

Symbols	Meaning	Unit
A_t	Surface area of target	m^2
C_b	Bypass capacitance	F
C_L	Load capacitance	F
c_o	Light velocity	3×10^8 m/s
d	Laser beam aperture diameter	m
d_{sn}	Traveling distance of target for each scan	m
D_r	Separation distance of parallel laser beams	m
PRF	Pulse repetition frequency	Hz
E	Electron energy	$1\ eV = 1.602\times10^{-19}$ J
E_r	Detector received energy	J
E_t	Transmitter transmitted energy	J
F	Focus distance of lens	m
G	Detector gain	dB
G_t	Transmitter gain	dB
h	Height of scanning line	m
H_{vmt}	Moving target contour at vertical plane	
I_{cc}	Collector current	A
I_{max}	Maximum peak current	A
k	Boltzmann constant	1.3807×10^{-23} J/ °K
K_a	Aperture illumination constant	$1/e^2$
L_{ap}	Approximated target contour length	m
L_m	Measured target contour length	m
m	Number of targets	
M	Molecular weight	
n	Number	
N_{d1}	Number of measured data at detector 1	
N_{d2}	Number of measured data at detector 2	
N_m	Number of measurement	
N_{md1}	Number of measured data by detector 1 for target m	
N_{md2}	Number of measured data by detector 2 for target m	
N_n	Number of measured data for scanning number n	
N_s	Number of scanning	
P_{av}	Average power	Watts
P_{max}	Maximum power	Watts
P_r	Received optical power	Watts

P_t	Transmit optical power	Watts
q	Electron charge	1.602×10^{-19} Coloumb
r	Target range	m
$r_{md1,\,p}$	Ranging per measurement for target m from detector 1	m
$r_{md2,\,p}$	Ranging per measurement for target m from detector 2	m
R_{air}	Air constant	8.135×10^{7} arg/degree
R_b	Decoupling resistance	Ω
R_L	Load resistance	Ω
t	Time	s
t_{crr}	Time of correlation signal	s
t_f	Fall time	s
t_d	Pulse width (FWHM)	s
t_g	TOF from radar system to ground surface	s
t_m	Measured time	s
$t_{m,\,crr}$	Measured time difference from correlation approach	s
$t_{md1,\,d}$	Measured TOF of m-th target by detector 1	s
$t_{md2,\,d}$	Measured TOF of m-th target by detector 2	s
$t_{md1,\,m}$	Measured time of m-th target by detector 1	s
$t_{md2,\,m}$	Measured time of m-th target by detector 2	s
$t_{md1,\,s}$	Scanning time of m-th point target by detector 1	s
$t_{md2,\,s}$	Scanning time of m-th point target by detector 2	s
t_n	Measured time for n number of data	s
t_{prf}	Periodic time duration for pulse repetition frequency	s
t_r	Rise time	s
t_{vpt}	TOF for perpendicular radar placement to target	s
t_{hpt}	TOF for horizontal radar placement to target	s
T_c	Ambient temperature	°C
T	Temperature	°K
v	Velocity	m/s
v_m	Measured velocity of moving object	m/s
v_{crr}	Velocity from correlation approach	m/s
v_{d1}	Velocity from detector 1	m/s
v_{d2}	Velocity from detector 2	m/s
v_r	Actual approximated velocity of moving target	m/s
V_{cc}	DC supply voltage for transmitter pulse generator	V
v_{mm}	Measured velocity for m-th target	m/s
$v_{m,\,crr}$	Velocity for m-th target by correlation approach	m/s
v_{st}	Velocity from start-stop approach	m/s

V_{t1}	Threshold of decision for detector 1	V
V_{t2}	Threshold of decision for detector 2	V
W_{hmt}	Moving target contour at horizontal plane	
W_{md1}	Contour signal for m target by detector 1	
W_{md2}	Contour signal for m target by detector 2	
$\hbar$	Plank constant ($\hbar = h/2\pi$)	6.63×10^{-34} Js
α	Critical angle	Degree
β	Angular direction of moving target	Degree
χ	Adiabatic coefficient	
ϕ	Angular direction	Degree
η_d	Quantum efficiency	
λ	Wavelength	m
η_{at}	Atmospheric transmission factor	
η_{sys}	Laser system transmission factor	
η_t	Transmission coefficient of transmitted laser beam	
η_r	Transmission coefficient of reflected beam from target	
θ_d	Divergence angle	Degree
θ_t	Laser beamwidth	Radian
ρ_T	Target reflectivity	
σ	Radar cross section	
σ_T	Stefan-Boltzmann constant	5.67×10^{-12} W cm^2 °K^{-4}
τ_d	Pulse duration	s
ΔL_{err}	Error length of target	
$\Delta N_{md1,\ err}$	Number of error detection for m -th target at detector 1	
$\Delta N_{md2,\ err}$	Number of error detection for m -th target at detector 2	
$\Delta t_{md1,\ err}$	Scanning error time for m -th target at detector 1	s
$\Delta t_{md2,\ err}$	Scanning error time for m -th target at detector 2	s
Δv_{err}	Error velocity of target	
Ω	Solid angle	Steradian
Ω_t	Solid angle of transmitted laser beam	Steradian
Ω_r	Solid angle of reflected beam from target	Steradian

List of Abbreviations and Acronyms

ADS	Advanced Design System
A/D	Analog-to-Digital
AlGaAs	Aluminium Gallium Arsenide
APD	Avalanche Photodetector
APG	Avalanche Pulse Generator
BFL	Back Focal Length
BJT	Bipolar Junction Transistor
CW	Continuous Wave
EM	Electromagnetic
EN	European Standard
EU	European Union
FMCW	Frequency Modulated Continuous Wave
GaAs	Gallium Arsenide
GPIB	General Purpose Interface Bus
HFT	High Frequency Technique
IEC	International Electrotechnical Commission
IR	Infrared
LASER	Light Amplification by Stimulated Emission of Radiation
L-C	Inductive-Capacitive
LIDAR	Light Detection and Ranging
MPE	Maximum Permissible Emission
N. E. P.	Noise Effective Power
NF	Noise Figure
NIR	Near Infrared
O/E	Optical-to-Electrical
PRF	Pulse Repetition Frequency
RADAR	Radio Detection and Ranging
RCS	Radar Cross Section
SH	Single-Heterostructure
S/N	Signal-to-Noise
SNR	Signal to Noise Ratio
STC	Sensitive Time Control
TEM	Transverse Electromagnetic
TOF	Time-of-Flight
USB	Universal Serial Bus
UV	Ultra Violet

Abstract

In this research work, new exploration of a pulse laser radar system is presented with two splitted parallel laser beams for the measurement of precise velocity of moving vehicles along with their contours and ranging distances. The emission of optical pulses is eye-safe, and hence the radar can be classified as a class-1 laser system. The laser emission comprises powerful and ultrashort optical pulses using the modulation concept of highly dynamic carrier injection into the active zone of a single-heterostructure laser diode. The emitted laser pulses have a wavelength of 904 nm. Two splitted laser beams are produced from one laser. These two laser beams are transmitted in parallel with a base separation distance of 28.8 cm. Transmitted parallel laser beams consist of a fast sequence of very short laser pulses with a rise time of 28 picoseconds and a pulse width (FWHM) of 32 picoseconds. Two broadband photodetectors with high sensitivity (50 A/W) are axially installed to their corresponding transmitted laser beams in order to avoid any beam detection interference between each other. Two synchronized optical reference signals are taken from the laser transmitter to the photodiodes via optical fibers having core diameters of 125 μm each. The photodetection technique is optimized to achieve the highest performance of the photoreceivers of the developed laser radar for detection of the moving targets. The range detection of targets is performed according to the time-of-flight principle. The velocity of vehicle is determined by the correlation of measured contours, detected by both photodetectors. The target detection is performed from the time difference between the reference pulse and the detected signal from moving targets. Moreover, the radar system can be used for the detection of bi-directional and multiple automotive targets in a highly congested traffic. Experimental measurements are performed in laboratory and real-life environments. The length and height are determined along with the velocity of the moving targets. Finally, the velocity for a car based on contour measurement is experimentally evaluated.

Zusammenfassung

In dieser Dissertation sollen neue Forschungsergebnisse und Erkenntnisse mit einem Pulslaserradarsystem mit zwei parallel aufgeteilten Laserstrahlen für die genaue Messung der Geschwindigkeit, der Entfernung und der Kontur von sich bewegenden Fahrzeugen vorgestellt werden. Die Emission der optischen Impulse ist augensicher, so daß das Radar als Klasse-1 Lasersystem klassifiziert werden kann. Die Laseremission basiert auf leistungsstarken ultrakurzen optischen Impulsen, die auf der Grundlage des Konzepts der sehr dynamischen Ladungsträgerinjektion in die aktive Zone einer Einfach-Heterostruktur-Laserdiode erzeugt werden. Die emittierten Laserpulse haben eine Wellenlänge von 904 nm. Zwei Laserstrahlen werden durch Teilung des Laserstrahles einer Laserdiode gewonnen. Diese beiden Laserstrahlen werden parallel zueinander mit einem Basisabstand von 28,8 cm ausgesandt. Die ausgesandten parallelen Laserstrahlen bestehen aus einer schnellen Folge von sehr kurzen Laserpulsen mit einer Anstiegszeit von 28 Pikosekunden und einer Pulsbreite (FWHM) von 32 Pikosekunden. Zwei Breitband-Photoempfänger mit hoher Empfindlichkeit (50 A/W) sind axial zu den entsprechenden Laserstrahlen installiert, um Interferenzen zwischen ihnen bei der Strahldetektion zu vermeiden. Zwei synchronisierte optische Referenzsignale werden aus dem Lasersender zu den Photodioden über optische Fasern mit einem Kerndurchmesser von jeweils 125 mm übermittelt. Die optische Empfangseinheit wurde dahingehend optimiert, dass bewegte Ziele von dem neu entwickelten Laserradar einwandfrei detektiert werden. Die Erkennung der Zielentfernung erfolgt nach dem Impulslaufzeitprinzip. Die Geschwindigkeit des Fahrzeugs wird durch die Korrelation der von beiden Photoempfängern gemessenen Konturen bestimmt. Die Zielerkennung erfolgt aus der Zeitdifferenz zwischen dem Referenzimpuls und dem detektierten Signal des beweglichen Zieles. Darüber hinaus kann das Laserradarsystem für die Erkennung von bidirektionalen und von mehreren automotiven Zielen auch in sehr dichtem Verkehr eingesetzt werden. Experimentelle Messungen sind im Labor und in einer realen Umgebung durchgeführt worden. Länge und Höhe von bewegten Zielen sowie deren Geschwindigkeit sind bestimmt worden. Schließlich wird die Geschwindigkeit eines Automobils auf der Grundlage von Konturmessung experimentell evaluiert.

Chapter 1

Introduction

The motivation of this thesis has been focussed from the pioneering research and development results of the Department of High Frequency Engineering (HFT) at the University of Kassel in the field of near field laser ranging, based on the time-of-flight (TOF) principle.

A milestone in the HFT laser radar technology was the invention of the generation of ultra-short and very high power laser pulses. A typical optical pulse used for the laser system under investigation has a peak power of 470W, and a pulse width of 32 ps (FWHM). A key parameter for the accuracy of ranging is the optical pulse rise time, which is typically 28 ps.

Such laser spikes have great advantages for various applications. According to the international safety rules, the emitted pulse fulfils the single pulse criteria, i.e. the pulse energy is much lower than the permitted limit value. Moreover, the emission of a pulse train can be done with very high pulse repetition frequency (PRF) without reaching the limit value of the permitted averaged optical power. Thus, the laser spikes are totally eye-safe so that the system under investigation can be grouped as class-1 laser system according to [1].

Due to the eye-safe nature of the emission of a high repetition rate, the laser spikes can be applied to the extended sampling techniques as described in [2]. In this case, the time (range) determination is done with time-converted and time-extended pulses instead of real pulses, which comprises, according to the sampling principle, a multiple of single measurement events.

The application of the time-extended sampling principle is very useful in time domain sensor systems, because signal processing in the sampled region is cost effective, and noise and temperature effects have minor influence on the system accuracy.

The invention of the laser spikes has a further key advantage regarding high spatial ranging, which is very important for 3D-imaging [3]. The provided laser power of single-heterostructure laser diodes by applying the novel modulation scheme of ‘high dynamic

carrier injection' is approximately 80 times higher than the optical power operating the laser diode under rated conditions. This extremely high increase in optical power makes it possible to use laser diodes with smaller aperture. As a result, laser beams with smaller laser spots at a given distance can be realized. This makes spatially high resolution 3D imaging possible. A 3D scanning laser radar is reported in [4], and it has focused on the measurement of glowing crankshafts of trucks. Another 3D scanning laser radar with high lateral resolution of 100 µm for orthopaedic surgery is reported in [5].

The goal of this thesis is to extend the single-beam laser radar concept (see Figure 1.1) to a double beam radar concept (see Figure 1.2) that opens new application fields regarding the identification of moving vehicles. The interesting measurement parameters are the height and the length of the moving vehicles. The control of vehicle velocity is of growing importance with the increasing traffic density. Literature about laser radar systems for velocity measurement can be found in [6-14].

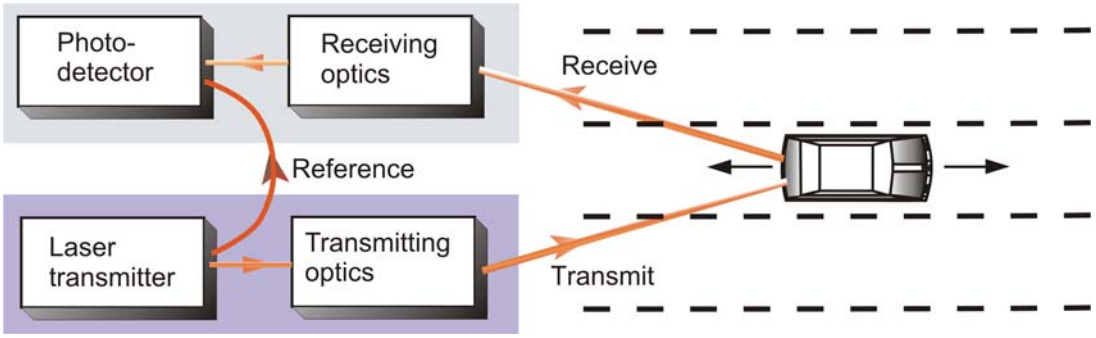

Figure 1.1 Single beam laser radar.

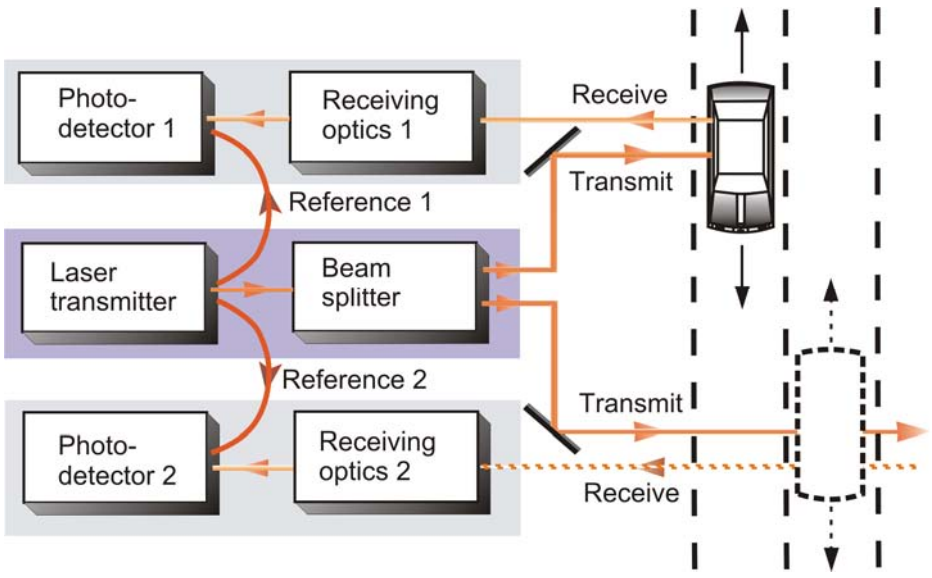

Figure 1.2 Double beam laser radar system.

In the new system, two parallel laser beams are produced from a single laser transmitter. Two photodetectors (photodetector 1 and 2) are placed coaxially with both laser beams as shown in Figure 1.2. The double beam laser radar system is placed perpendicular to the direction of the moving vehicles. In case of single beam laser radar, the system is placed towards the direction of the moving vehicle. It is mainly used for velocity measurement. Using the double beam laser system, the type of a moving vehicle can be easily evaluated by detecting the range, length and height along with the velocity of the vehicle. Moreover, two references (reference 1 and 2) are used to detect the velocity of bi-directional moving vehicles, as shown in Figure 1.2.

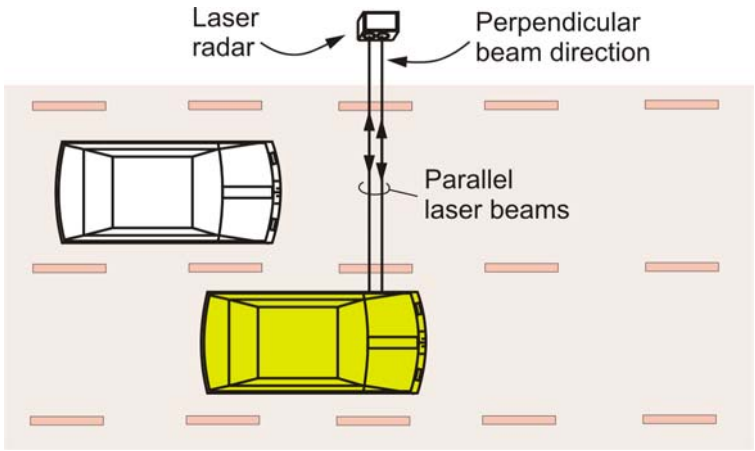

(a)

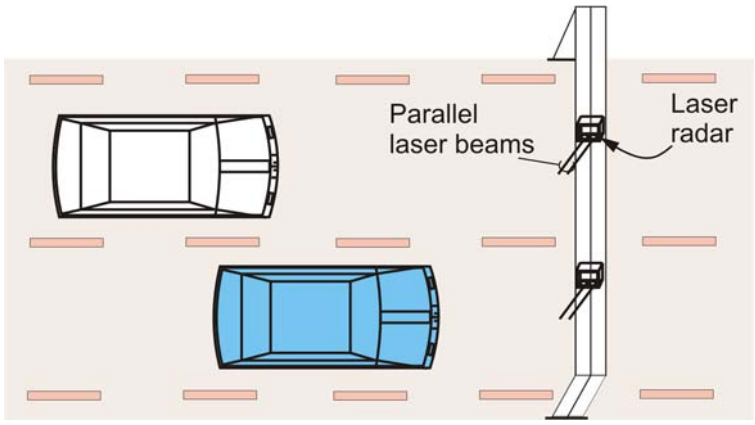

(b)

Figure 1.3 Basic velocity measurement set-up of analysed pulse laser radar with parallel beams [system placed (a) aside the road, and (b) above the road].

The velocity measurement using the double laser radar can be performed from aside the road and also from above the road, as shown in Figure 1.3(a) and 1.3(b). The laser beam is produced with a very small laser spot size of approximately 1 mm diameter.

This means high resolution detection and, therefore, precise vehicle velocity determination in high traffic zones.

Following systems are in use for traffic control:

Microwave radar: The microwave radar radiates electromagnetic (EM) waves. It suffers from high beam divergence and therefore, it is only suitable for very short distance detection tasks [15-19]. At velocity measurement, it has low angular resolution and the spatial beam resolution also changes along with distance. For instance, resolution changes from one lane to the others (in Figure 1.4, on lane 1 and lane 2). Moreover, it is necessary to use complex signal processing techniques for the microwave radars [20, 21]. Furthermore, the cosine effect (in Figure 1.4, cosϕ) is another drawback of such systems [18, 22] in the application of velocity measurement.

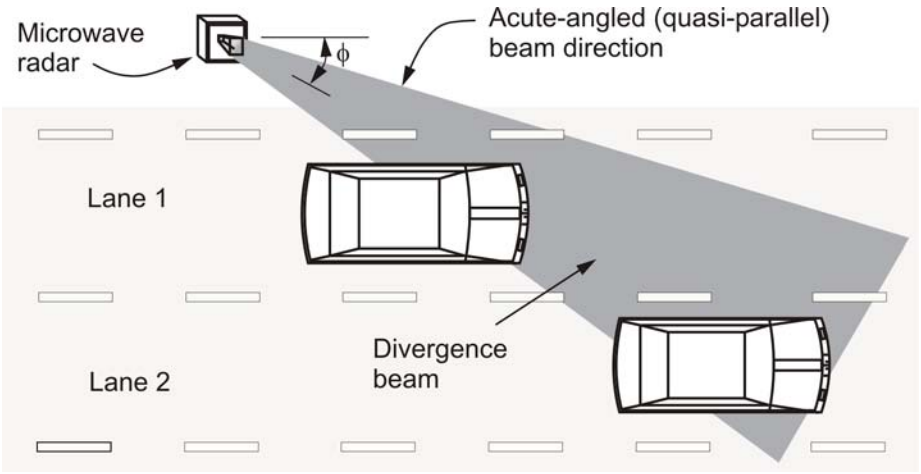

Figure 1.4 Schematic view of the cross-the-road radar system for vehicle velocity measurement. The angle ϕ (in degree) is typically the angular direction of radar system to street (commonly it is from 10 degree to 60 degree).

Optical radar: For velocity measurement [23, 24] it is necessary to setup precisely a retro-reflector or optical receiver at the opposite side of the system to measure the vehicle velocity. As a result, the overall system remains complicated.

Doppler radar: The frequency modulated continuous wave (FMCW) principle is basically used in the Doppler radar system. It is suffering from frequency shifting error in moving target identification [9, 25]. For instance, if two or more vehicles are in the measurement area, it is very difficult to measure the velocity by using a Doppler radar [22] because of the frequency shifting of multiple vehicles.

To emphasize this research, a new pulse laser radar concept with parallel laser beams is developed to measure the velocity of vehicles with high accuracy.

In Chapter 2, the theoretical background of the laser beams and the target properties are described. The external factors which influence the performance of the laser radar are described. Finally, the rules and regulations about the application of laser systems are presented.

In Chapter 3, the fundamental background of the pulse radar as a velocity meter is described. The functions to represent the pulse radar as velocity meter are evaluated. At the end, the influencing factors, the limitation of the laser system, and the range of the laser radar system are described.

In Chapter 4, an overview of the developed laser radar with parallel laser beams as precise velocity meter is reported. The design, simulation, fabrication and characteristics of the hardware modules are presented (a block diagram of different hardware modules of the radar system is shown in Figure 1.2). In the laser transmitter, a GaAs laser diode is used to generate eye-safe ultra-short laser pulses. A clock synchronized trigger pulse generator is used to trigger the avalanche pulse generator. Two avalanche photodetectors are developed as broadband receivers. The optical system comprises transmitting and receiving optics. The transmitting optics are used to produce two parallel laser beams from a single laser transmitter. The receiving optic are used to filter out the unwanted optical signal and to focus the reflected laser pulses from the target on the photodiodes. Towards the end, the analysis and optimization of the developed laser system is performed to reduce the signal to noise ratio (SNR).

In Chapter 5, the radar signal processing and the developed software for the laser radar system, especially for evaluating the velocity, contour and ranging of the dynamic targets are presented. The different topology of target detection (velocity and contour) and their relationships are described. The evaluation of signal-to-noise ratio for the measurement methodology is described. The target detection range by the developed laser radar system is evaluated. The measurement technique of velocity and contour of different movable targets is discussed. Target detection and velocity measurement system for a single target, bi-directional moving targets and multiple targets are explained. The relative variations of the velocity for other external factors are realized.

In Chapter 6, the practical velocity measurement for a test car is performed. Different scanning surface areas of a test car are selected to demonstrate the effective property of the car surfaces to detect the velocity, contour, and length of the car. Finally, a complete present status, data sheet and ratings of the new pulse radar velocity meter are also given.

In Chapter 7, conclusion, further improvements and future work are presented.

Chapter 2

Laser Radar Basics

In this chapter, the background of the laser beams and the properties of targets are demonstrated. The theoretical and mathematical concepts of laser radar are described for the ranging of objects. Moreover, it is also a keen criterion to develop mathematical concepts, computational technique and an analytical scheme to describe the desired performance of the radar system. For instance, keen concepts are basics to develop the hardware and software of radar system. At the end, the international rules and regulations for the commercial uses of laser systems are described.

Moreover, the backgrounds of the laser radar sensor system can be found in [27-31].

2.1 Radar Range Equations

In general for radar system, the target identification is evaluated from the precise range detection and from the properties of received signals. The radar emitted signal is specified by the properties of the electromagnetic wave propagation. The electromagnetic wave propagation can be replaced by the radar equation [32, 33] as

$$P_r = \left(\frac{P_t G_t}{4\pi r^2}\right).\left(\frac{\sigma}{4\pi r^2}\right).\left(\frac{\pi d^2}{4\pi r^2}\right).\eta_{at}.\eta_{sys} \qquad (2.1)$$

where P_r is the received signal power, P_t is the transmitted signal power, r is the range of target in meters, d is the aperture diameter in meters, η_{at} is the atmospheric transmission factor, σ is the radar cross section, η_{sys} is the laser system transmission factor and G_t is the transmitter gain.

The pulsed laser radar sends a laser pulse train in a certain direction to detect the targets. The detection of target, whether it is static or moving, is considered to be the evaluation of discrete point detections. Every sample of detection can be considered as

the range of target, as shown in Figure 2.1. The range of target is represented by r, and it can be represented as

$$r = \frac{c_o t}{2} \tag{2.2}$$

where for the pulse laser radar system with TOF principle, the time t is the required elapsed time for a laser pulse transmitted from the transmitter, reflected by the target and received by the receiver. If the target is in r distance from the transmitter and from the receiver, then the time t means the EM wave travels twice the r distance at the light velocity of c_o (light velocity in vacuum is 3×10^8 m/s). Actually, the EM wave propagation velocity in air medium is depending upon the weather condition and temperature, and it will be described in Chapter 4.

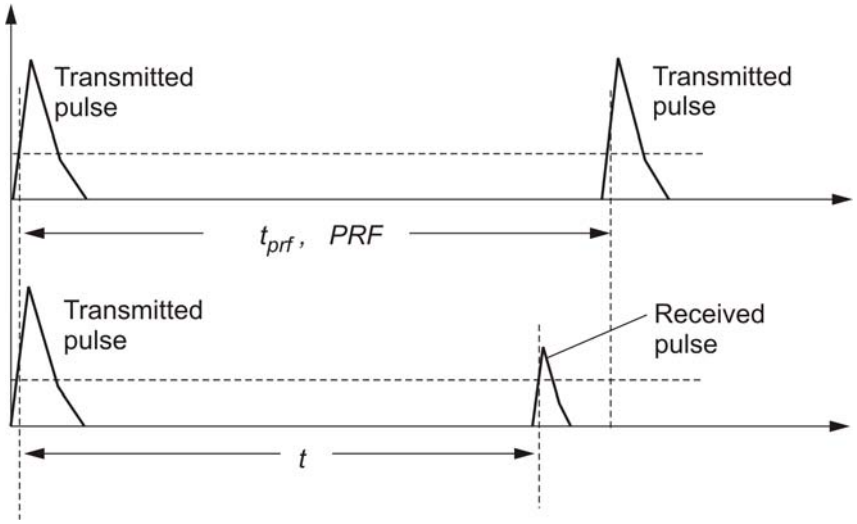

Figure 2.1 PRF and time ambiguity of pulsed radar.

The maximum range of laser radar represents the maximum distance of a target from the radar at which detection is possible. From Figure 2.1, it can be easily evaluated that the target must be between the time ($t_{prf} = 1/PRF$) of two discrete radiated pulses due to pulse repetition frequency. Therefore, for any position of target, if the time difference between transmitted laser pulse and received pulse is t, then the maximum time (t_{max}) must be less than or equal to t_{prf} in order to fulfil the detection criteria without considering other ambiguity factors. The maximum range (r_{max}) without ambiguity can be represented as

$$r_{max} = c_o t_{prf} / 2 = c_o / (2PRF) \tag{2.3}$$

Ideally, the detection of target is considered from the detections of all point targets as shown in Figure 2.2. In case of the discussed application, the detection of target is considered as extended target, because the spot size of the laser beam is larger than point target. Therefore, the reflected signal detected by receiver is from the extended surface of target.

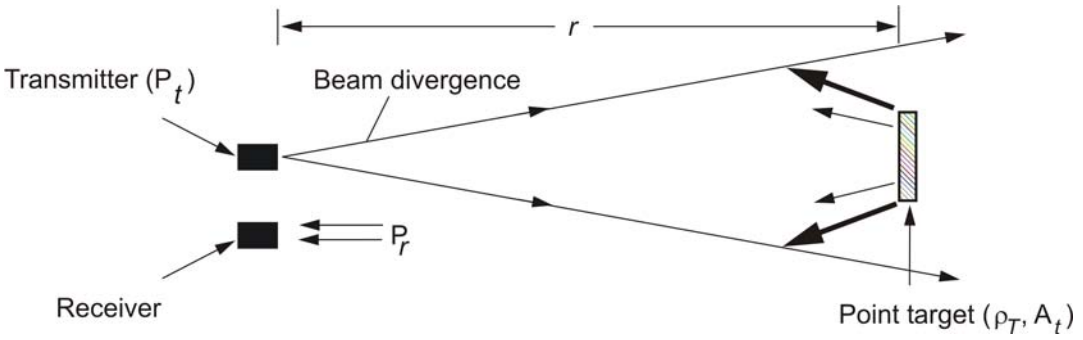

Figure 2.2 Schematic of the detection of point target.

In case of point target: The point target [34] is smaller than the transmitted beam footprint (see Figure 2.2). The scattering area [radar cross section (RCS) of target] is $\sigma = 4\pi\rho_T A_t/\Omega$ [35-37], where ρ_T is the target reflectivity, A_t is the target surface area, and Ω is the scattering steradian solid angle of the target. The scattering area of point target (σ) can be assumed as constant because of the surface area of target A_t is constant. The receiving power in (2.1) has no dependency on the target scattering area (σ). From the range equation (2.1), it can be represented as the receiving power is reciprocal proportional to the fourth power of range

$$P_r \propto \frac{1}{r^4} \tag{2.4}$$

In case of extended target: The surface area of target is larger than the incident laser beam area. The entire incident laser beam is involving in the reflection from target surface, as shown in Figure 2.3. The scattering area of a target (σ) has direct influences on the receiving power in (2.1). The received signal [38] has range square dependency. From the range equation (2.1), it can be represented as the receiving power is reciprocal proportional to the square of range

$$P_r \propto \frac{1}{r^2} \tag{2.5}$$

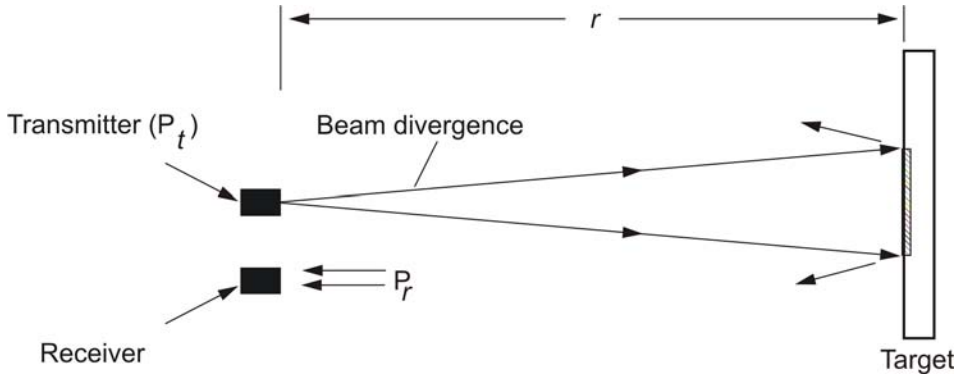

Figure 2.3 Schematic of extended target detection.

The targets under consideration are extended targets. However, the reflectivity of targets depends on the surface properties of the targets. For instance, mirror type targets have specular reflection and diffuse type targets have larger scattering reflection. They are described as:

(a) *Mirror type target*: The target redirects the incident wave toward the radar system as shown in Figure 2.4. In typical mirror targets, the probability of reflected wave distribution associates with their specular facets [39]. Such targets follow the law of reflection, where the angle of reflection is equal to the angle of reflection.

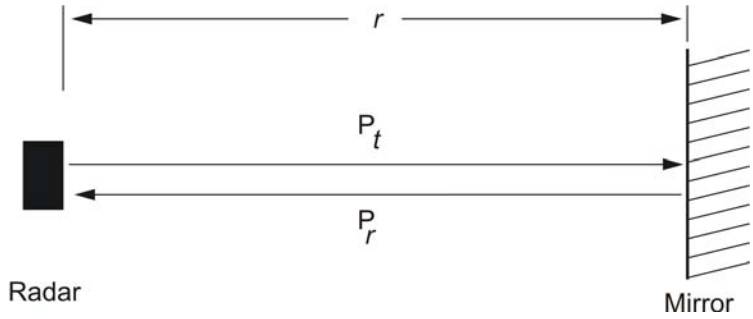

Figure 2.4 Reflectivity of mirror type target. Specular reflection.

(b) *Lambertian target (diffuse target)*:

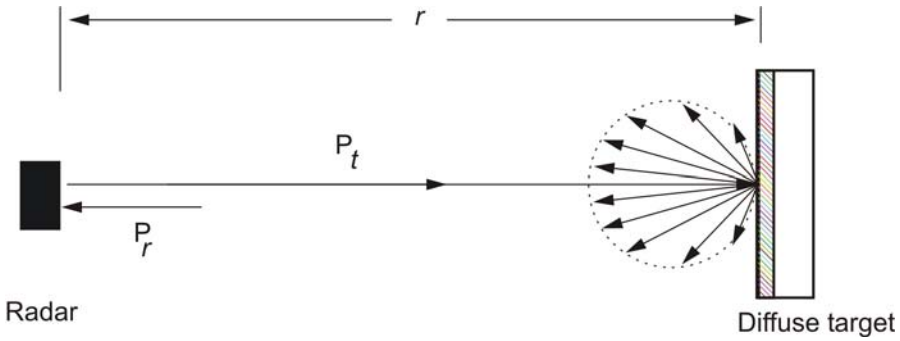

Figure 2.5 Reflectivity of diffuse target. Large scattering reflection.

A pure diffuse target has a large scattering field due to the granular surface properties of the target [40]. For a completely nonspecular surface, the reflected light will spread over a hemisphere as shown in Figure 2.5. Since the reflected light spread over as a hemisphere, therefore the scattering steradian angle will be equal to 2π.

The diffused target with specular spots refers to the standard target in radar technology as shown in Figure 2.6. The scattering diffuse target (Lambertian target) has a reflection with a solid angle of π steradian. The reflectivity varies with the colour of the surface [41, 42]. In our case, the target is considered as a diffused target with specular spots. For instance, the vehicle body has metal surface, and the surface colours of vehicles are different. Therefore, the reflectivity of the vehicle surface is depending on the vehicle surface colour.

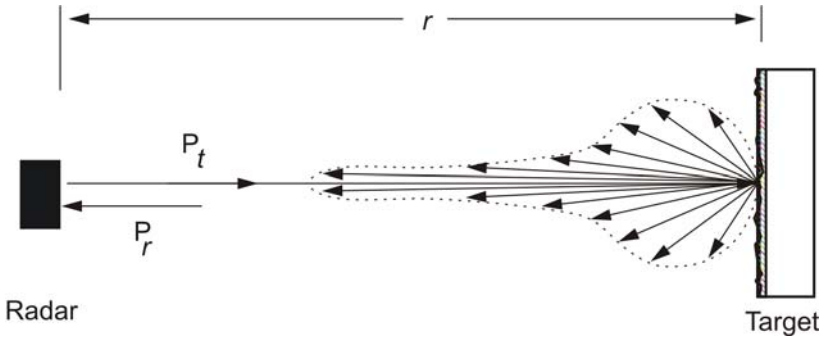

Figure 2.6 Scattering reflectivity of diffuse target with specular spots.

2.2 Weather Effects

The radiated laser light pulses are reflected, redirected, diverted, and absorbed. Those are nominally influenced by noise sources [32, 43, 44]. The weather effect is another most considerable external noise on laser radar system. The rain, fog, snow, temperature and sunlight are considered as weather effects and they directly influence the performance of the laser radar system.

In raining condition, the detection probability decreases proportionally to the amount of raindrop in per unit area, since it scatters the laser beam drastically [45]. Fundamentally, the signals with noises are detected by the detector with different ranges of the targets. The noise signal due to rain can be evaluated and extracted by using a sensitive time control (STC) unit on the signal processing module [46]. The functions of the STC are to evaluate and to extract the noise signal due to rain.

In foggy weather, the transmitted laser beam is scattered but the effect is less than with rain or snow, and it is easy to extract by using STC. The correlation principle can be used to reduce the noise effects due to rain and fog, and it is described in [45].

During snowing, if it is light snowing it is possible to solve the problem by STC. But if it is heavy snowing than it is very difficult to extract. Therefore, during heavy snowing the developed laser system is recommended to be used under a bridge. More details on laser radar emplacements are reported in Chapter 3. Moreover, the beam scattering due to bad weather (rain, snow, fog and dust) is also depending on the pulse width of the transmitted laser beams [47, 48]. The effect of bad weather is less on ultra-short laser pulses than short laser pulses (for example, millisecond pulse width), and therefore, in this work, ultra-short laser pulses (picoseconds) are used.

The sunlight decreases the detector signal-to-noise (S/N) ratio, and in case of sun within 10 degrees of the laser beam the radar can become blind [49]. Therefore, the laser radar placement should not be within 10 degree to the sunlight. To avoid the noise signal due to sunlight, the laser radar system can be placed in opposite direction to the sun. The reduction of noise signals can be controlled by using matched optical filter in the receiving optics, more details are given in Section 4.5.2.

2.3 Laser Safety Regulations

There are several standardizations concerning the design and application of sensor systems, and they are regulated by international, national and regional basis. The varieties of laser systems are widely spreaded into the area of applications. As a result, it is categorized according to the laser exposure characteristics. For the safe use of a laser system, they are standardized according to its maximum permissible exposure (MPE) power for its operating wavelength and its exposure time. The MPE has been established in order to protect human beings from any hazardous laser radiation. It is mentioned that the laser safety standard was published in 1984 by International Electrotechnical Commission (IEC) named IEC 825 [50]. The standard IEC 825 has been updated several times and later on it has valided in 2001 as IEC 60825-1:2001 [1], and the German version in [51]. The European standard EN 60825-1 [52] is equivalent to IEC 60825-1 and applies throughout the European Union (EU). Latest, IEC standard is revised by IEC 60825-1:2007 [53]. The commercial uses of laser sensors are classified according to IEC 60825-1. It is also reported that the class-1 laser has lowest energy exposure, and it is commercially used to prevent any risk. In

this research work, a class-1 Gallium-Arsenide (GaAs) laser diode is used with an operating wavelength of 904 nm (see, Section 4.2). The laser radiation may damage the human body if the secured limit is exceeded. But, on human eyes and on skin the laser radiation effect is stronger. The eyes are vulnerable to laser radiation from about 400 nm to 1400 nm [54, 55]. For eye safety, the safe MPE for class-1 laser for the wavelength (λ) of 700 nm to 1050 nm is represented in Table 2.1. The correction factor are used as

$$C_4 = 10^{0.002(\lambda - 700)} \tag{2.6}$$

$$\begin{aligned} C_6 &= 1 && \text{for } \alpha < \alpha_{min} \\ &= \alpha / \alpha_{min} && \text{for } \alpha_{min} < \alpha < \alpha_{max} \\ &= \alpha_{max} / \alpha_{min} && \text{for } \alpha_{min} < \alpha < \alpha_{max} \end{aligned} \tag{2.7}$$

where α is the critical angle from the laser source to the eye, the minimum critical angle is α_{min} [54, 55], and it is $\alpha_{min} = 1.5$ microradian for $t < 0.75\text{s}$ and $\alpha_{min} = 2t^{3/4}$ for $0.75\text{s} \le t < 10\text{s}$. The maximum of critical angle is α_{max}, and it is $\alpha_{max} = 100$ microradian for the eye.

Table 2.1 Eye safe MPE for class-1 laser ([1, 54])

Emission period, t (s) / Wavelength, λ(nm)	10^{-13} to 10^{-11}	10^{-11} to 10^{-9}	10^{-9} to $1.8\text{x}10^{-5}$	$1.8\text{x}10^{-5}$ to 10
700 nm to 1050 nm	$1.5\text{x}10^{-4}C_4C_6$ (Jm^{-2})	$2.7\text{x}10^{4}C_4C_6t^{0.75}$ (Jm^{-2})	$5\text{x}10^{-3}C_4C_6$ (Jm^{-2})	$18t^{0.75}C_4C_6$ (Jm^{-2})

Chapter 3

Double-Beam Laser Radar Concept

In this chapter, the theoretical and analytical background of the double-beam laser radar system for vehicle velocity measurement is explained. The properties of pulse radar velocity meters are described. The theoretical part includes the pulse laser radar system and the velocity measurement systems. The correlation between radar system and target velocity are demonstrated. The analytical part includes the functions to represent the pulse radar as velocity meter. The influencing factors, limitations and ranges of the developed laser systems are given.

It is already mentioned in this research work that the laser radar with two parallel beams is used to detect the precise velocity of moving targets such as for vehicle with its contour, length, range and moving direction. The used two splitted parallel laser beams have similar optical characteristics. The reason of using two splitted parallel beams has two basic backgrounds. First, the target can be detected from the known laser beam separation distance. Second, it can achieve the precise accuracy on velocity measurement by evaluating the correlation of both detector signals.

Two high-sensitive photodetectors have been placed parallel with both laser beams to detect the vehicles and moving targets. Therefore, the developed laser radar can be deployed in different ways as shown in Figure 3.1. Two emplacements of this laser radar system for velocity measurement are the horizontal direction to mobile target plane and the vertical direction to a mobile target plane.

In the horizontal placement of the laser radar system, both laser beams are parallel to the ground plane and toward the side plane of moving targets such as vehicles, shown in Figure 3.1(a). The radar system can be installed in a car. In Figure 3.1, it is shown that two detectors D_1 and D_2 measure the time Δt to cross both parallel laser beams by any target. The parallel separation between both laser beams is realized at 28.8 cm. More details are reported in Chapter 4. In case of urban road and highway, the arch of a road curve for two laser beams can be considered as straight line,

therefore, the laser system as vehicle velocity measurement can also be placed on the curvature of a road and a highway.

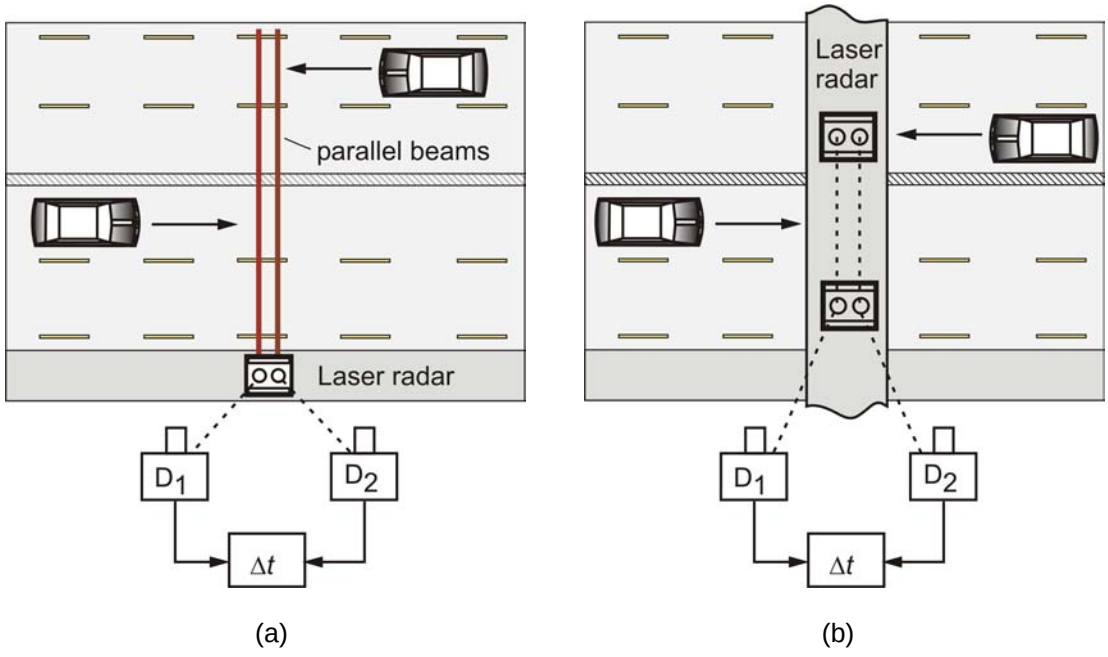

Figure 3.1 Emplacement of laser radar: (a) horizontal, and (b) vertical to the moving targets.

In the vertical placement of the laser radar system, both laser beams are perpendicular to the ground plane. Most possible placements of the radar system can be under a bridge as shown in Figure 3.1(b). For the efficient measurement of velocity, both laser beams and the target direction are to be in the perpendicular plane. For example, for vehicle velocity measurement the vehicle direction is just perpendicular to both of the laser beams as shown in Figure 3.1(b).

3.1 Legal Margins and Errors on Velocity Measurement

It is often a remarkable limit of the application of a measuring instrument due to the lack of measurement accuracy. Fundamentally higher accuracy of the measuring device insists of a higher acceptance of that device. The measuring result should not be beyond the specification in order to achieve the reliable performance. For instance, the measurement error of the velocity measurement system for vehicles is also limited, and in Germany it is regulated by the German norm [56]. The regulation of velocity can sometimes vary, and the variation ranges are depending on the speed limits. According to the German norm, the maximum error ranges allowed for vehicle velocity measuring devices at traffic system are represented in Table 3.1 [56] as

Table 3.1 Margin of allowed error in traffic system ([56])

Actual Velocity (v_r) in km/h	Margin of Error (Δv)
Less than 100	Less than 3 km/h
More than 100	The ratio of $\Delta v/v_r$ should be less than 3%

However, there are several causes of errors on velocity measurement by using a pulse radar system. The fundamental causes are reported in the following sections.

3.2 Start-Stop Velocity Measurement System

The fundamental way to measure the velocity of moving targets by using the analysed radar system is the simple start-stop approach. In the start-stop system, the radar counts the number of detected pulses from the reflected pulses by moving targets. For detecting the specific target (such as vehicle) velocity, the counting of scanning pulses is just started when that target enters the first laser beam. The counting is just stopped when that target go-out from the second laser beam, as shown in Figure 3.2. Very simply, two splitted parallel laser beams have a specific separation distance and it is D_r. For known D_r, the counter records the time from the detected start pulse up to the time of detected stop pulse. Therefore, the velocity of the target can be measured from the counting of received pulses and it represents the time differences of start-to-stop pulses. For instance, a target with a velocity of v is intercepted any of start beam and the same time radar has begun to receive reflected pulses by the target. Meanwhile, the radar has also begun to count the number of scans (N_n) until the receiver has received the stop detected pulse (last pulse) from that target. Now, due to the fixed pulse repetition frequency (PRF) of the radar, the measured time (t_m) can be described as

$$t_m = \frac{N_n}{PRF} \tag{3.1}$$

Ideally, if the target crossed the laser beams perpendicularly as shown in Figure 3.2(a), then the measured velocity by start-stop would be

$$v = \frac{D_r}{\Delta t} \tag{3.2}$$

Moreover, practically the targets might not be crossed 100% perpendicular to the laser beams, as shown in Figure 3.2(b). Therefore, the distance that the target has crossed can be denoted as D_t, and it can be described as

$$D_t = \frac{D_r}{\sin\beta} \tag{3.3}$$

where β is the angle between the directions of target to laser beams as shown in Figure 2.4(b). The angle β can be described as

$$\tan\beta = \frac{D_r}{D_d} \tag{3.4}$$

where D_d is the difference of target ranging distance has detected by first and second detectors. However, the angle β can be measured from the contour of moving targets, and it has been reported in Chapter 5 and in Chapter 6. From the measured time t_m and the known laser beam separation distance D_r, the measured velocity (v_m) of moving target by start-stop system can be represented for the direction of β as

$$v_m = \frac{D_t}{t_m} = \frac{D_r.PRF}{N_n \sin\beta} \tag{3.5}$$

For the target travelling perpendicular to direction of laser beams then $\sin\beta = 1$, and D_t can be considered as D_r. As a result, the measured velocity from (3.5) can be rewritten as

$$v_m = \frac{D_t}{t_m} = \frac{D_r}{t_m} = \frac{D_t.PRF}{N_n} = \frac{D_r.PRF}{N_n} \tag{3.6}$$

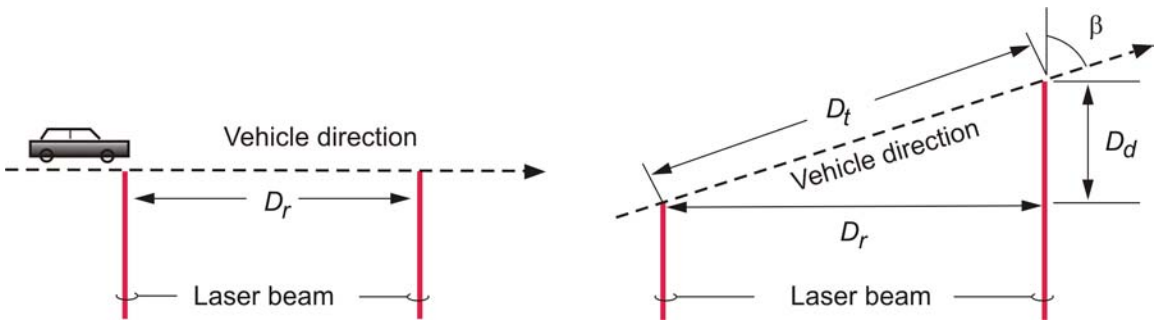

(a) (b)

Figure 3.2 Velocity measurement by parallel beam laser radar: (a) perpendicular to target, and (b) angular direction to target.

***Error Due to PRF in the Start-Stop System*:** The velocity measurement based on the start-stop system is functioning with the measurement of detected laser pulses and the time to take to cross both laser beams by the moving target. In start-stop system, the maximum error can be occurred when the target (vehicle) crosses the two beams just after a laser pulse has emitted. In Figure 3.3, the start and the stop pulses are described as Pl and Pr, respectively. In start pulse counting, the laser pulse of 2Pl in the starting laser beam does not detect the target and it detects by the pulse 3Pl. The same error can also occur in the case of the stop pulse, and it may not detect the pulse 2Pr and it detects the pulse 3Pr. As a result, the maximum time error can be counted [57] as

$$t_{err,\,\max} = 2t_{prf} = 2/PRF \tag{3.7}$$

Again, it can be pointed out that the error due to pulse repletion frequency (PRF) in start-stop system is lower at higher repetition frequency. But, pulse repetition frequency cannot be very high because it should not be the case of exceeding permissible limit of MPE [52]. More explanation about the limitation of repetition frequency and the characteristics of laser transmitter is described in Chapter 4. On the other hand, the error level can be reduced by using very fast photodetection technique, and it will be described in Section 4.4 and Section 5.2.

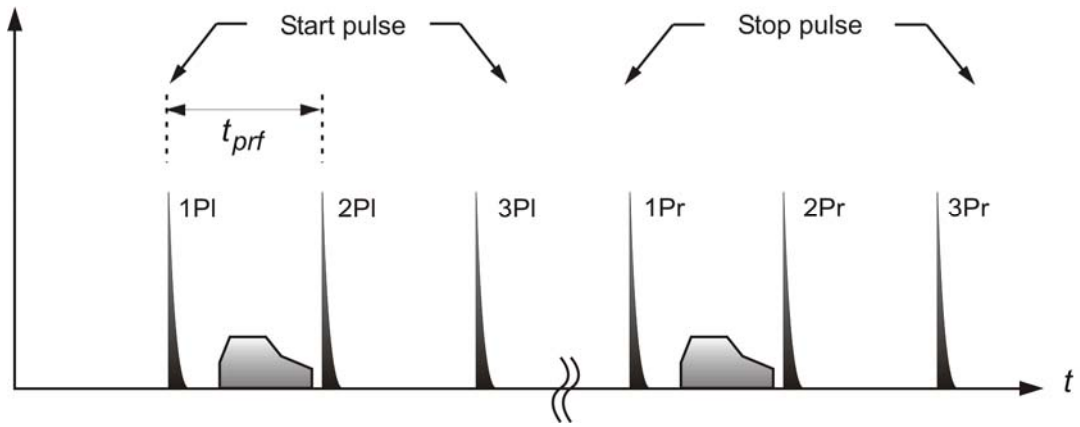

Figure 3.3 Start-stop measurement errors due to repetition frequency.

In (3.5), it is described that the measured velocity by start-stop system is represented as $v_m = D_t/t_m$. If the time t is needed to cross both laser beam with distance D_r, then the velocity v_r can be rewritten as

$$v_r = D_r/t \tag{3.8}$$

Now, if Δt_{err} (difference between exact and measured time) is the error time, which introduced the error velocity of Δv_{err} , then (3.8) can be written as

$$v_r \mp \Delta v_{err} = D_r / \left(t \pm \Delta t_{err}\right) \tag{3.9}$$

Therefore, from (3.8) and from (3.9), it can be written as

$$\frac{\Delta v_{err}}{v_r} = \frac{\Delta t_{err}}{t \pm \Delta t_{err}} \tag{3.10}$$

The maximum of the error velocity can occur for the maximum time error in the start-stop system, which is $\Delta t_{err,\,\max} = t_{err,\,\max} = 2/PRF$. From (3.9) and (3.10), the maximum error of velocity yields

$$\left(\frac{\Delta v_{err}}{v_r}\right)_{\max} = \frac{2v_r}{3.6D_r.PRF + 2v_r} \tag{3.11}$$

From Table 3.1, for vehicle velocity of $v_r \leq 100$ km/h, the error velocity Δv_{err} should be ≤ 3 km/h. In this case, (3.11) becomes

$$\Delta v = \frac{2(v_r)^2}{3.6D_r.PRF + 2v_r} \leq 3 \text{ km/h} \tag{3.12}$$

It follows that

$$D_r \times PRF \geq \frac{2(v_r)^2 - (3 \text{ km/h}) \times 2v_r}{3.6 \times (3 \text{ km/h})} \quad \text{for} \quad v_r \leq 100 \text{ km/h} \tag{3.13}$$

Again from Table 2.4, for a vehicle velocity of $v_r > 100$ km/h, the ratio of error velocity should be $\Delta v_{err}/v_r \leq 0.03$. In that case, (3.11) yields

$$D_r \times PRF \geq 17.96 v_r \quad \text{for} \quad v_r > 100 \text{ km/h} \tag{3.14}$$

From (3.11) and (3.12), it can be noticed that the lower the vehicle velocity, the lower is the error level. Therefore, this laser radar system can also measure very low velocity compared to a Doppler radar. In this work, the separation distance of both laser beams was primarily chosen as 28.8 cm due the easiest feasibility of installing all laser radar modules (see Chapter 4). The functional and acceptable range of pulse repetition frequency for the measurement of precise vehicle velocity system is represented in Figure 3.4 for the laser beam separation distance $D_r = 28.8$ cm. It is demonstrated that higher pulse repetition frequency is better to evaluate velocity precisely within allowed MPE.

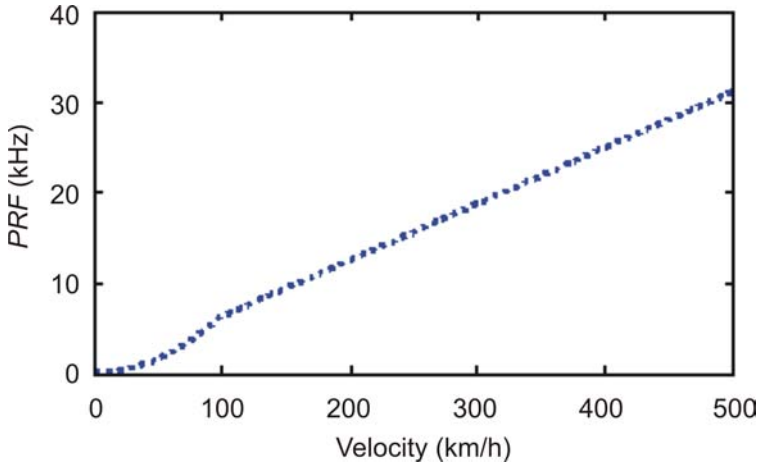

Figure 3.4 *PRF* and velocity ranges. It includes the maximum permissible errors.

3.3 Contour of Moving Targets

The precise velocity measurement system has been given much priority due to the ability to ease the prediction of vehicle velocity and identification also in heavy traffic congestions. Meanwhile, it is highly demanding to evaluate the types of a vehicle along with its velocity. Due to traffic regulations, there are different speed limitations for different types of vehicles, and it has increased the safety in the traffic system. Fundamentally, the classes of vehicles have been separated according to their load capacity and their surface dimensions. There are six major groups of vehicles reported by Hobson, Roe and Hawley [58], and they are represented in Table 3.2. Now, if the velocity traffic radar system is also able to precisely detect the classes of vehicles and ranging along with their velocities, then it will also be possible to know the vehicles infringes and their existing speed limit. The differentiation of velocity allocation and existing velocity can easily be identified, and it is very useful information for the road traffic planers. It is well known in traffic system, to alleviate the traffic congestion the interested information is the types of vehicles and the running velocities of those vehicles [57].

Table 3.2 Six major groups of vehicles ([59])

Types of Vehicle	Motor-bikes	Cars	Light Goods Tracks	Medium Goods Tracks	Heavy Goods Tracks	Buses
Length (m)	2	3.2 to 5	5 to 8	8 to 11	11 to 20	12

From the developed pulse laser radar system, it is easily possible to detect the length, height and contour of mobile targets along with the velocity, especially of vehicles; they are briefly represented in Chapter 5 and in Chapter 6.

3.4 Measurement of Vehicle Length

The length of a moving target can easily be detected by using the information from any of the detector laser signals. Moreover, by using the information from any of the two laser beams, the system can determine the length of the vehicle. If the radar system counts the number of detection from a moving target to cross both parallel laser beams the length of the moving target can be evaluated. For a certain pulse repletion frequency (PRF), the measured length L_m of the moving target can be represented as

$$L_m = v_m t_m = \frac{v_m N_n}{PRF} = \frac{D_r}{(t_m)^2} \tag{3.15}$$

where N_n is the number of detected laser pulse, and t_m is the measured time to cross both laser beams by target.

***Error on Length Measurement*:** From the error time of (3.7) and the length measurement of (3.15), the maximum error of target length ΔL_{err} can be described as

$$\Delta L_{err} = \frac{2v_r}{3.6PRF} \tag{3.16}$$

There are also some reasons of error on length measurement such as laser beam width, rise time, temperature effect. However, those factors are related to radar system development. Therefore, there influencing factors are governed by the radar development reported in Chapter 3 and Chapter 4.

3.5 Measurement of Vehicle Contour

As it is discussed the double beam laser radar can measure in horizontal and in vertical direction to the moving target. Therefore, two dimensional horizontal and vertical contours also can be measured by this laser radar.

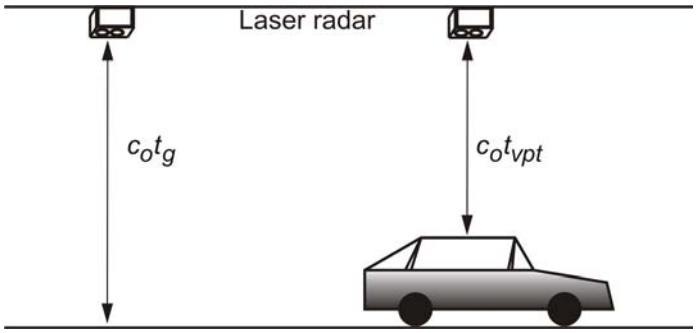

Figure 3.5 Contour measurements on vertical direction.

In case of contour measurement from vertical direction, the system can measure height and length of the target. However, to measure the height and vertical contour of vehicles this laser radar should be vertical to the vehicles (targets) direction, as shown in Figure 3.5. Now, if the required time of laser pulse reflected from the ground is t_g , the required time of laser reflected pulse from the vertical-surface of vehicle is t_{vpt} , then the time difference between t_g and t_{vpt} represents the height of the vehicle surface per measurement. By the radar detected vehicle velocity v_m , the travelling distance of vehicle for each scanning can be described as

$$d_{sn} = \frac{v_m}{PRF} \tag{3.17}$$

Therefore, if the received number of scanning pulse from vertical direction of N_{vn} is detected from the vehicle, the detected length of vehicle L_{mvc} by using vertical contour can be presented as

$$L_{mvc} = d_{sn} N_{vn} = \frac{v_m N_{vn}}{PRF} \tag{3.18}$$

Similarly, the height of vehicle for each measurement H_{mpt} (height of moving target) can be presented as

$$H_{mpt} = \frac{c_o \left(t_g - t_{vpt} \right)}{2} \tag{3.19}$$

The vertical contour of that vehicle (moving target) H_{vmt} can be described as an envelope signal for N_{vn} number of scanning and for each scanning travelling distance of d_{sn} as

$$H_{vmt}(n) = \sum_{n=0}^{N_{vn}} \left[d_{sn}(n).H_{mpt}(n) \right] = \sum_{n=0}^{N_{vn}} \left\{ d_{sn}(n). \frac{c_o . \left[t_g(n) - t_{vpt}(n) \right]}{2} \right\} \tag{3.20}$$

where $n = 1, 2, 3, ..., N_{vn}$ and $H_{mpt}(n)$ is measured heights of n^{th} scanning.

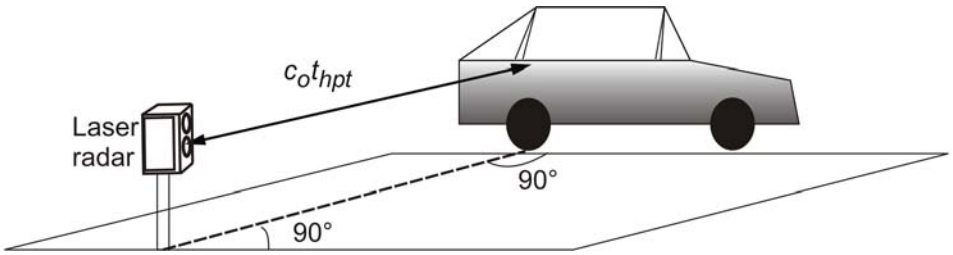

Figure 3.6 Contour measurements on horizontal direction.

In case of contour measurement from horizontal direction, the developed laser radar system can measure the length and the horizontal contour of moving targets. The system emplacement is shown in Figure 3.6. For a vehicle (or any moving target) which intercepts the laser beams, the required time of laser reflected pulse from each measurement of the point horizontal-surface of vehicle is represented as t_{hpt}. With the target velocity v_m, the distance travel of each scan is described as $d_{hn} = v_m / PRF$. From the detected number of scanning pulse in horizontal direction (N_{hn}), the length by horizontal contour (L_{mhc}) of the moving target can be represented as

$$L_{mhc} = d_{hn} N_{hn} = \frac{v_m N_{hn}}{PRF} \tag{3.21}$$

Now, if the ranging distance of each measurement of horizontal-surface from target is r_{hpt}, then it can be described as

$$r_{hpt} = \frac{c_o t_{hpt}}{2} \tag{3.22}$$

The minimum distance of moving target can be represented as $r_{hpt,\,\min}$ from any minimum detected time of $t_{hpt,\,\min}$ in (3.22) for the detected N_{hn} number of scanning from that moving target. The horizontal contour of the target of W_{hmt} is an envelope signal from N_{hs} number of scanning and for each scanning travelling distance of d_{hn}, and it can be described as

$$W_{hmt}(n) = \sum_{n=0}^{N_{hn}} \left\{ d_{hn}(n).\left[r_{hpt}(n) - r_{hpt,\,\min} \right] \right\} = \sum_{n=0}^{N_{hn}} \left\{ d_{hn}(n).\frac{c_o.\left[t_{hpt}(n) - t_{hpt,\,\min} \right]}{2} \right\} \tag{3.23}$$

However, for better resolutions of radar detected signals, the received signals can be averaged on several discrete signals. As it is a pulse laser radar system, the system will count all detected signals for each scanning. Most of all reflected pulses will be from the front surface panel of the desired moving target. Therefore, simply by evaluating all received signals from the surface contour of the moving target, the radar system will be represented the two dimensional form of height or width (from vertical and horizontal measurement plane, respectively).

3.6 Velocity Measurement Using Measured Contours

By using the temporally taken contours of the radar system from both detectors, the precise velocity of vehicles such as moving targets can be evaluated. To perform the precise velocity from both contours, the correlation of both time signals is preferred. By correlation, the precise detection time that the vehicle takes to run the base distance D_r between the two laser beams is obtained from the superimposition of both contours, as shown in Figure 3.7.

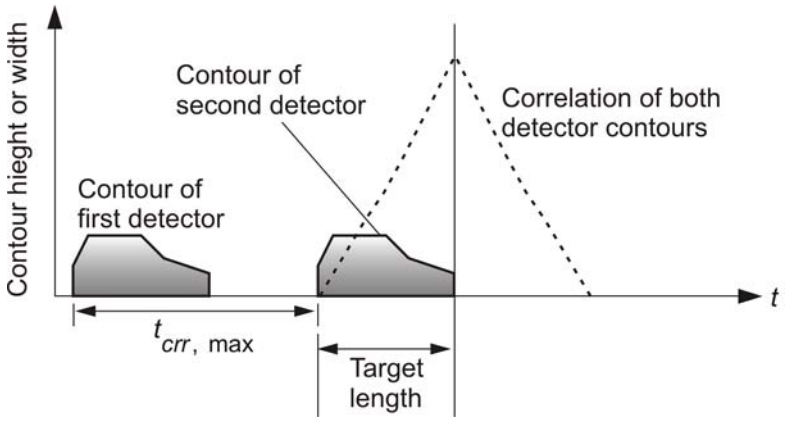

Figure 3.7 Precise velocity measurement from target contours.

In correlated signal, detected time signals of every point targets from first detector are cumulatively conjugated with every point targets of second detector as represented by the equation (with a temporary variable ℓ)

$$R_{X,Y}(\ell) = \sum_{n=0}^{N_{tn}} X\left[(n-\ell)t_{prf}\right] \times Y(nt_{prf}) \tag{3.24}$$

where ($R_{X,Y}$) is the correlation signal of both detected contours, $X(n)$ is the n-th sample of first detector, $Y(n)$ is the n-th sample of second detector, and N_{tn} is the

total number of scanning taken by the radar system in the measurement. The correlation of both detector signals (3.24) have the maximum time $t_{crr,\,\max}$, and it is the point of maximum correlated signal as shown in Figure 3.7. The time $t_{crr,\,\max}$ is precisely same as the time difference of both detected contours. The maximum of $R_{X,Y}$ is obtained as $R_{X,Y,\,\max}$ for $\ell = \ell_{\max}$. The maximum difference of time can be represented as $t_{crr,\,\max} = \ell_{\max} t_{prf}$. Since the distance between both parallel laser beams D_r is fixed (see Section 3.2), so the measured velocity by using correlation (v_{crr}) can be described as

$$v_{crr} = \frac{D_r}{t_{crr,\,\max}} = \frac{D_r}{\ell_{\max} t_{prf}} \tag{3.25}$$

***Error on Velocity from Measured Contour*:** The temporal detected contours from both detectors are correlated to evaluate the precise velocity. Therefore, in this case, the maximum temporal error may occur when one detector has measured the contour length twice more than other detector. It may happen due to the mismatches of photoeceivers, and it can be identified from the error in length measurement. However, such error can be found out if the numbers of detected laser pulses are not the same. The system can be designed to extract the photoreceivers mismatches. For instance, it can be seen from Figure 3.7 that the maximum of the correlation time can be displaced by t_{prf}, and it may cause the maximum error on time based contour measurement. From Section 3.2, it can be demonstrated that the error is exactly half from the start-stop system. Moreover, since the whole contour is used to correlate for the velocity evaluation, therefore, the accuracy of this method is not only depending on the first detected signal.

Chapter 4

Double-Beam Laser Radar Realization

In this Chapter, the realized laser radar system and its main system components are described. Afterwards, the complete system is characterized, and measurement results are discussed.

4.1 System Overview

A block diagram of the analyzed pulse laser radar system is depicted in Figure 4.1.

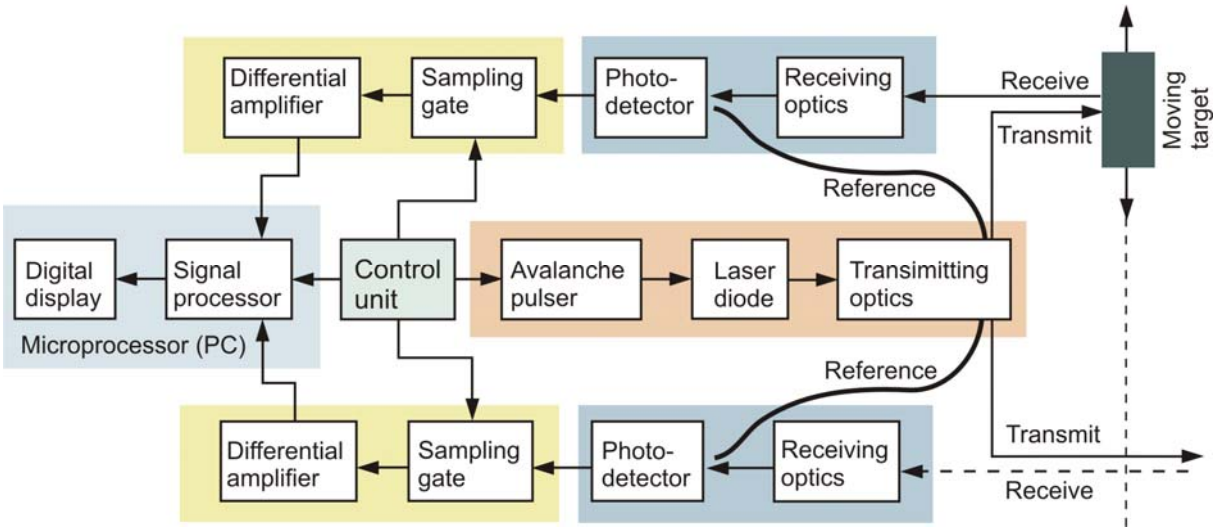

Figure 4.1 Schematic block diagram of the developed pulse laser radar.

The laser radar system mainly consists of the following modules:

- Laser transmitter
- Photodetector (in each measurement channel)
- Optical system
- Control unit
- Receiver down-converter

The laser transmitter generates and emits picosecond laser pulses. The photodetectors should have the same characteristics in order to achieve the synchronized photodetection technique. The broadband high sensitive avalanche type photodetectors are used to convert the optical signals to electrical signals (O/E converter). The optical system comprises the transmission optics and the reception optics. The transmission optics is used to split-up the laser beam into two parallel beams. The reception optics is used to filter the unwanted noise signals and to produce the micrometer focus point for the receiving echo pulses on to the active area of the photodiodes. The control unit is used to control the pulse repetition frequency of the laser transmitter. It also generates the synchronized reference pulse for the laser transmitter and for the sampling units. The down-converter converts the fast electrical signals from the photodetectors to slow down for further signal processing. Finally, the radar signals are analyzed and programmed for detecting the moving target such as vehicle velocities (see Chapter 5).

The radar system is synchronized by a control unit [2], and it is operated at a repetition frequency of 37.5 kHz. The repetition frequency controls the triggering of the avalanche current pulse generator. The avalanche current pulse is used to generate powerful short laser pulses from the used single-heterostructure laser diode of type LD-62. In the transmitter optical system, the combination of two biconvex lenses is used to produce the laser beam with similar aperture, and this beam is splitted into two laser beams by using an optical beam splitter. These two laser beams are used to measure the contour of the moving targets as shown in Figure 3.1. Part of the reflected pulse echo is detected via the receiving optics by the photodetectors. Two reference signals are also coupled out from the transmitted laser beams, and they are directly focused on both photodiodes via optical fibers. The broadband biasing circuit is used to activate the photodiode and to transmit the optical to electrical (O/E) signal for further signal processing. Finally, the received signals from both photodetectors are down-converted by using time-extended sampling principle [2]. They are amplified to perform further signal processing. The time interval between the reference signal and the measured signal is proportional to the ranging distance of moving target. The time differences from both reference and detected signal are used to detect the moving targets (vehicle). By evaluating time significant points from the measured signals, it is elaborately possible to evaluate the 2D contour of the movable targets and their velocity.

4.2 Radar Transmitter

As a module of the pulse laser radar system, the laser transmitter is considered as the core module to be developed. The characteristic of the laser transmitter determine the overall performance of the radar system. The laser transmitter comprises a pulse generator to stimulate the SH AlGaAs-GaAs laser diode of type LD-62 in a gain guided Q-switching mode [59-70]. The laser diode (LD-62) chip was manufactured by Laser Diode Lab. Inc., USA. Meanwhile, the fabrication of single-heterostructure laser diode has been stopped, and only double-heterostructure laser diodes are manufactured because of their higher temperature stability. In this case the modulation of the highly dynamic carrier injection principle can not be applied because the heterojunction barrier cannot be severely influenced. Nevertheless, the fabrication of single-heterostructure laser diodes is very simple and cheap, so that, in a given case, fabrication can be restarted. The avalanche transmitter is a bipolar transistor [71], and it activates the laser pulse generator [72]. The avalanche pulse generator and the laser spikes generator are considered as the radar transmitter.

4.2.1 Realized Laser Transmitter

The realized laser transmitter has a load capacitor C_L of 470 pF, as shown in Figure 4.2. The resistance R_M is chosen as 0.5Ω for the measurement of the pumping current. The trigger signal is taken from a pulse generator in the control unit; see Figures 4.2(b) and 4.2(c).

The cross sectional view of the SH GaAs LD-62 laser diode is shown in Figure 4.3(a). The light emitting active area is 2.032 μm×152.4 μm of the p-GaAs area of the laser diode. The fundamentals of SH laser diodes are found in [64], [73-76]. The laser pulses induced are based on the extremely fast and strong carrier injection into the active area of the laser diode operating in a Q-switched mode [70]. The lasing operation is controlled by the supply voltage V_{cc} and by the trigger signal. Under rated operating condition, moderate carrier density is injected into the active area of the laser diode. In this case, the index profile of asymmetric optical waveguide and especially the pn-junction are not sufficiently decreased. At very high pumping current pulse, the high concentration of carriers decrease sharply the refractive index properties and attribute a negative value contribution of the real part of the refractive index. As a result, high carrier injection has suppressed the commonly observed laser mode indicated by the

dotted line in Figure 4.3(c). Further increase of the pumping current pulse still increases the carrier density in the active region. It can change or suppress the optical refractive index in such a way that the laser can be radiated as a powerful and very short single laser pulse with a shorter wavelength [72]. Whereas, the maximum rated radiant optical power is only 6W [77], and the peak power has achieved 450W in this work.

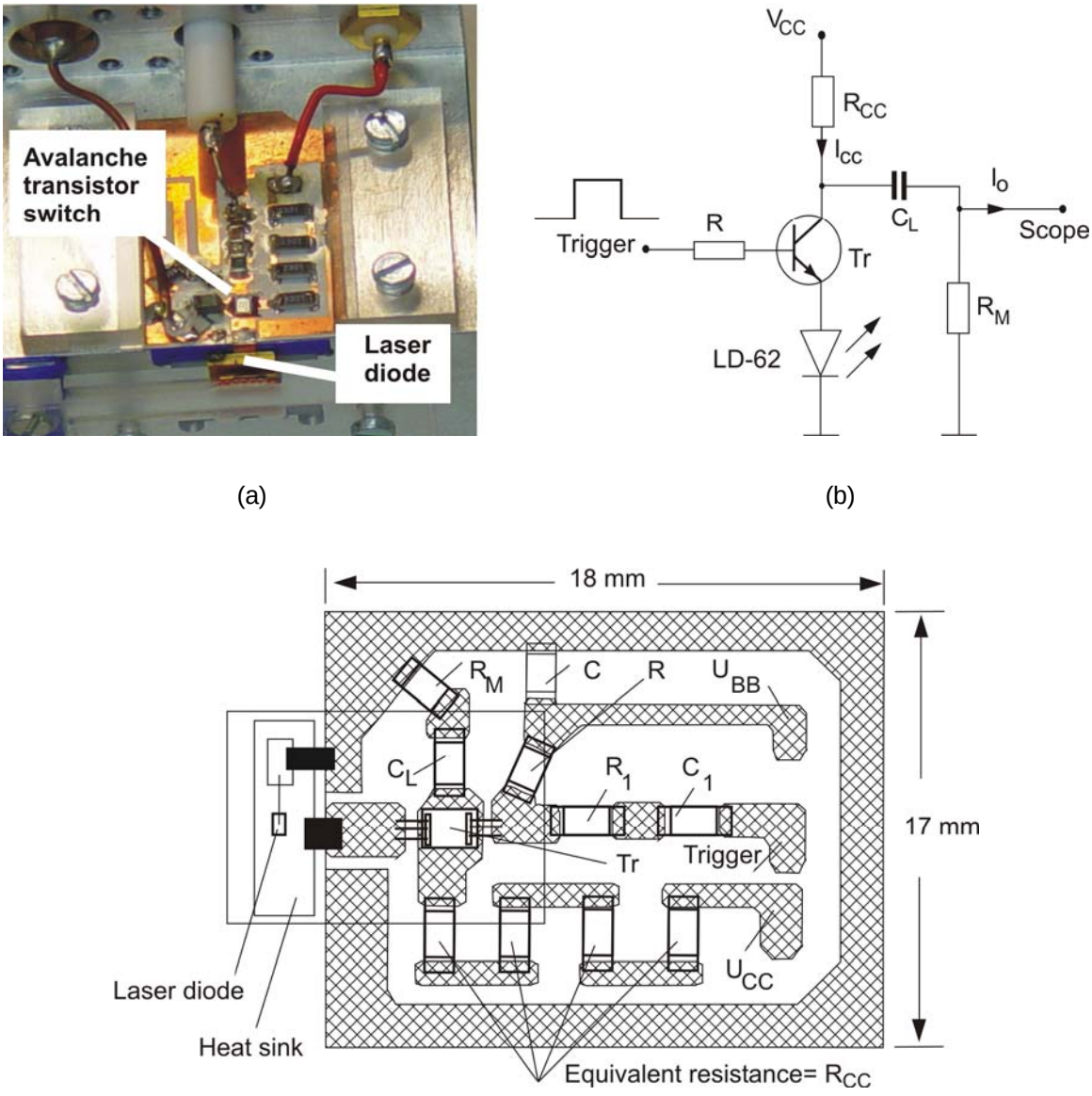

Figure 4.2 Laser transmitter: (a) Picture, (b) circuit diagram, and (c) layout of avalanche pulse generator with integrated laser diode LD- 62 [70].

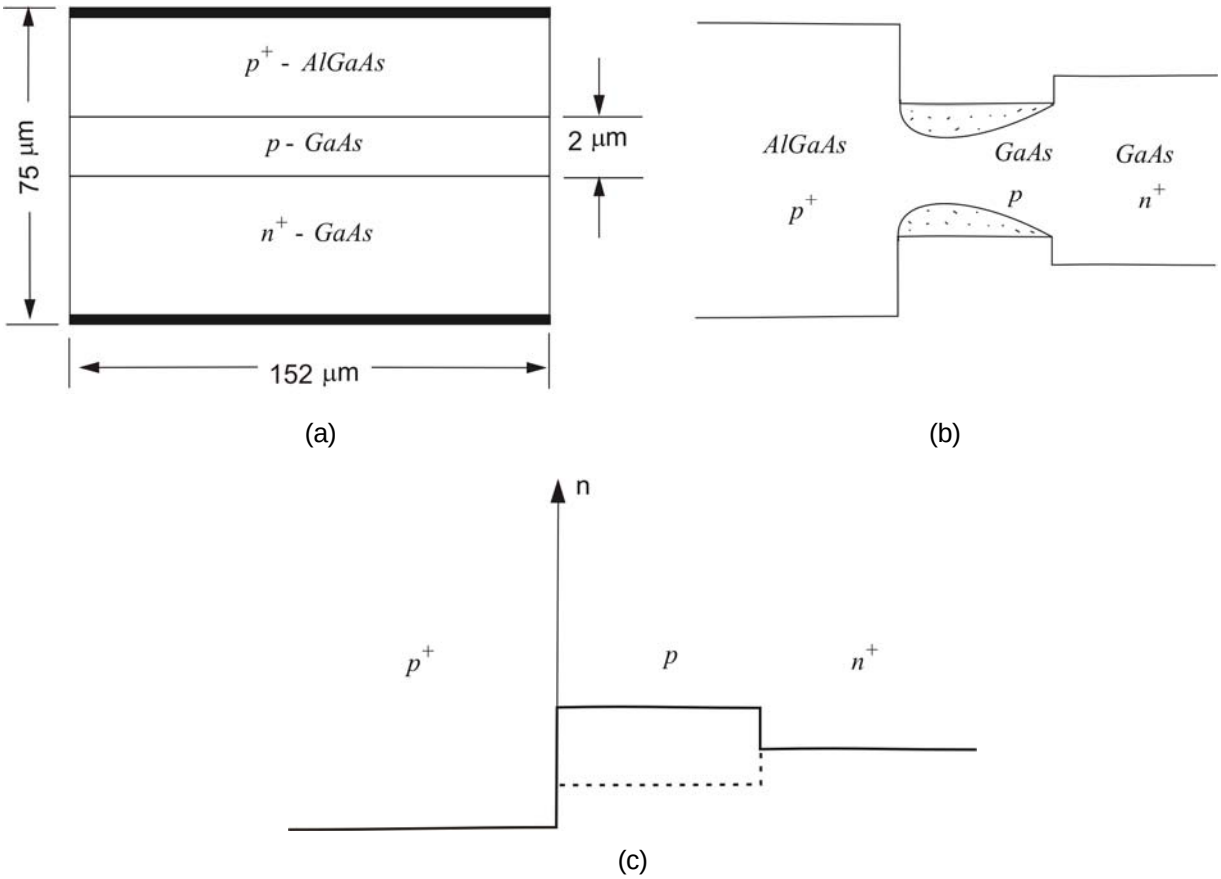

Figure 4.3 Laser diode LD-62: (a) Schematic structure with active area of 2.032 µm ×152.4 µm, (b) simplified band structure of LD-62, and (c) refractive index profile [70].

4.2.2 Experimental Characterization

A laser transmitter, already available in the department of HFT, was used for generating the high power picosecond laser pulses [78-80]. This laser transmitter comprises a bipolar power transistor operating in avalanche characteristics with a discharging capacitor C_L of 470 pF and a load resistance R_M of 0.5Ω. Measurements have been performed to evaluate the laser pulse properties and the effects of external parameter variation on the laser pulses. To demonstrate the characteristics of the laser transmitter, principally the behavior of optical laser pulses is considered.

The block diagram of the measurement setup is shown in Figure 4.4. A 20 MHz pulse generator (HM 8035, Hameg) with 5V peak produces the trigger pulse. The supply voltage V_{CC} and current I_{CC} are measured by digital multimeters (Voltcraft ® GS 6520). The photodetector model v1002 (60 GHz, 3 dB, power conversion rate 2 mV/mW) from the company of New Focus Inc., UK, with a Schottky diode is used to convert the optical signal to an electrical signal [81] (O/E converter). The output of the avalanche transistor circuit stage [see Figure 4.2(b)] is connected with sampling scope head HP

54124T via 60 dB attenuator and 170 cm long coaxial cable (UT 85). The Schottky photodiode in the photodetector is connected to the laser diode (LD-62) via a multimode optical fiber (50 µm diameter, 190 cm long). The photodetecter is connected to the sampling scope via RG coaxial cable (RG 58A) with 35 cm length and 40 dB attenuator. The reason of using attenuators is to tackle failures of any components in the measurement system. The operating temperature of the laser diode [70] is controlled by a Peltier element (temperature controller).

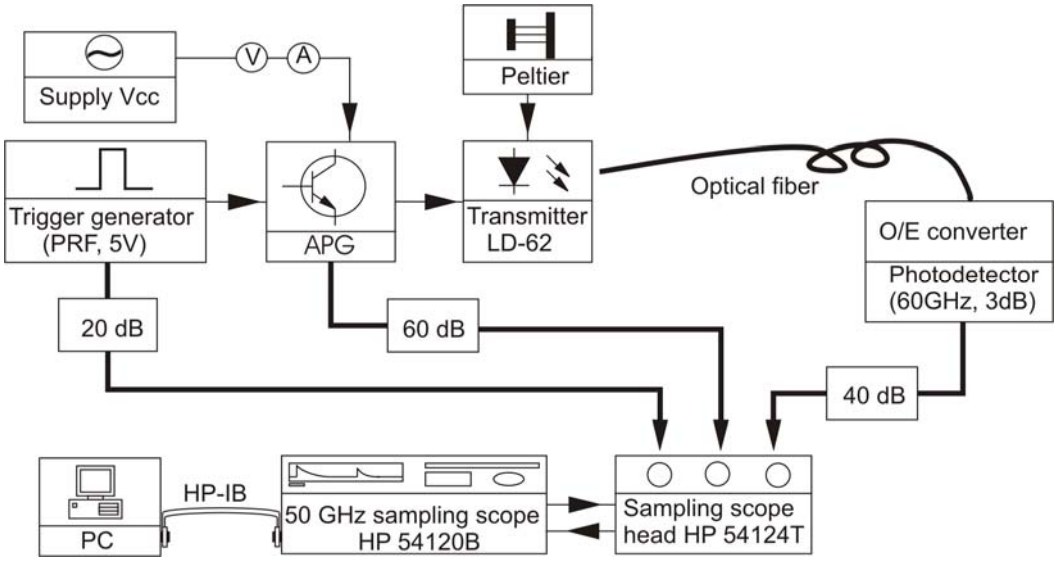

Figure 4.4 Measurement setup for laser transmitter characterization.

The light intensity, bandwidth of the laser pulse and temperature are very important functions to evaluate the characteristics of laser pulses by using O/E converter. Therefore, the selection of the photodetector is very important because it may produce a distortion of the signal wave shape. The use of a 60 GHz Schottky diode with high cut off frequency ($f_{max} \leq 25$ GHz) assures the detection of distortionless impulses. In addition to the Schottky diode, the measurements can also be performed with fast MSM photodiodes. Both types of photodiodes are working within the linear range, but MSM photodiode has higher temperature non-linearity [70, 82].

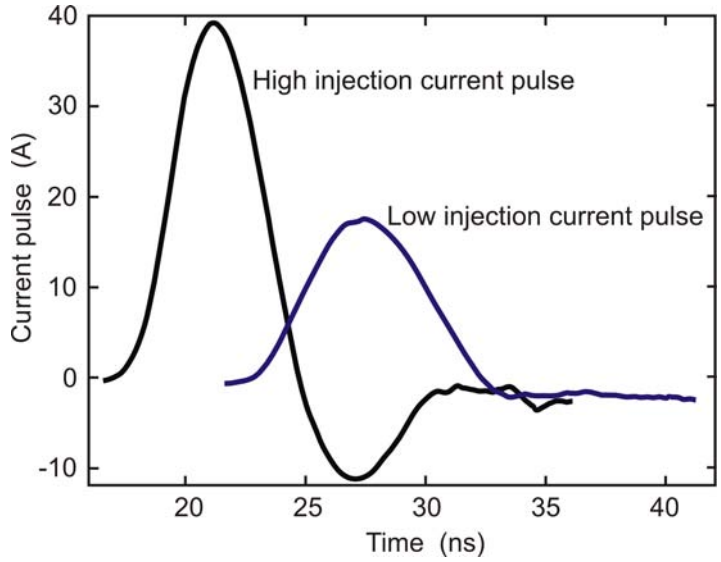

(a)

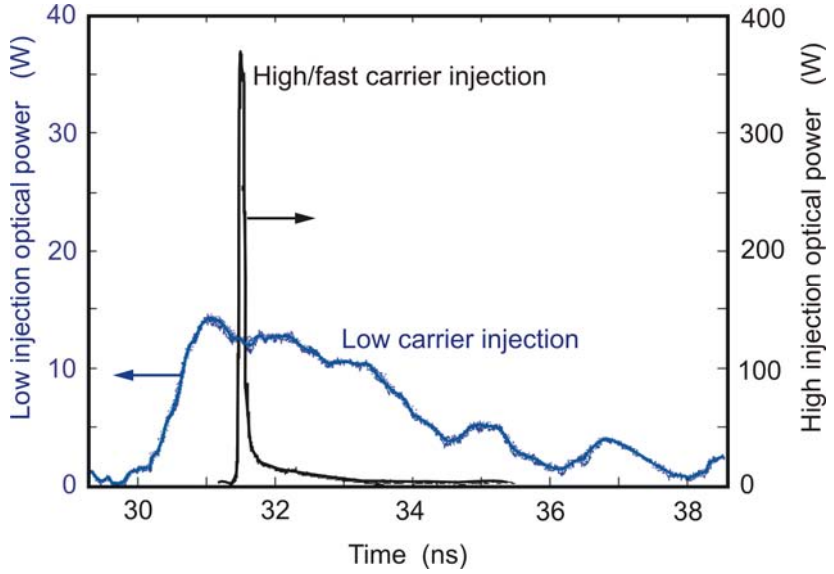

(b)

Figure 4.5 (a) Measured pumping current pulses. The low injection current pulse with $I_{max} = 16.8$ A, rise time 2.69 ns, fall time 4.09 ns, pulse width 7.24 ns (FWHM) at the supply voltage V_{CC} of 239V. The high injection current pulse with $I_{max} = 39.2$ A, rise time 2.26 ns, fall time 2.35 ns, pulse width 4.02 ns (FWHM) at the supply voltage V_{CC} of 310V. **(b)** Measured stimulated low injection and high injection optical laser pulses. At low injection, the laser pulse generated $P_{max} = 13.7$ W, $t_r = 832.0$ ps, $t_f = 5.06$ ns, and $t_d = 3.08$ ns. At high carrier injection, the laser pulse generated $P_{max} = 371.5$ W, $t_r = 28.2$ ps, $t_f = 121.0$ ps, and $t_d = 32.30$ ps.

Based on the measurement, it is evaluated that the pulse repetition frequency has no significant effect on the characteristics of the laser transmitter. The measurements are performed simultaneously from a pulse repetition frequency of 1 kHz to 40 kHz. However, it is also evaluated that the avalanche breakdown action begins at the

supply voltage of 239V. At the supply voltage of 239V, the measured current amplitude is 16.8A and the pulse width (FWHM) is 7.24 ns. The current pulse is increased further by increasing the supply voltage, for instance at 310V. At the supply voltage of 310V, the current pulse peak is 39.2A and the pulse width is 4.02 ns (FWHM), as shown in Figure 4.5(a) and Figure 4.5(b). It is realized that at a lower supply voltage, the carrier injection into the active area of the laser diode is not strong enough to produce a substantial negative contribution of refractive index. As a result, the laser diode has also produced a laser pulse with a peak value of 13.7W; see Figure 4.5(b). A further increase of the supply voltage has induced stronger and sharper laser pulses. The strong carrier injection into the laser's active area has been produced by gradually increasing the pumping current pulse. From the measurement result, it is evaluated that the laser diode emits an optimum pulse at the supply voltage of 310V. In this case, the pumping current pulse peak of 39.2A has produced an optical peak power of 371.5W. The measured laser pulse parameters for the supply voltage of 310V are: Optical peak power P_{max} = 371.5W, rise time t_r = 28.20 ps, fall time t_f = 121.0 ps and pulse width t_d = 32.30 ps (FWHM). It has increased the rated optical power by a factor of 62 for an operating temperature of 23°C.

It can be demonstrated that, at a lower supply voltage, the charge carrier velocities are mostly insufficient to produce the complete avalanche multiplication action. As a result, the free carrier charges still exist in the active area of bipolar devices such as in BJT transistor (Tr). At a higher supply voltage, the electron-hole pair recombination process is drastically increased. The breakdown at a higher supply voltage is near to being saturated, which implies that the possibility of existing free carrier charges on the active area is approximately zero [82-84]. Such circumstances can be approximated as a very high carrier injection. In high carrier injection, the injection current is 2.5 times higher than the low injection current, as shown in Figure 4.5(a). As a result, the laser pulse (371.5W) generation at a high injection current is drastically increased, and it is approximately 27 times higher than the low injection laser pulse (13.7W), shown in Figure 4.5(b). From the measurement samples, it has also been realized that the laser pulses are not significantly increased with a growing supply voltage V_{CC} above 315V. This is because of the saturation occurred, and there is no significant amount of carriers free to take part in the recombination process.

It is also realized that the delay of laser pulse radiation also changes with the change in the pumping current injection pulse. The cause of the delay time changing on the laser pulses is dependant on the time of the carrier recombination process. For instance, more free charge carriers still exist in the active area of LD-62 at the lower current injection pulse. As a result, the carrier recombination process becomes faster at the higher pumping current injection process, and which is recombined for faster laser pulse generation. Therefore, the delay time of the laser pulse generation decreases for a faster carrier recombination process, and consequently it also produces the short laser impulses.

***Relationship of Laser Impulses and Operating Temperature*:** The temperature variation of the injection current pulse is given in Figure 4.6(a), and the reaction of the optical pulse is shown in Figure 4.6(b) for the supply voltage V_{CC} of 310V. It is observed that the laser pulses are varied with the change of temperature. The laser impulses are decreased with the increase of temperature. The reason for this is that the increase of temperature increases the loss of photon energy at the laser diode. As a result, the peak of optical pulse decreases at higher temperatures as shown in Figure 4.6(b).

It is observed that the delay time of the current pulse is decreased with the increase of temperature; see Figure 4.6(a). The delay time of the current pulse is decreased by 0.40 ns for the temperature increase from 17 °C to 28 °C. The reason is the increasing of thermal energy at higher temperatures, and it has increased the carrier velocity. But, in case of the laser pulse, the delay time is increased by 0.55 ns for the temperature increase from 17 °C to 28 °C, see Figure 4.6(b). The reason for the additional time delay in the laser pulses is the increase of photonic energy loss at a higher temperature. At higher photonic energy losses, the additional time is needed to recombine the same carrier charge in the LD-62 laser diode. As a result, at the higher temperature the delay time is increased and the peak value of the laser pulse is also decreased.

The measurement results of Figure 4.6(a) and Figure 4.6(b) show that the temperature variation should be controlled to minimize the uncertainty of laser system performances. Power control and relative signal processing technique can be the effective solutions to minimize the temperature effects on laser sensor performance.

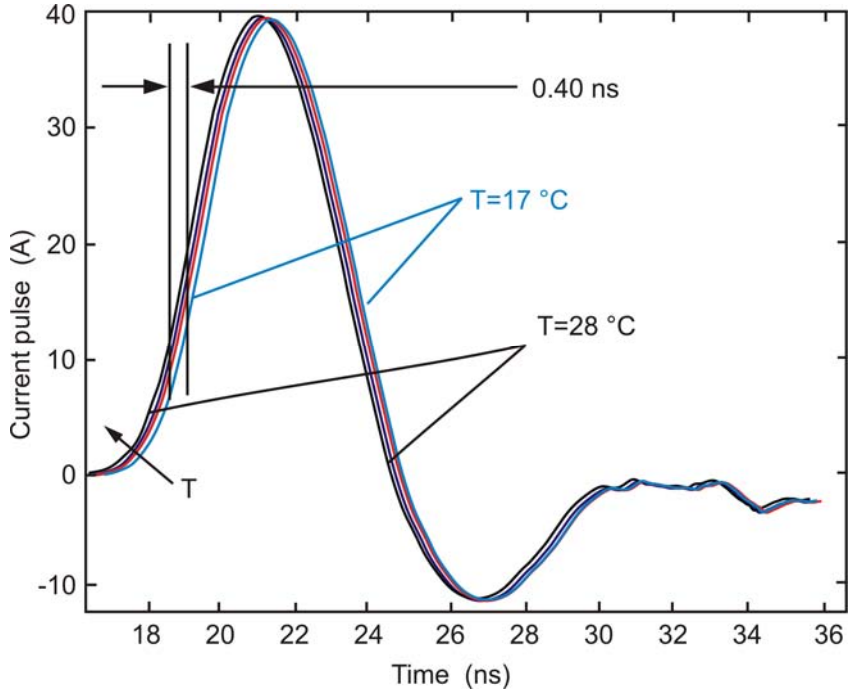

(a)

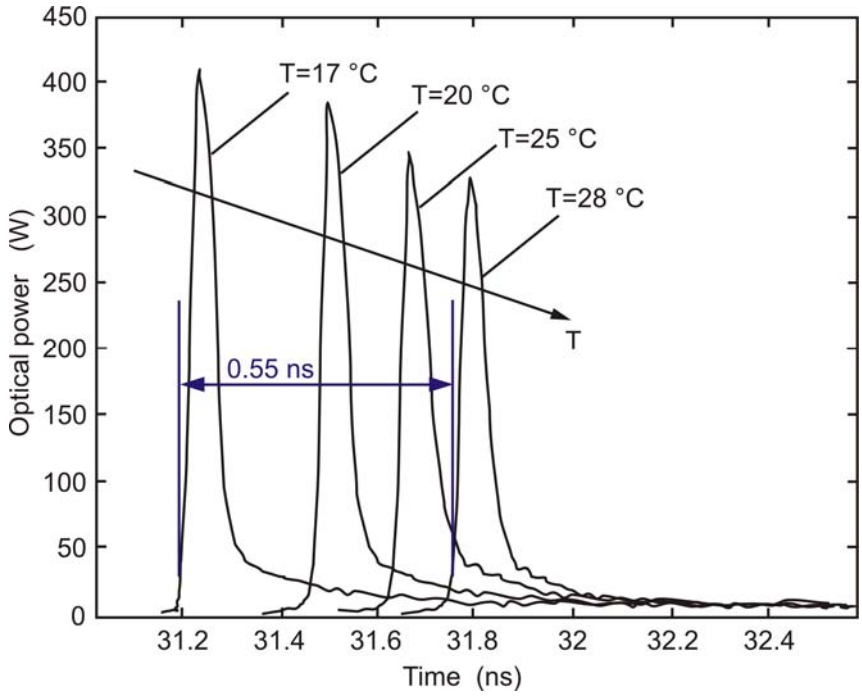

(b)

Figure 4.6 Measured (a) variation of current pulse due to temperature changes at supply voltage of 310V, and (b) corresponding changes of laser pulses.

***Nonlinearity and Temperature Effects*:** In order to carry out the analysis, it is important to evaluate the variation of the optical pulse characteristics due to the change of supply voltage and laser diode temperature. From the measurement result, it has been evaluated that for supply voltage in the range of 239V to 270V, the

characteristic curves are strongly nonlinear. This is due to the beginning of the avalanche breakdown voltage. Therefore, the supply range is reported here from 270V to 325V.

The relative peak value change of the optical pulse is presented in Figure 4.7(a) as a function of supply voltage V_{CC} for different constant temperatures and in Figure 4.7(b) as a function of temperature for different selected supply voltages V_{CC}. From those relatively compared illustrations, it is clear that the temperature variation on peak power plays an important rule up to 310V. The nonlinear variation due to the temperature changes is not significant at the supply voltage of 310V; see Figure 4.7(b). Above 315V the nonlinear variation is again relatively higher than 310V, as shown in Figure 4.7 (b).

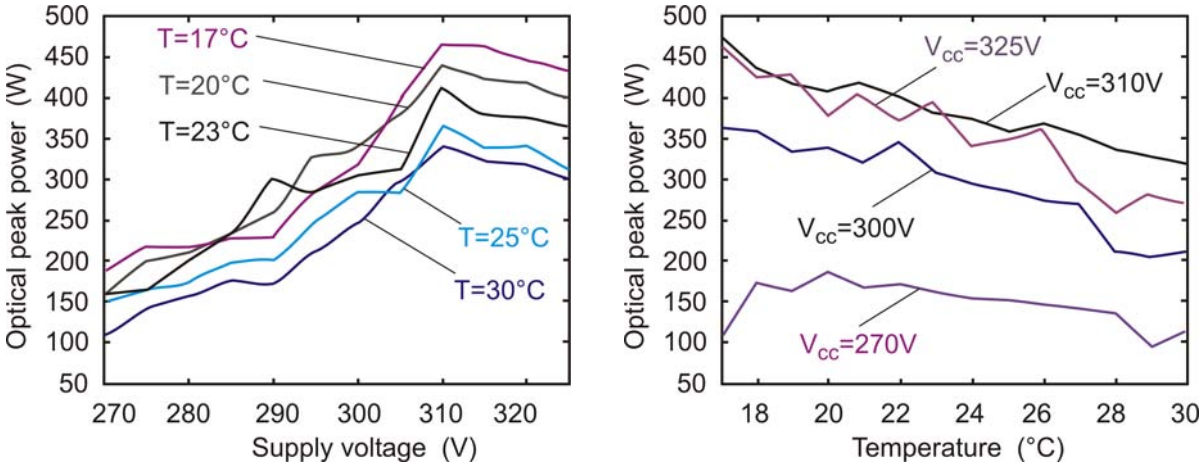

(a) (b)

Figure 4.7 (a) Peak of optical pulse as a function of biasing supply voltage V_{CC}, and **(b)** peak of optical pulse as a function of temperature T °C.

The pulse width (FWHM) of the optical pulses is presented in Figure 4.8(a) as a function of supply voltage V_{CC} for different constant temperatures, and in Figure 4.8(b) as a function of temperature for different selected supply voltages V_{CC}. It is realized that the pulse width (FWHM) is nonlinearly decreased with the increase of supply voltage. From Figure 4.8(b), it can be seen that the variation of pulse width (FWHM) for the change of temperature are mostly significant up to 310V, and above 320V it is again highly nonlinear. The highest nonlinear variation is again observed at supply voltage of 270V, and it is because of the beginning of avalanche breakdown.

The dependencies of the rise time of optical pulses are presented in Figure 4.9(a) as a function of supply voltage V_{CC} for different constant temperatures, and in Figure

4.9(b) as a function of temperature for different selected supply voltages V_{CC}. From Figure 4.9(a), it is realized that the rise time decreases with the increase of supply voltage, and it has nonlinear variation with the changes of temperature. But, at the supply voltage of 310V the nonlinear variation is about 1.4 times less than that at the supply voltage from 270V to 325V. In Figure 4.9(b), it is also presented that the variation of rise time for the changes of temperature are mostly significant up to 310V, and above 320V the nonlinear variation is again increased. The most significant variation is also realized at the supply voltage of 270V. Therefore, it can be abstracted, by considering the optical peak power, pulse width (FWHM) of the laser impulse and the rise time, that the best selection of supply voltage would be 310V.

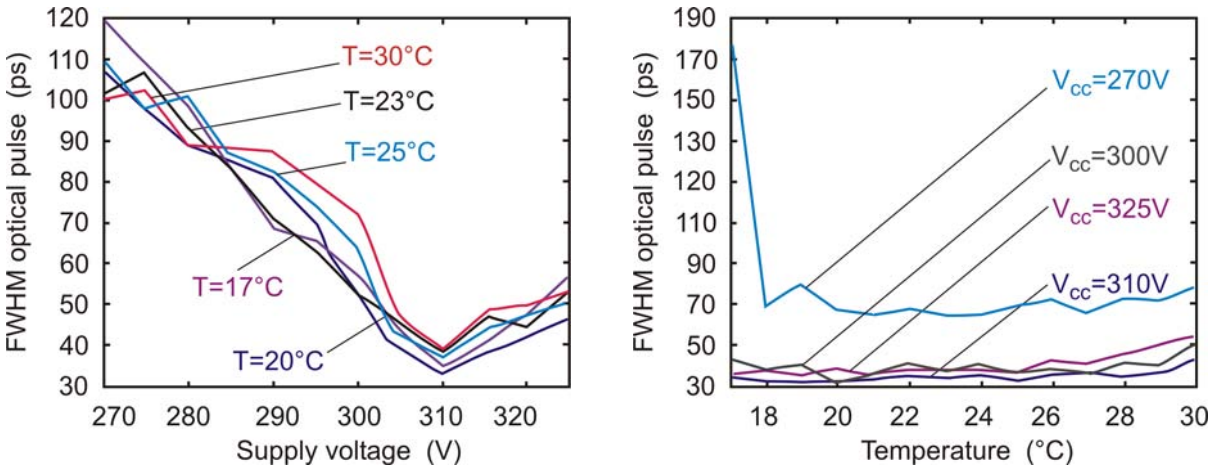

(a) (b)

Figure 4.8 (a) FWHM of optical pulse as a function of supply voltage V_{CC}, and **(b)** FWHM of optical pulse as a function of temperature T °C.

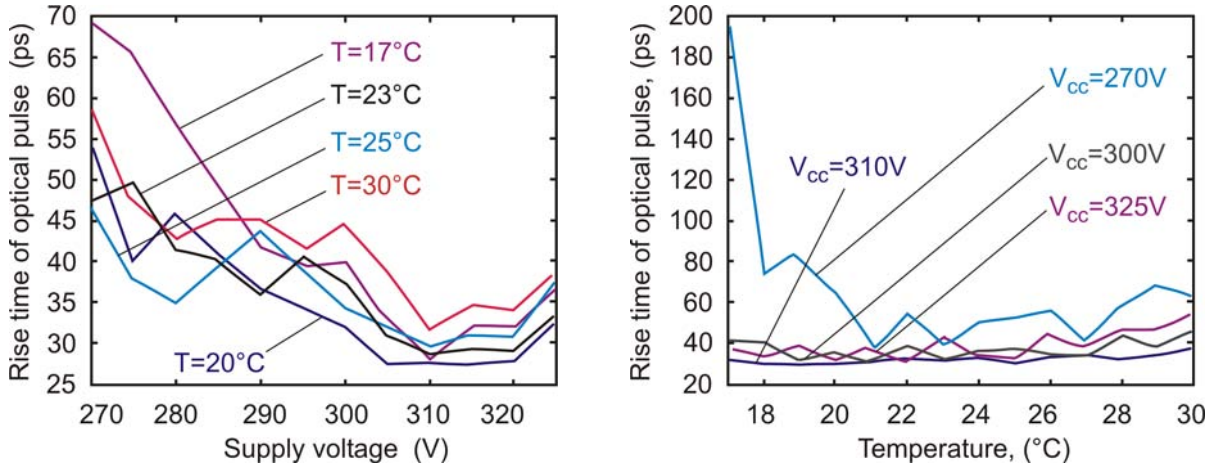

(a) (b)

Figure 4.9 (a) Rise time of optical pulse as a function of supply voltage V_{CC}, and **(b)** rise time of optical pulse as a function of temperature T °C.

***Evaluation of Transmitter Parameters*:** The average optical power of the laser transmitter is measured by using an optical power meter (Model 66XLA from Photodyne Inc.). It is evaluated that the increase of pulse repetition frequency (*PRF*) has also increased the average optical power because more optical power is radiated per unit time. The average optical power P_{av} is the numerical integration of the optical pulse train $P(t)$ over the pulse duration time τ_d. With a pulse repetition frequency (*PRF*) it can be presented as

$$P_{av} = PRF \int_0^{\tau_d} P(t)dt \tag{4.1}$$

According to the measurement results (see, Figure 4.10) and [70, 72, 84], it is demonstrated that higher average optical power is radiated with higher pulse repetition frequency, and it can also be realized from (4.1). The pulse repetition frequency should be controlled in order to ensure the eye-safe operation of the laser diode [53]. The average power (4.1) is proportional to the pulse repetition frequency [70] for a laser system.

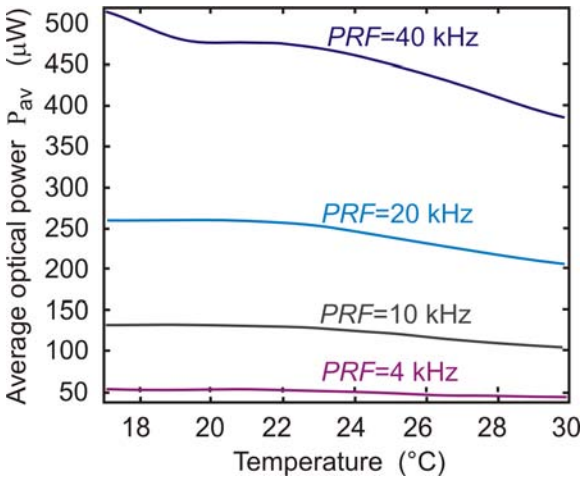

Figure 4.10 Relation between PRF and optical average power.

The temperature effects on the optical power (P_{av}) is higher in higher pulse repetition frequency; the relative variations of the optical power are shown in Figure 4.10. Fundamentally, the peak value of collector current I_{CC} does not change with the change of temperature from 17 °C to 30 °C, see Figure 4.6(a). But, at higher pulse repetition frequency the impedance of the LD-62 laser diode varies with the temperature [70, 72]. Therefore, at a pulse repetition frequency of 40 kHz the temperature variation is most significant. As a result, at 40 kHz the average optical power is decreased from 520 μW to 380 μW for the temperature increase of 17 °C to

30 °C. In contrast, at 4 kHz it is decreased from 55 µW to 42 µW, as shown in Figure 4.10.

It is already realized in Section 3.2 that the velocity error is lower for higher pulse repetition frequency. Therefore, the choice of the pulse repetition frequency selection should be as high as possible to obtain precise velocity measurement. Moreover, the exposure of the laser pulse train due to higher pulse repetition frequency must not exceed the allowed MPE limit of class-1 [53]. The MPE of class-1 laser emission for a wavelength of 904 nm is equal to 0.988 mW. For the evaluation of vehicle velocity up to 500 km/h a minimum pulse repetition frequency of 30 kHz is evaluated (see Section 2.4). Introducing additional factors for precise measurement of the vehicle velocity, the repetition frequency has been chosen as 40 kHz. The generated maximum average optical power of the developed laser transmitter is 525 µW for 40 kHz, and it is approximately half of the allowed MPE according to [44]. Therefore, for *PRF* = 40 kHz, the developed laser radar is eye-safe and classified as a class-1 laser system.

4.3 Control Unit

The function of the control unit is to synchronize the timing signals for the radar transmitter and for the sampling modules. The synchronized reference of the repetition pulses for the transmitter and sampling unit are used to eliminate the time difference error on sampling techniques. Three output signals are generated, and these three synchronized trigger pulses have a pulse repetition frequency of 37.5 kHz, as shown in Figure 4.11. This pulse repetition frequency is set to utilize the high bandwidth of sampling data acquisition and higher accuracy in velocity measurement techniques within safe operation [53] of a laser system. The design and simulation are performed with SPICE and the circuit is fabricated on FR4 substrate. The measurement of the output pulses is performed by using an Agilent Oscilloscope 54641A (350 MHz) and with CAT-1 (TT-MF312, 1.2m long, 600V) probe connectors.

The frequency control is provided by a quartz stabilized oscillator of 20 MHz. This frequency is converted to 37.5 kHz by two frequency dividers. They are frequency divider A and frequency divider B, as shown in Figure 4.11(b). The operation of the frequency divider A is functioning with high-speed Si-gate CMOS devices, where two counters are functioned. They are a ripple counter and a decade counter, and they are used to produce a selectable pulse repetition frequency from 26 kHz to 6.66 MHz. There are three outputs from decade counter 74HCT4017 as shown in Figure

4.11(b). The output signals from the decade counter are taken for producing the synchronized pulse repetition frequency signals for the avalanche pulse generator and the sampling units.

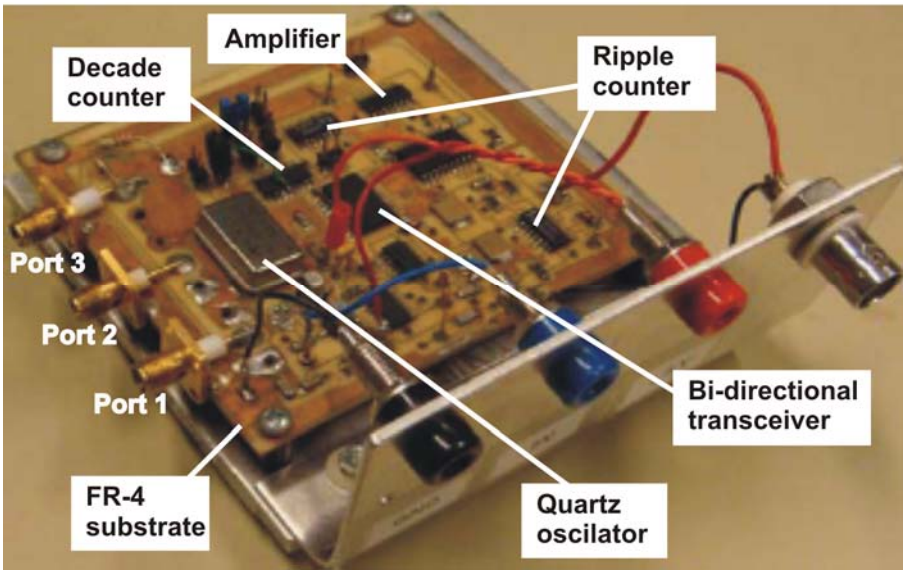

(a)

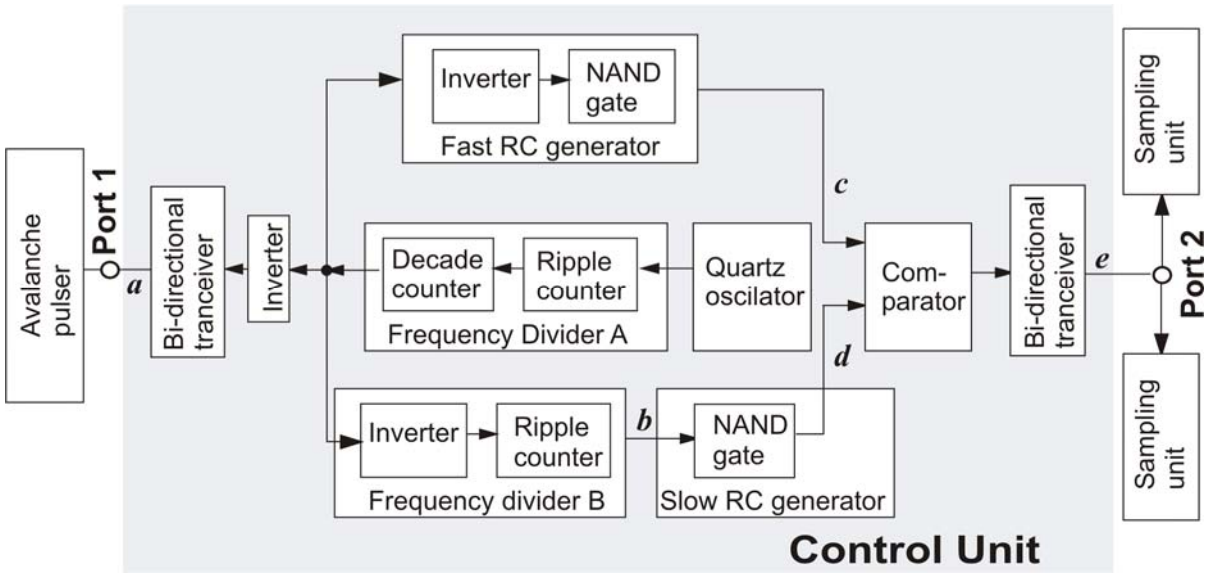

(b)

Figure 4.11 Pulse generator of the control unit (*PRF* = 37.5 kHz): (a) circuit diagram with the size of 8 cm × 8.5 cm, fabricated on FR4 substrate, and (b) schematic functional block diagram.

In this circuit module, first, the 20 MHz signal from the quartz oscillator is fed into a 12-stage binary ripple counter 74HCT4040 [85] and it has a single stage propagation delay of 8 ns. Second, the output of the ripple counter is feed into a 74HCT4017 decade counter (with 10 decade outputs) [86]. The output pulse of frequency divider A with active high has pulse width of 500 ns (FWHM) and PRF of 3.33 MHz. For

producing the pulse repetition frequency for the avalanche pulse generator, the first output signal from 74HCT4017 is again fed in high-pass filters after series buffering and amplifying by 74HCT4049 [87]. The high-pass filter is differentiated to positive and negative pulses. At the end, the differentiated signal is again fed into a 74HCT245 bi-directional transceiver digital logic IC device [88]. It has produced the pulse repetition frequency with sharpening pulse [53], and it is denoted by signal ***a*** in Figure 4.11(b). The signal ***a*** is with a pulse repetition frequency of 37.5 kHz. It is measured at the fabricated circuit port 1 as shown in Figure 11(a). The measured characteristics parameters of signal ***a*** from port 1: Amplitude of 5.40V, rise time (10% to 90%) of 10 ns, and pulse width of 30 ns (FWHM), as shown in Figure 4.12(a). This output signal is used for triggering the avalanche laser transmitter, as depicted in Figure 4.11(b).

Another output signals from the frequency divider A (after 74HCT4017 decade counter) are fed in a frequency divider B and in a fast RC generator, as shown in Figure 4.11(b). The input signals of the frequency divider B and in the fast RC generator are buffered by using hex inverting shifter 74HC4049. The output of frequency divider B (after second ripple counter 74HCT4040 Si-gate CMOS IC) is 20 Hz. It is the input of the slow RC generator and it is denoted by signal ***b***. The charging time constant for the fast RC-generator τ_f is 260 ns. For the slow RC generator the characteristic constant τ_s is 360 ms. Output signals from both RC generators are fed into a comparator (NE521) [89]. The delay slope of the output signal of the comparator is shifted in time at each clock signal and the resulting time shifting is relative to the synchronized frequency sampling. For $\tau_s >> \tau_f$, it can be presented according to [2] as

$$\Delta t \approx T_f \times \tau_f / \tau_s \tag{4.2}$$

where Δt is the system time resolution, which is 19.2 ps. T_f is the time period of the fast RC generator. The output signal of the comparator has been fed to high-pass filters to generate positive and negative pulses. The differentiated positive and negative pulse signals have been fed into a 74HCT245 bi-directional transceiver. It has produced the signal ***e***, shown in Figure 4.11(b), according to [90]. The signal ***e*** is also with a pulse repetition frequency of 37.5 kHz, and it is measured from fabricated circuit port 2. The characteristics parameters measured from port 2 are: Amplitude of 4.95V, rise time (10% to 90%) of 10 ns, the pulse width (FWHM) is 29 ns, as shown in Figure 4.12(b). This trigger signal will be used for the sampling unit.

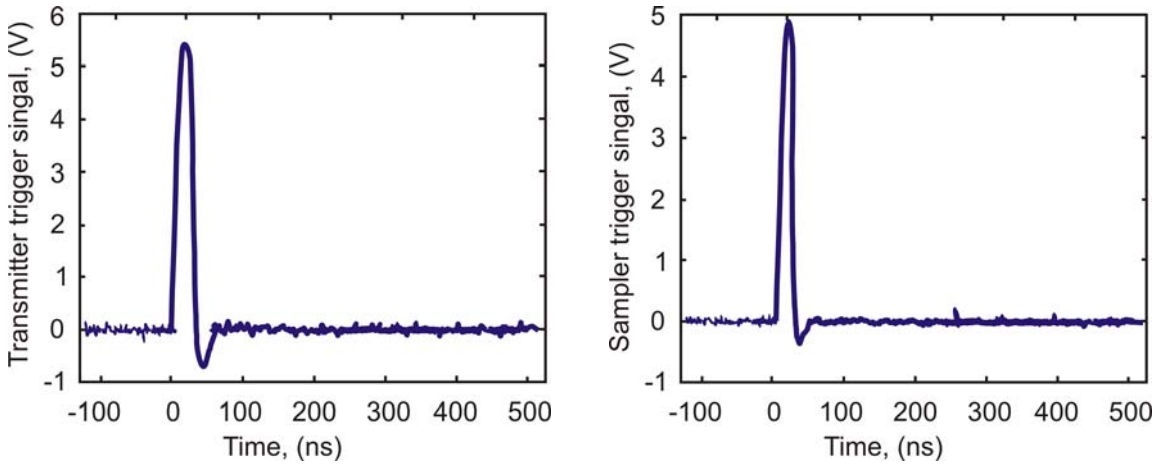

(a) (b)

Figure 4.12 Measured trigger signals of the control unit: (a) trigger signal for laser transmitter (peak value: 5.4V, rise time: 10 ns), and (b) trigger signal for the sampling unit (peak value: 4.95V, rise time: 10 ns).

The third output signal from frequency divider A (after 74HCT4017 decade counter) is fed into the inverting buffer CMOS IC. This is an inverted trigger signal and it is measured from the fabricated circuit port 3, in Figure 4.11(a). The trigger signal delay between transmitter and analog to digital (A/D) converter is measured to be 50 ns, and it is used to evaluate the output sampled pulses from sampler. Moreover, this signal will be the reference signal for analog to digital (A/D) converter.

4.4 Radar Receiver

The block diagram of the receiver is shown in Figure 4.13. Since two receivers are used in this laser radar system, two photodetectors are used with same properties to detect the optical signals. They are used to convert the received optical powers to electrical signals. The APD series of APD230 type diode chips are taken from Silicon Sensor Int. [91]. The APD230 photodiode has high gain spectral responsivity (50 A/W), low noise dark current (0.6 n/A) and very low optical power detection [noise effective power (N. E. P.) typically 10^{-14} W/Hz$^{1/2}$] for $M = 100$ at 800 nm. The function of the photodetector is to detect the ultra-short laser signal with rise time of 28 ps, pulse width of 32 ps (FWHM. Therefore, high sensitivity and broadband photoreception system is necessary to detect the optical signals without distortion. In these circumstances, the avalanche photodiode (APD) is providing the highest sensitivity [92-96]. Moreover, the APD is also operated at high frequency. It has higher gain and higher conversion rate of optical signals to electrical signals than MSN photodiode and PIN photodiode [92].

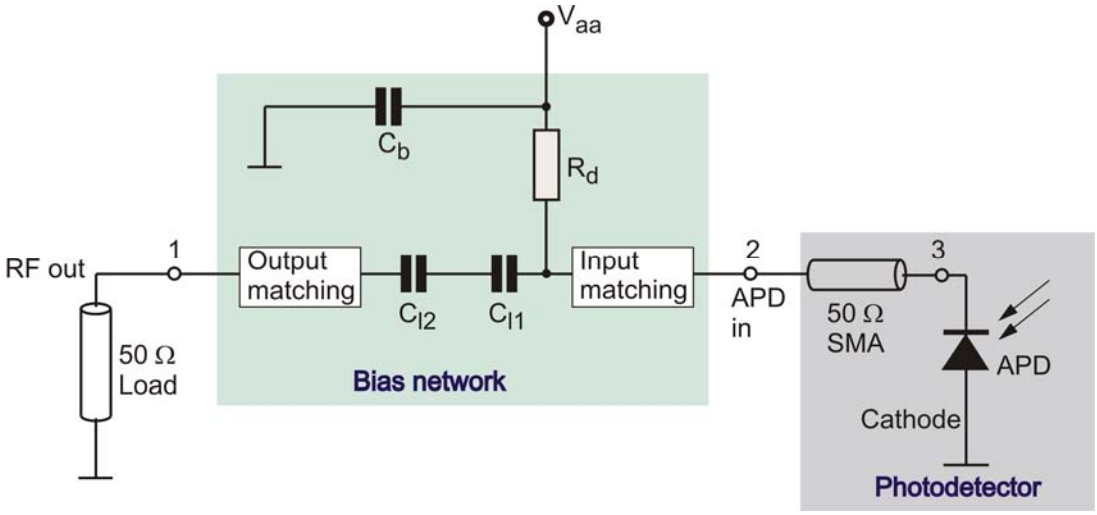

Figure 4.13 Block diagram of the developed photodetector circuit. The APD230 chip is mounted on a 50Ω SMA female connector with cathode grounding.

There are two parts in the photodetector as shown in Figure 4.13. They are the APD photodiode, and the biasing circuit network. The APD photodiode is used to detect the optical signals and to convert the optical signal into electrical signals. Therefore, it functions as an O/E converter, see Figure 4.13. The biasing circuit network is used for biasing the photodiode and transmitting the O/E converted signals from the photodiode to the receiver downconverter for further signals processing. Since different targets have different reflectivities, the reception of the laser pulse from targets will vary from target to target. Therefore, the broadband biasing circuit is necessary to perform the detection in wide varieties of targets. The characteristics of designed and fabricated biasing network are reported in Section 4.4.1. The photodiodes (APD230 chip) are mounted and fabricated on 50Ω SMA female connectors. The reason of choosing the 50Ω SMA female connector to fabricate the APD chip is to reduce the parasitic effects, and it is also reported in Section 4.4.2. The characteristic signal responses of the developed broadband photodetectors are demonstrated in Section 4.4.3.

As shown in Figure 4.13, bypass capacitor C_b of 10 nF is used to bypass the AC oscillation from the power supply. It is also used to produce the spurious free DC supply voltage V_{aa} for the biasing network. The decoupling resistance R_d of 22 kΩ is used to control the current flow of the APD diode. The blocking capacitors C_{l1} and C_{l2} with a value of 330 pF and 330 pF, respectively, are used. Therefore, the effective blocking capacitive value is 165 pF. The blocking capacitors isolate the RF signal from high voltage DC supply voltage V_{aa}. The reason for using two blocking capacitors in series is to reduce the risk of capacitor failure and to avoid any damage

of the sampling scope. For example, it has secured measuring instruments and sampling devices from high voltage overloading.

4.4.1 Design and Fabrication of Bias Network

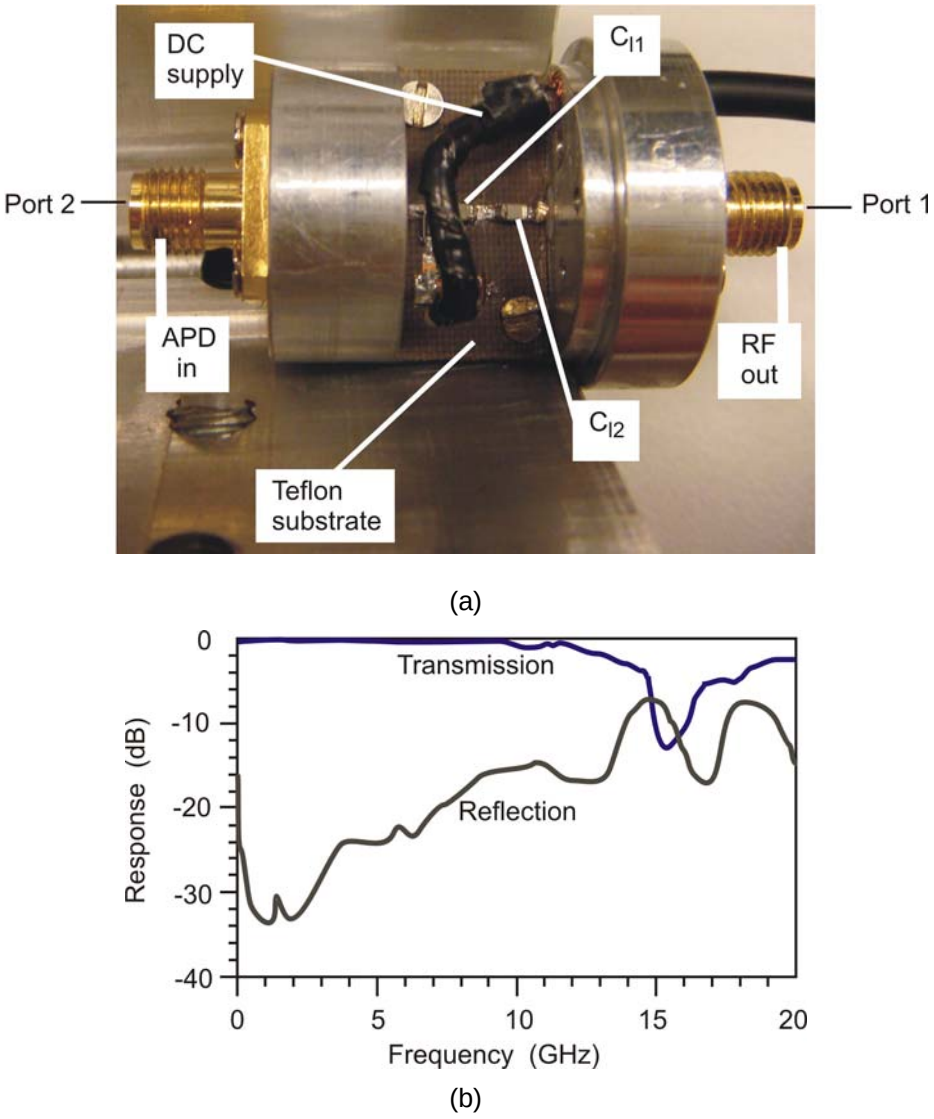

Figure 4.14 Broadband and high voltage bias network: (a) fabricated biasing circuit on Teflon substrate with area of 10.5 × 17 mm^2, and (b) measured transmission and reflection coefficients.

The high supply voltage is needed for the avalanche operation of bipolar transistors and diodes [76, 91]. To detect very short laser pulse [rise time 28 ps, pulse width (FWHM) 32 ps] the photodetector have to be also very fast system. Therefore, the lumped elements of the biasing network have to function also at high voltage and high frequency. But at high frequency, the parasitic effect is the main obstacle to design a broadband biasing circuit. Eventually, high frequency devices rated lumped elements are not designed for operating at high voltages. Therefore, intensive simulation and design are used to develop the biasing circuits. The biasing circuit is

designed and simulated by advanced design system (ADS) [97]. The SMD chip type lumped elements are used to minimize parasitic effects. Input and output matching networks with 50Ω microstrip lines are used to achieve the broadband properties of the biasing network, as shown in Figure 4.14.

The designed biasing circuit is fabricated on Teflon substrate with a relative permittivity of 2.51 [98] in hybrid technology [99-105] and circuit substrate size of 10.5×17 mm^2. The APD input impedance and the RF output impedance of the biasing circuit network is matched to 50Ω. The fabricated biasing circuit block is shown in Figure 4.14(a), and the measurement result of the S-parameter is presented in Figure 4.14(b). The anode terminal of the APD device is connected to a coaxial 50Ω SMA female connector. The RF output signal is taken from 50Ω load RF out terminal of the fabricated bias network as shown in Figures 4.13 and 4.14(a). From Figure 4.14(b), it is evident that the transmission loss is less than 0.8 dB up to 10 GHz, and from 10 GHz to 13.5 GHz it is less than 3.0 dB. The reflection loss from the APD terminal to the RF output terminal with 50Ω load is less than –15 dB up to 13 GHz. Therefore, it is evaluated that the operating frequency range of the bias network is from 0 to 13.5 GHz. Moreover, this broadband biasing network is operating and functioning up to 300V. Finally, two biasing circuits are developed with the same ratings.

4.4.2 Fabrication of APD Chip on SMA Connector

Direct bonding of APD230 chip (shown in Figure 4.15) on inner conductor of 50Ω SMA-connector is a fast choice to achieve photodetectors characteristics with less parasitic effects. The 50Ω connector is chosen because of the biasing network output which is equivalent to 50Ω. The SMA connector is taken to have the broadband frequency range, and it is functioning from DC to 18 GHz. The parasitic effects are a drawback factor to the fabrication of high sensitive (50A/W) devices like APD230 chip on the device housing. The bonding wire characteristics and used device mounting have to be designed and fabricated with special care. In micrometer (the diameter of active area is 230 μm and the chip diameter is 760 μm) chip devices (APD230), micrometer changes of bonding wire on mounting surface can be the cause for the failure of device functions. According to [91], the APD230 chip size is 760×760 μm^2, the chip raster size is 800×800 μm^2, the diameter of the active area is 230 μm, and the rise time is 180 ps. The cathode ring dimension is 75 μm. The separation

between the cathode ring and the anode surface is only 24 μm. The types of bonding and housing have to be analysed to improve the photodetector characteristic response. Therefore, the bonding is done to the cathode ring to the brass ring surface as shown in Figure 4.16 and Figure 4.17. The anode is connected to the inner conductor of the used SMA connector with the APD chip backside potential.

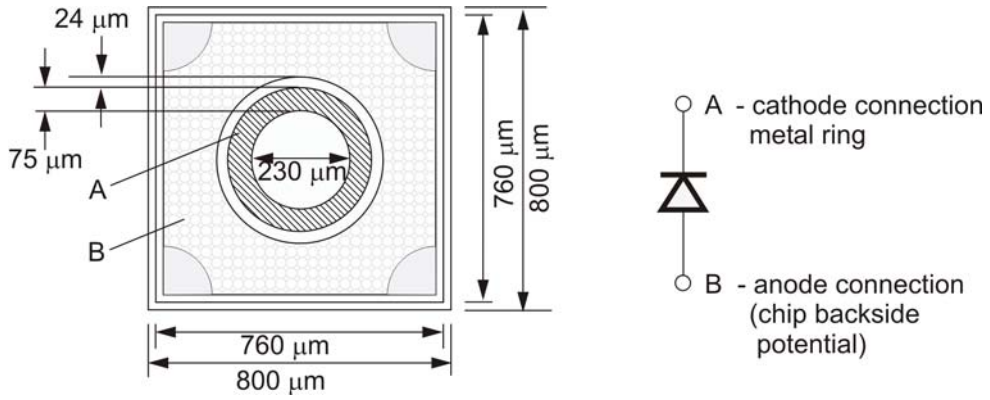

Figure 4.15 APD230 photodiode: (a) chip surface with active area with diameter of 230 μm, and (b) circuit symbol.

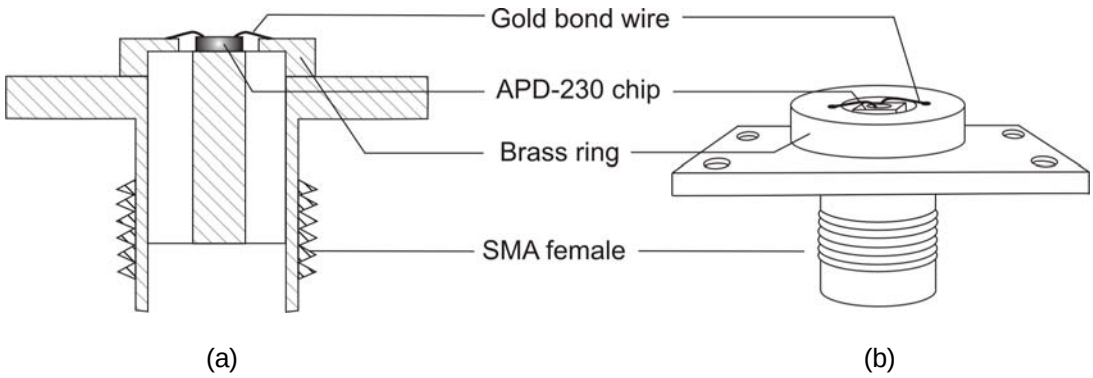

Figure 4.16 APD230 chip placed on SMA connector: (a) cross sectional view, and (b) 3D view.

A brass ring with 7 mm outer diameter and 1.8 mm inner diameter is fixed on the SMA connector to bond the APD230 cathode terminal, as shown in Figure 4.16. The inner surface diameter (1.8 mm) of the brass ring is evaluated to optimize the distance from the APD chip to the brass ring conduction. The reason is to reduce the inductive effect between APD230 to the brass ring. The 13.5 GHz bias network is terminated with a 50Ω SMA female connector. It is selected to connect with anode of APD-230 via SMA housing. Therefore, the 50Ω SMA male-male adapter is necessary to connect the biasing circuit with APD photodetector. Approximately 2 mm long gold wires with diameter of 25 μm are used to bond the APD chip to the brass ring, as shown in Figures 4.16 to 4.18. The characteristics of the bonding gold wires can be

equivalently described by inductive-capacitive (L-C) passive circuits. The bonding wires are tested for series and tangential connections to the APD with the brass ring in order to reduce the parasitic effect on the bonding. The series type bonding is considered as the bonding of gold wire on cathode ring with zero degree phase shift to the bonding point on brass ring (see, Figure 4.17). The tangential type bonding is considered as the bonding of gold wire on cathode ring within 90 degree phase shift to the bonding point on the brass ring (see, Figure 4.18). The conductivity of the gold wire bond is 4.55×10^{7} S/m. The cross-sectional view of the bonded APD230 chip on 50Ω SMA female-connectors is shown in Figure 4.16(a). The bonded APD chip on SMA housing is shown in Figure 4.16(b).

***Reduction of Parasitic Effects*:** The separation between the cathode ring and the anode surface is only 24 μm, as shown in Figure 4.15(a). The diameter of the used bonding wire is 25 μm. Therefore, a very important point of concern is to evaluate the bonding type on cathode ring, since its diameter is only 75 μm. The series bonding is presented in Figure 4.17.

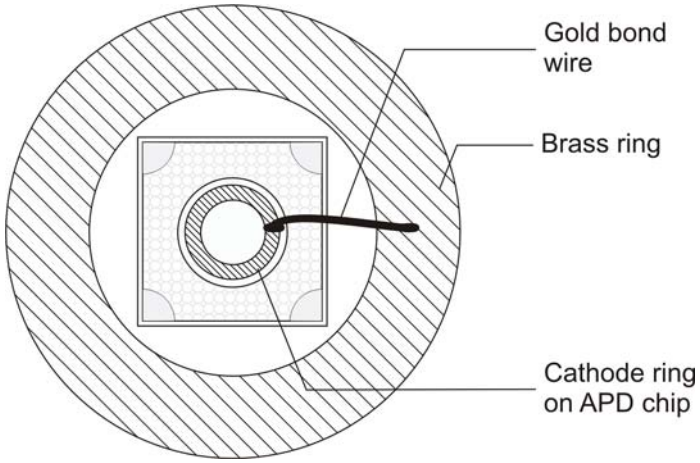

Figure 4.17 Series gold wire bonding of APD230 chips with brass ring. Bonding wire diameter is 25 μm.

It is given in Table 4.1 that the series bonding with one wire has 5.8V less peak response and rise time 50 ps higher than the one wire tangential bonding in Figure 4.18(a). Therefore, the tangential wire bonding is considered as the preferable bonding. But, the number of tangential wires directly influences the characteristics of the photodetector. Measurements have been performed to evaluate the effect of different combinations of wire bonding on the APD characteristics; it is reported in Section 4.4.3. It is also realized that the placement of the bonded wire on the cathode

ring is very important, it should not overlap on the APD surface (active area or in cathode ring to anode surface). The bonding wire overlapping on APD surface has reduced the efficiency of APD characteristics parameters.

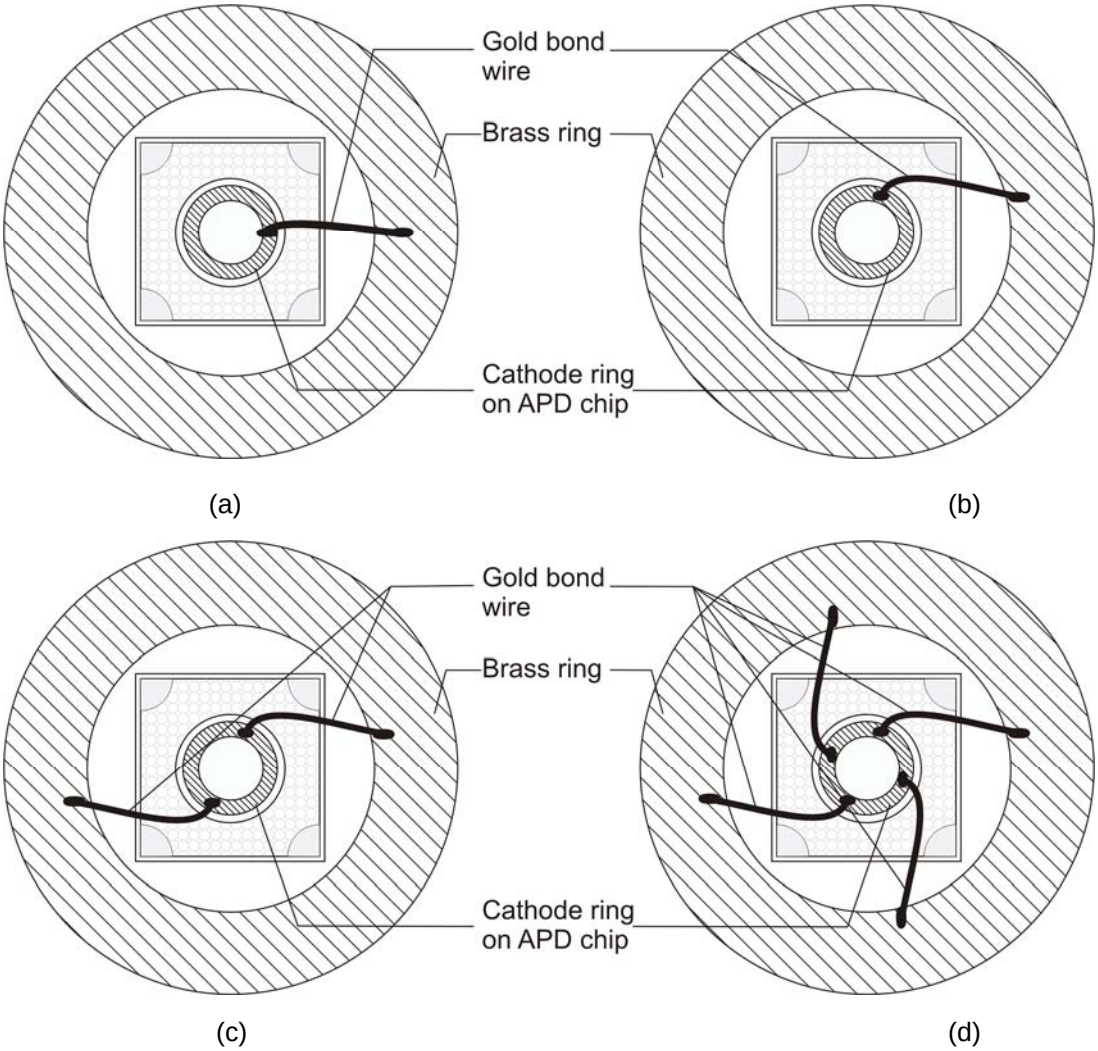

Figure 4.18 Tangential gold wires bonding of APD230 chips with brass ring: (a) one tangential wire bonding, (b) two tangential wire bonding, (c) three tangential wire bonding, and (d) four tangential wire bonding.

Different numbers of tangential bonding wires for APD contact is presented in Figure 4.18. Four types of bonding conditions have been analyzed: one wire, two wires, three wires, and four wires. The comparison of the bonding effects are given in Table 4.1. Every measurement is taken four times for ensuring the results given in Table 4.1. Furthermore, for each measurement four APD230 chips are taken into consideration. Since the optical excitation is measured, the optical excitation power should be precisely the same to perform such measurements. To have a unique input of optical excitation to APD all compared data are presented for laser signals with an optical power of 355W (peak). From the measurement, it is evaluated that the better

APD response is within 160V to 230V bias range. The best response is found for 160V bias supply. Therefore, the output characteristics of the photodetectors are presented for 160V bias supply in all following steps of representations.

From the measurement results, it has also been evaluated that two-wire bonding is better than one-wire bonding. The four-wire bonding is better than any other bonding (one-wire, two-wire and three-wire) and it has given a maximum efficient output of the APD photodetectors. Fundamentally, the number of increasing bonding wire should improve the device performances. In this case, the alignments of bonding wires are also having effect to the APD performance. For instance, in case of three-wire tangential bonding, the peak response is reduced by 5V and the rise time is increased by 5 ps compared to the two-wire tangential bonding, as shown in Table 4.1. The possible reason is due to the different angular separation of three bonding wires; they are 90, 90, and 180 degrees on the cathode ring, as shown in Figure 4.18(c).

Table 4.1 Comparisons of different bonding effect on APD responses.

Number of Bonding wire	Detected pulse peak (volts)	Rise time (ps)	Pulse width (FWHM) time (ps)	Fall time (ns)
Series one wire	18.2340	152.60	560.50	3.2650
Tangential one wire	24.0324	102.50	490.42	2.4820
Tangential Two wire	40.3725	95.45	425.65	2.4596
Tangential Three wire	35.5623	99.10	460.80	2.4650
Tangential Four wire	47.8858	84.20	410.10	2.4230

It has been shown that the type of bonding and the number of used bonding wires play an important rule on the characteristics of the photodetector. Principally, the series type of bonding should have better performances than the tangential bonding due to the shortest bonding wire. However, this could not be obtained. In this case, the tangential bonding has better responses than the series bonding. The reason is that the parasitic effects is higher at series bonding, since the distance between the cathode rings and the anode surface edge is only 24 μm. It has increased the parasitic effects during series bonding because the distance between the bonding wire and the anode surface is less than 24 μm, as shown in Figure 4.17. There are two reasons which were realized during the series wire bonding. First, it was not possible to bond the gold wire on the

cathode ring without overlapping on the APD active surface because of the very short diameter. Second, the distance between the bonding wire and the anode surface was very close compared with the tangential type wire bonding. As a result, tangential wire bonding has dominated the efficient operation of APD output.

4.4.3 Measured Results

The characteristics of the developed photodetecter are presented in this section. The reason for this measurement is to select the optimum bias dependant parameters for the evaluation of the photodetector characteristics.

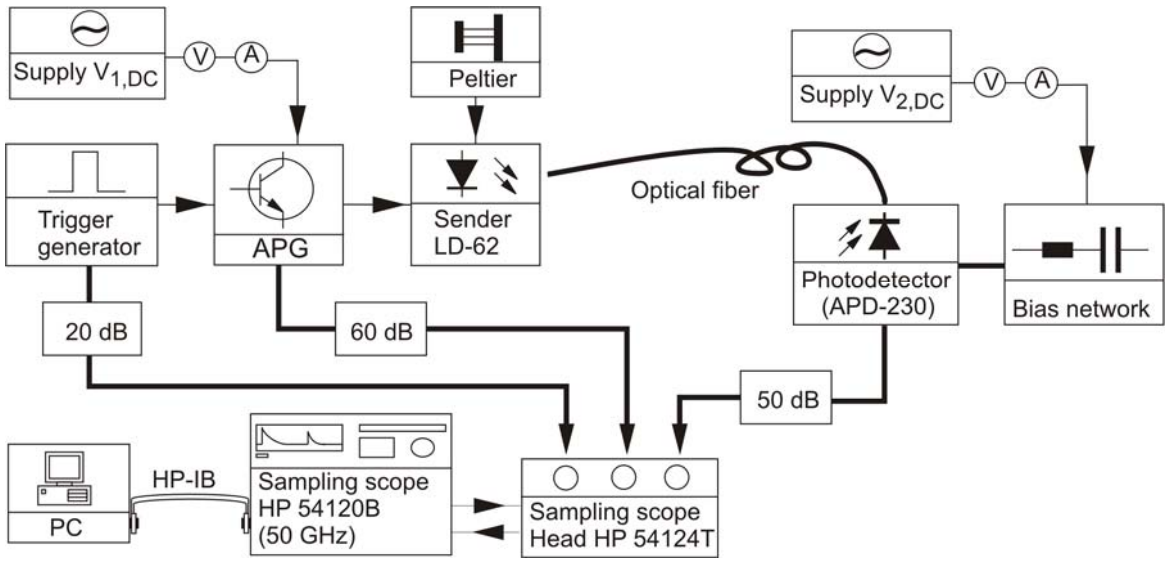

Figure 4.19 Block diagram of the measurement setup for the characterization of the APD device.

The measurement setup is shown in Figure 4.19. Different attenuators (20 db, 60 dB and 50 dB) are used at the outputs of the measuring devices to prevent the measurement instruments from any danger. The APD photodetector described in Section 4.4.2, is functioning with a broadband biasing network (reported in Section 4.4.1). Pulse repetition frequency of 37.5 kHz is used to trigger the avalanche pulse generator (APG) and the sampling scope. The avalanche pulse generator (APG) has a bias supply $V_{1,DC}$ of 310V, and it has produced optical peak power of laser pulse $P_{opt,i}$ of 355W using a LD-62 diode. The temperature of the LD-62 laser diode is controlled by a peltier. The optical excitation signal for the avalanche photodiode is taken via a multimode optical fiber (73 cm long, and core diameter of 125 μm) at a temperature of 22 °C. The APD is activated through the bias network supply of $V_{2,DC}$.

The measured avalanche breakdown of the APD230 (active area is 0.042 mm^2) photodetector has been found to be 148.2V at a temperature of 22 °C. It is illustrated in Figure 4.20(a). The specified breakdown voltage at the data sheet of the company (Silicon Sensor GmbH) is within 120V to 190V [91]. The measurement of breakdown voltage can be used to realize the impact ionization of electrons and holes, the avalanche multiplication length, the charge density on the active zone [106]. Here, it is used to measure the current and to protect the device from destruction due to high current [107]. Moreover, it is also practically used for selecting the operating range of APD.

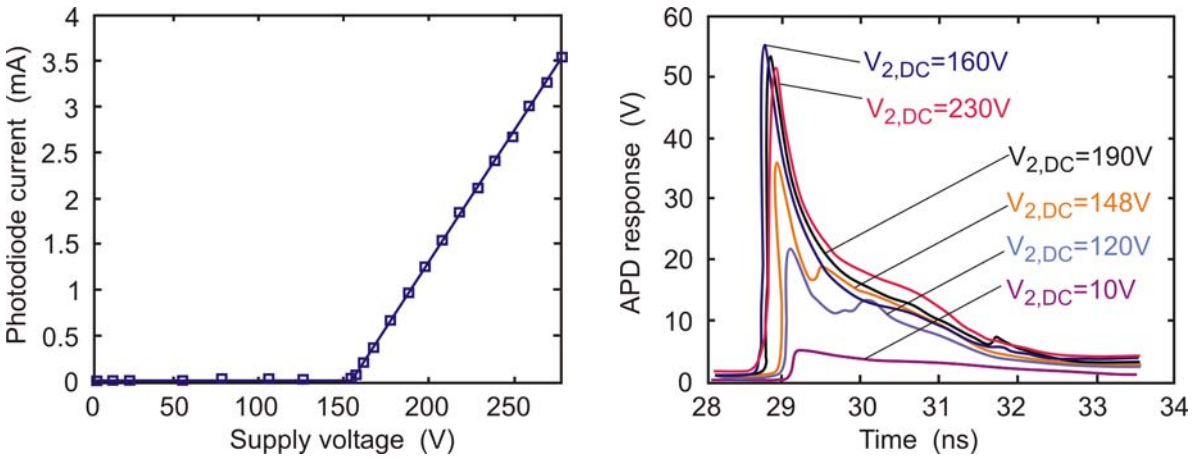

(a) (b)

Figure 4.20 Measured response of the APD-230 photodetector: (a) avalanche breakdown, and (b) pulse response for different supply voltage.

It is observed that the change of current versus supply voltage is stronger at higher bias voltage, especially after breakdown, as shown in Figure 4.20(b). The reason is due to the increase of electron velocity and electric field, and they have increased the avalanche multiplication. The increase of current is measured up to 225V, but after 230V it is again decreased. The decrease of APD characteristic response after 230V is illustrated in Figure 4.21. Therefore, for further increase of optical excitation power after complete avalanche breakdown, the probability of carrier recombination is not increased. In this case, the existence of free electron and hole pairs are almost approximately zero. Therefore, only the thermal effect is increased on APD. The increase of the thermal effect is the reason of the decreasing of the photodetector characteristic responses due to thermal loss. For instance, it is realized in rise time, pulse width (FWHM), fall time of response as shown in Figure 4.21.

It is also realized that at the beginning of the avalanche breakdown the characteristic parameters of the APD such as rise time, pulse width (FWHM) and fall time are strongly nonlinear. Above breakdown the characteristics parameters variations are insignificant. The theory of APD nonlinearity is reported in [108-110]. However, for a supply voltage ($V_{2,DC}$) from 120V to 155V, the APD peak pulse response increases approximately by 15V. For the supply voltage from 155V to 200V, the APD peak pulse varies only by 3V. Again from supply voltage of 200V to 250V the APD peak varies by 10V, as shown in Figure 4.21. Therefore, the stable operation of APD is realized at the supply voltage range of 160V to 190V. The better operation of APD is realized at 160V with respect to any other operating condition. The measured characteristics parameters for supply voltage ($V_{2,DC}$) of 160V are: Peak response voltage of 48V, rise time of 84 ps (including the rise time of 7 ps of the used sampling scope), pulse width (FWHM) of 410.10 ps, and fall time of 2.50 ns.

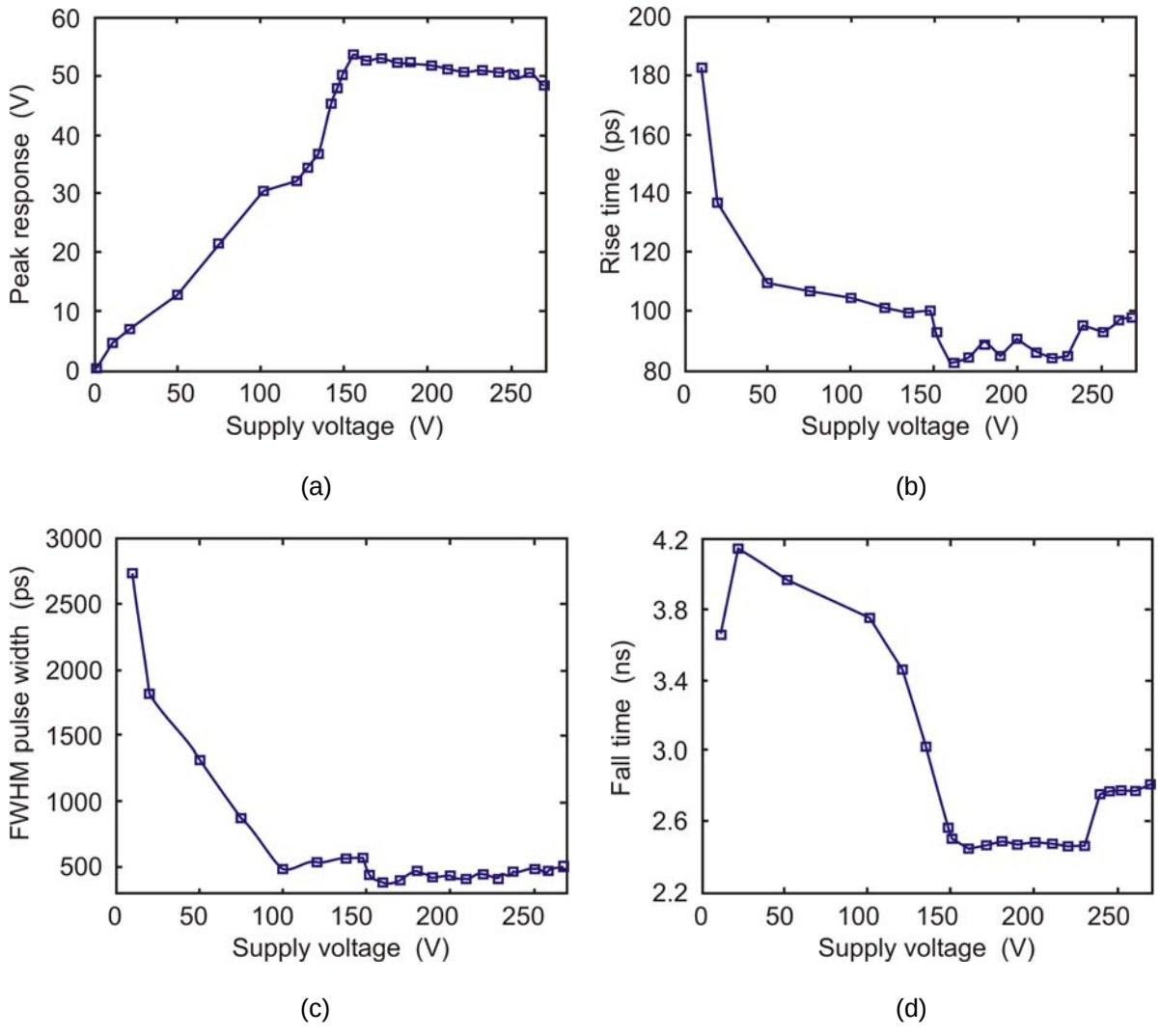

Figure 4.21 Characteristics of the photodetector response: (a) detected peak voltage, (b) rise time, (c) pulse width (FWHM) time, and (d) fall time.

4.5 Optical System

In laser radar the optical system is used for laser light transmission and reception. Therefore, the performance of the laser transmitter and the photodetectors are directly dependent on the property of the optical system. The optical system of laser radar has two parts: First, the optical transmission system for generating two parallel laser beams, and second, the optical reception system for focusing the received signals from targets. The block diagram of the optical system is shown in Figure 4.22.

In the laser transmitter, the laser pulse generator generates very short and high peak laser pulses. The transmission optics first produces a laser beam which is then splitted into two separate laser beams, as shown in Figure 4.22. The splitted two laser beams produce two parallel laser beams (laser beam 1 and 2) by using 90 degree beam deflectors (90° beam deflector 1 and 2). The reason of using one transmitter instead of two transmitters is to synchronize both laser beams. Moreover, two splitted laser beams from one laser generator can be easily synchronized. It has improved the system accuracy by extracting the time errors nonlinearity of both transmitted laser beams.

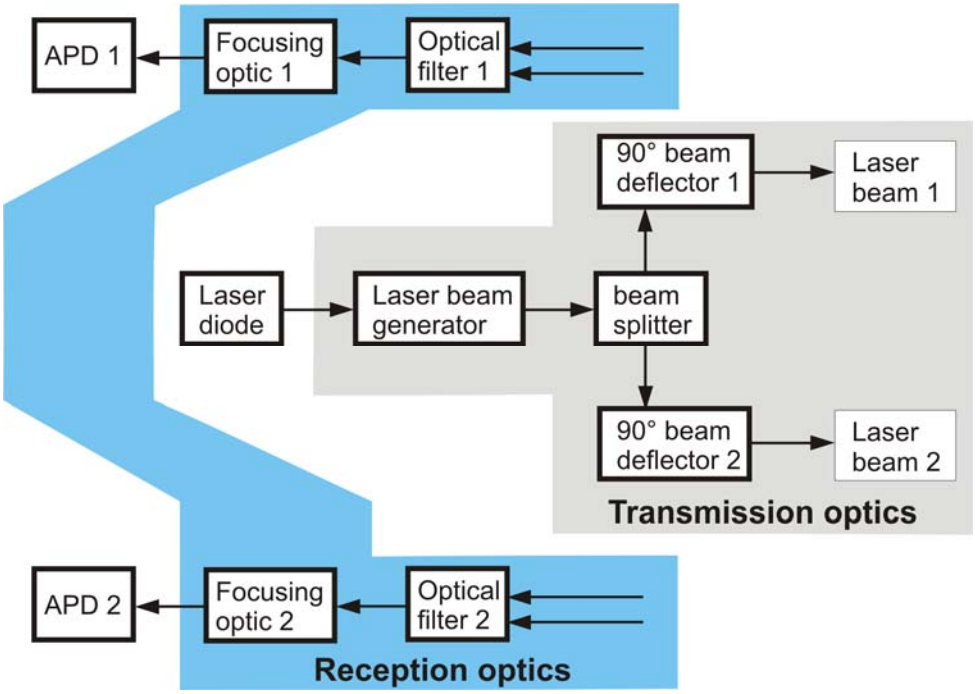

Figure 4.22 Block diagram of the optical system.

The reception optics can be compared to the telescopic part in a laser radar system [32, 55]. There are two optical reception systems as shown in Figure 4.22, and each for first and second photodetectors (APD 1 and 2). The reception optics (optical filter

1 and 2) filters the received laser signals and later on produces the micrometer focused point (by focussing optic 1 and 2) on the APDs, see Section 4.5.2.

4.5.1 Transmission Optics

The combinations of lenses, beam splitter and mirrors are used in the transmission optics to produce two parallel laser beams. The optical software SIGMA 2000 (from Kidger Optics Ass.) [111] is used to design and simulate the optical system. The main points of concern are the parallel laser beams adjustment, light intensity and spot size of the laser beams with respect to the variation of distance.

It is evaluated that the combination of two biconvex lenses produce approximately parallel laser beams up to several tenths of meters distance [57, 112]. It has produced the laser beam with the highest resolution and with minimum aberration [57]. The combination of planoconvex with planoconvex and planoconvex with biconvex lenses could be an alternative solution. But, due to the design simplicity, both lenses are taken as biconvex lenses. Broadband NIR antireflection-coated lenses (from Newport Ltd.) are used to increase the transmission refraction efficiency (reflection less than 0.5%) [113]. A schematic diagram of the laser beam generation is shown in Figure 4.23. The first lens L_1 with focus F_1 and the second lens L_2 with focus F_2 are used with the separation X_2. The distance between LD-62 to first lens L_1 is X_1. The distance between second lens L_2 to point of measurement B is X_d.

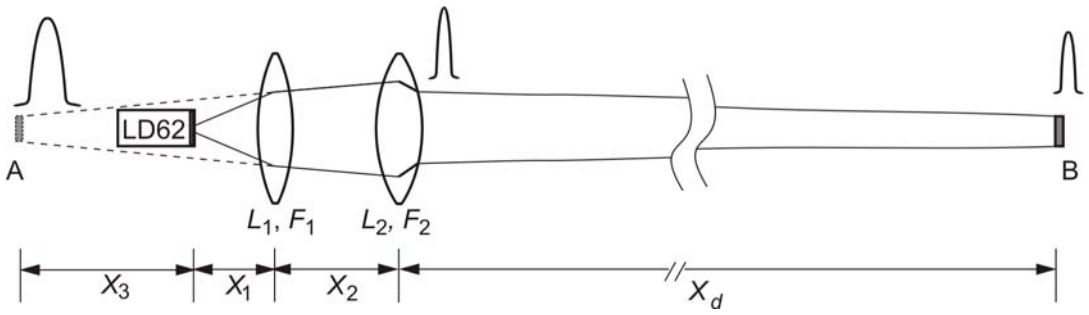

Figure 4.23 Schematic of the optical system for laser beam generation.

The beam divergence of the generated laser light is ±16 degrees from the LD-62 active area [77]. With a given diameter of lens L_1, the divergence has limited the distance between laser diode to the first lens L_1. So, it is a preliminary issue to place the first lens as near as possible to have low loss laser output. The first imaginary focused point is A because F_1 is greater than X_1, and it can be demonstrated as $F_1 \approx X_1 + X_3$.

According to the characteristics of biconvex lenses, if any light source is placed in the focus point of a biconvex lens then it will produce approximately parallel light rays. Therefore, the approximation of the placement of second lens is considered approximately as $F_2 \approx X_1 + X_2 + X_3$. It is evaluated that if the sum of X_1, X_2, and X_3 is greater than F_2 then the laser beam has produced another real focused image at the point B. Now, if the sum of X_1, X_2, and X_3 is smaller than F_2 then the laser beam has expanded according to the distance of the point of B. Therefore, the sum of X_1, X_2, and X_3 is taken as just greater or equal to F_2 in order to avoid the beam expansion. To avoid the loss of the laser beam, it is the best choice to place both lenses as closely as possible. From the optical system simulation and analysis, it is evaluated that the selection of lenses with $F_1 > F_2$ and with smaller X_2 has produced the Gaussian beam. Transverse electromagnetic (TEM) wave is produced [55] by the placement of the active area of the laser diode and both lenses L_1, L_2 are in an axis at zero angular positioning. The generated spot size is not the same along with the distance variation of X_d, but the variation is very low. For instance, the spot size is 6.6 mm at a distance of 1m. At a distance of 3m the spot size is measured as 6.54 mm. The spot size is 6.56 mm at the distance of 10m. The simulated beam spot by using SIGMA 2000 and the generated beam spot taken by CCD camera are shown in Figure 4.24. The laser beam intensity is realized as Gaussian beam and the highest light intensity is in the centre of the laser beam.

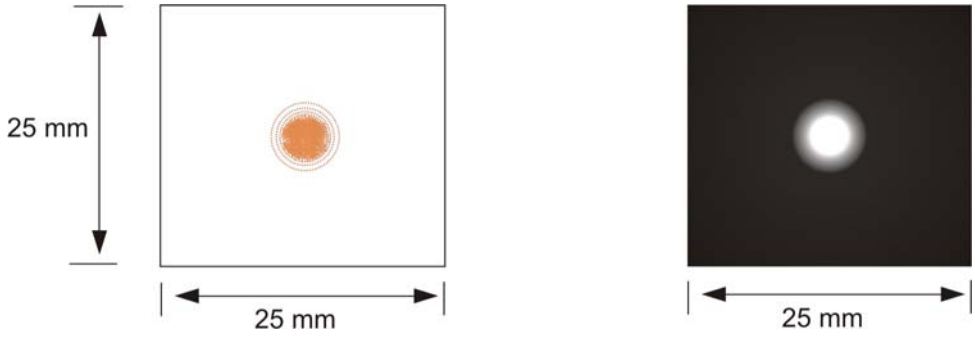

Figure 4.24 Transmitted laser beam spot: (a) simulated beam spot, and (b) generated beam spot at the distance of 1m.

The optical transmission system is shown in Figure 4.25. The laser beam produced by both biconvex lenses is splitted into two laser beams with a phase difference of 90 degrees. After splitting the beam from one laser transmitter LD-62, both laser beams are redirected by using mirrors (mirror 1 and 2). Silver coated antireflection dielectric

mirrors from Linos photonics Int. [114] are used to achieve a high reflectivity greater than 99%. Finally both laser beams appear as parallel laser beams with a separation distance of D_r , as shown in Figure 4.25.

To divide the laser beam a circular variable beam splitter [115] has been used. The function of the beam splitter is like that of a mirror, and it reflects a portion of the beam and lets the other portion propagate through it. The beam propagated through the beam splitter is again redirected by 90 degrees by using a UV fused silica prism [116] (from Linos Photonics Ltd.). By using UV silica mirrors 1 and 2 with silver coating, two parallel laser beams are produced with the separation of D_r . The reason for further redirecting the second laser beam by prism is to have the axial parallel position of both photodetectors. It is done to cover a wide range of target detection and to avoid the signal detection interferences.

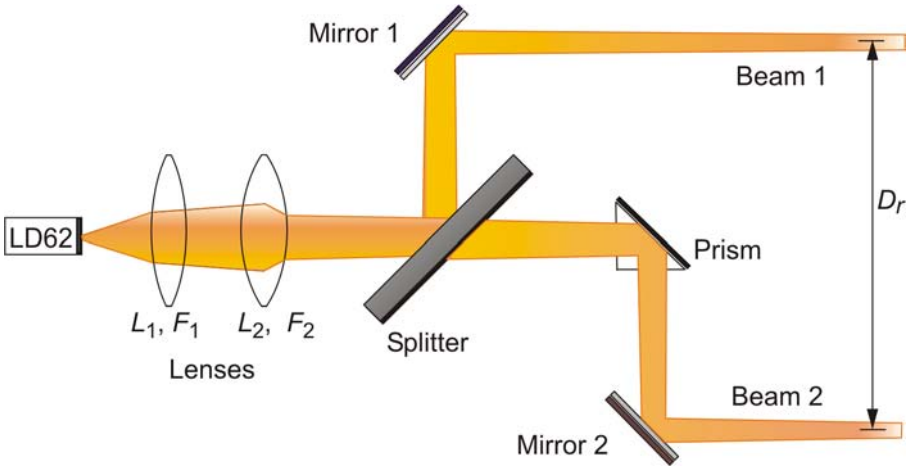

Figure 4.25 Schematic of the optical transmission system.

The measured average optical radiated power emitted by the LD-62 laser diode is 510 μW, and it is measured by an optical power meter (Model 66 LXA from Photodyne Inc.). This laser power is obtained for the avalanche pulse generator bias current of 7 mA with the pulse repetition frequency of 37.5 kHz. It has also been evaluated that the average optical power of laser beams 1 and 2 are equal (140 μW). Therefore, the sum of both laser beams average optical power is 280 μW from 510 μW total emitted average power. It is 230 μW less than the generated average power. So, the transmitting optical system has a power loss of 2.6 dB. The loss is occurred for the used transmitting optics, because of their refractive indexes and material properties.

4.5.2 Receiving Optics

The optical reception systems are the telescopic part of each IR photodetector, as it is reported in Section 4.4. The BK-7 optical lenses (From Newport Ltd.) are used within the wavelength range of 380 nm to 2100 nm. Since the reflectivity varies from target to target, the received laser signals will also vary. Moreover, the emitted laser signal has a wavelength of 904 nm. However, the received signal (focused laser light) should be highly inserted on the IR photodetectors active area to achieve the highest response by the photodetection system.

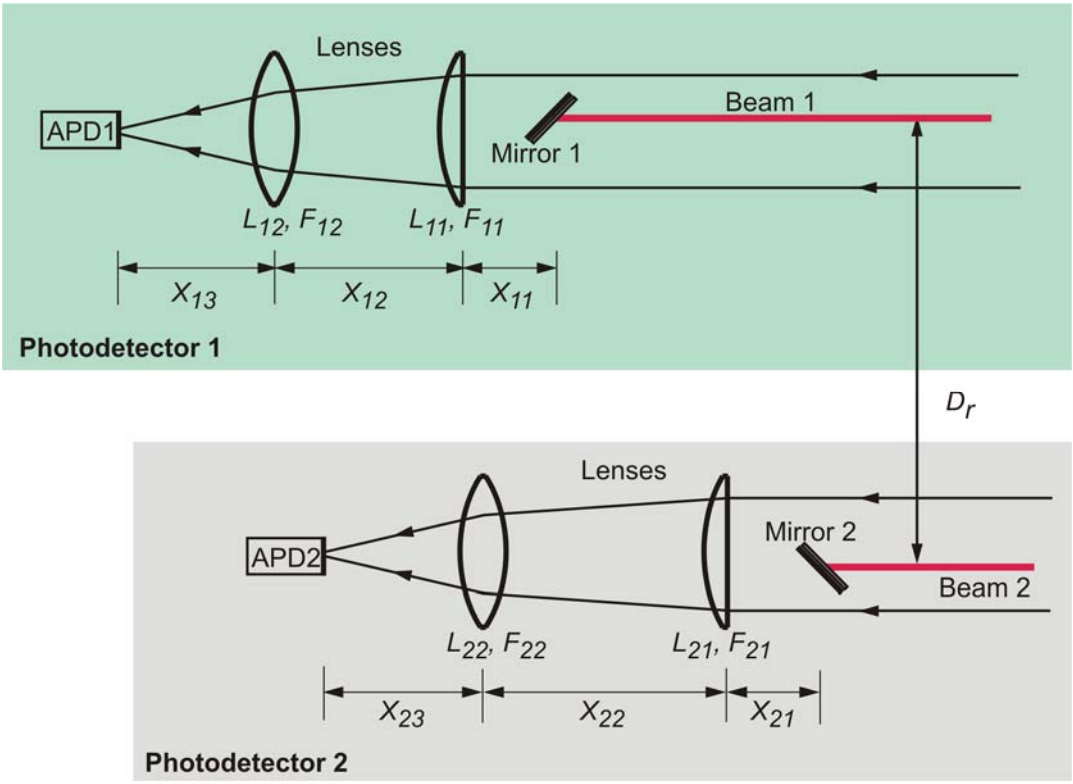

Figure 4.26 Optical reception system: The reception optics for photodetector 1, and the reception optics for photodetector 2.

The reverse principle of laser beam generation is used for the optical reception system to focus the reflected signal from targets. The combinations of two biconvex and planoconvex BK-7 series lenses are used for each optical detection system, as shown in Figure 4.26. The optical axis of each optical system has to be coincided with the emitted laser beam from both mirrors. The reason is to receive the laser beam only from corresponding transmitted laser beam. It has also been achieved the maximum detection range of photodetectors and omitted the cross interferences. Therefore, the receiving optical lenses have to be placed on an axis for each photodetector. The first lens of each optical reception system is placed just behind the transmitted mirrors to

avoid the shadow from the transmitted mirrors on the receptor. To increase the reception light power efficiency, a diameter of 50.8 cm is used for the first reception lenses.

The optical reception system for photodetector 1 is shown in Figure 4.26. The first lens L_{11} with a focus of F_{11} and the second lens L_{12} with a focus of F_{12} are used in this system. The distance between the mirror and the first lens is X_{11}, the separation between both lenses is X_{12} and the distance between lens L_{12} and photodetector 1 (APD1) is X_{13}. The optical reception system for photodetector 2 is also shown in Figure 4.26. The first lens L_{21} with a focus of F_{21}, the second lens L_{22} with a focus of F_{22} are used in this system. The distance between the mirror and the first lens is X_{21}. The separation between both lenses is X_{22}. The distance from the lens L_{22} and photodetector 2 (APD2) is X_{23}. According to the paraxial formula the focus point of both photoreception systems can be evaluated [117]. The focus point of first optical reception system F_{d1} is presented [118, 119] as

$$F_{d1} = \frac{1}{F_{11}} + \frac{1}{F_{12}} - \frac{X_{12}}{F_{11}F_{12}} \tag{4.3}$$

The distance of X_{13} from lens L_{12} to APD1 is presented by the back focal length (BFL) of the first photoreceptor, and it can be rewritten [118, 119] as

$$X_{13} = \frac{F_{12}\left(X_{12} - F_{11}\right)}{X_{12} - \left(F_{11} + F_{12}\right)} \tag{4.4}$$

Similarly, the focus point of second optical reception system F_{d2} is presented as

$$F_{d2} = \frac{1}{F_{21}} + \frac{1}{F_{22}} - \frac{X_{22}}{F_{21}F_{22}} \tag{4.5}$$

The distance of X_{23} from lens L_{22} to APD1 is presented as BFL of the second photoreceptor, and it can be rewritten as

$$X_{23} = \frac{F_{22}\left(X_{22} - F_{21}\right)}{X_{22} - \left(F_{21} + F_{22}\right)} \tag{4.6}$$

From (3.4) and (3.6), it is presented that the sum of both lenses focus should be higher than the separation between them. Therefore, the first lens is used as a planoconvex lens with $F_{11} > F_{12}$ and similarly $F_{21} > F_{22}$ to achieve the smallest separation between both lenses and optimum BFL to the photodetectors.

4.6 Signal and Data Processing

In this section the radar signal processing unit is described. A 4 channel 40 Gsa/sec real-time oscilloscope (DSO81204B, from Agilent Tech. Int.) is used to measure and process the output signals from both APD outputs. It is presented in Figure 4.27.

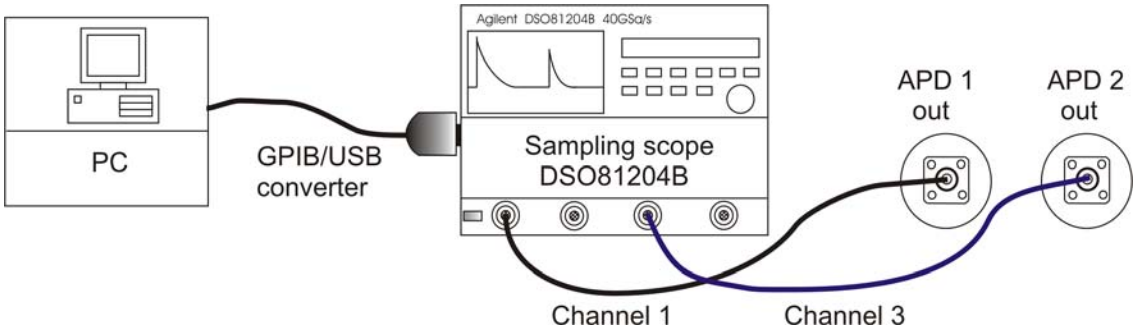

Figure 4.27 Schematic of the sampling and data processing units.

In Figure 4.27, it is shown that Channels 1 and 3 of oscilloscope DSO81204B are connected with the photodetectors. It is due to the internal coupling of the sampling oscilloscope, Channel 1 and Channel 3 are used to perform the measurement. Channel 1 is connected to the output signal of the APD 1. Channel 3 is connected to the output signal of the APD 2. Two 50Ω semi-rigid coaxial cables with the same length are used to connect the APDs to the sampling scope. The reason for using the same length of 105 cm long coaxial cables is to calibrate the time delays of both receiver signals. It has synchronized the reference signals from both detectors. As a result, it reduces the measurement error due to time-distance shifting. The sampled and digital data from the scope are transferred to the PC via a GPIB to a USB port converter (from Agilent tech.).

The functioning of the sampling scope is controlled with a PC by self-developed Matlab programming software. Finally, in the PC, the received sampled data are analyzed by using further developed software to evaluate the precision contour and velocity of targets.

It has been idealized that the target detection time depends on the rate of scanning. The number of average samples per measurement is directly related to the distance measurement accuracy. If the number of measurement is increased then the scanning speed is decreased. As a result, the accuracy of the measurement speed is also decreased. Therefore, a compromise has been made to reduce the number of measurement averages to increase the number of sampling point of scanning rate in the data processor. Several attempts are made during the measurement of target

tracking system. It is found that the substantial improvement is achieved by increasing the memory depths of the data processor.

After evaluating the measurement performances by the real-time oscilloscope (DSO81204B), the down-conversion process [2] with extended time sampling techniques can be used. The data processing can be done using a 8-bit A/D converter. However, the precise velocity of the target is evaluated from the received laser signals from each scanning. The topology of the developed software for precise vehicle velocity measurement is reported in Chapter 5, and the measurement of real time vehicle velocity is reported in Chapter 6.

4.7 Characteristic Data of the Realized Radar System

At the beginning, the performance of the developed laser radar is analyzed by carrying out the distance measurement for a diffuse target with ranging distances from 50 cm to 20m. The reason of choosing the largest ranging distance of 20m is that this laser radar is developed to track the vehicle velocity up to four lanes range. Generally, the maximum width of a street with four lanes is not more than 20m, according to German norm [50]. Moreover, if the laser radar is installed under a bridge then the distance of 10m is sufficient ranging to cover the tracking range. Therefore, 10m range is selected both for horizontal and vertical velocity measurement of moving targets (vehicles). Finally, the optical system for laser beam development is improved to cover the distance ranging up to 20m.

The typical optical signal detection by both photodetectors is presented in Figure 4.28 for a plane wooden block. The reflector is placed at 3.2 m in front of the laser radar. The detected response of APD 1 is shown in Figure 4.28(a) and the response of APD 2 is shown in Figure 3.28(b). It has also been measured for the detection range of up to 20m for the wooden block as reflector, and the detected responses are shown in Figure 4.28. The detected response of APD 1 is shown in Figure 4.29(a) and the response of APD 2 is shown in Figure 4.29(b). The reference signals are carried out from the LD-62 laser diode to the APD230 photodiodes via 55 cm long (125 μm diameter) multimode optical fibers. This measurement is performed for the laser diode bias of 310V at 20 °C, and the APD bias of 160V for each photodetector. The measured reference pulse of APD 1 has a peak value of 0.126V and a rise time of 110 ps. Moreover, the measured reference pulse of APD 2 has also a peak value of 0.126V, rise time of 110 ps. The detected peak response for the target (wood) distance at 3.2m is 0.125V, as shown in

Figure 4.28. But, for the ranging distance of 20m the measured peak response is 30 mV, as shown in Figure 4.29. The reception signal for 20m is approximately 4 times less than that for 3.2m. It is clear that the optical power receptions by the photodetectors are decreased with the increase of target distance due to the scattering effects. For longer distance the interference on the signal-to-noise ratio are much higher than for shorter target distance, as a result, the signal detection is lower.

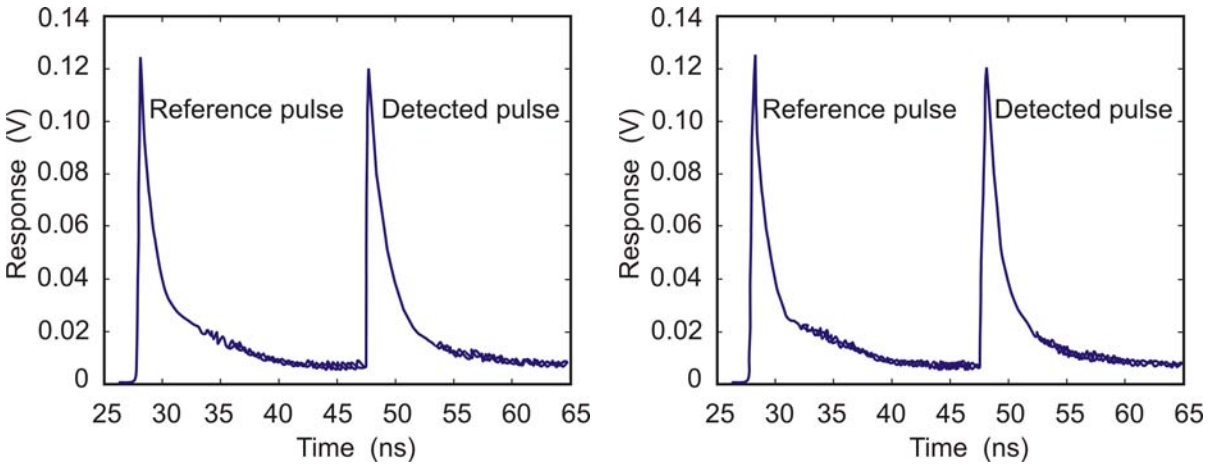

(a) (b)

Figure 4.28 Photodetector responses for a wooden block as reflector at 3.2 m ahead of the laser radar: (a) the APD 1 response, and (b) the APD 2 response.

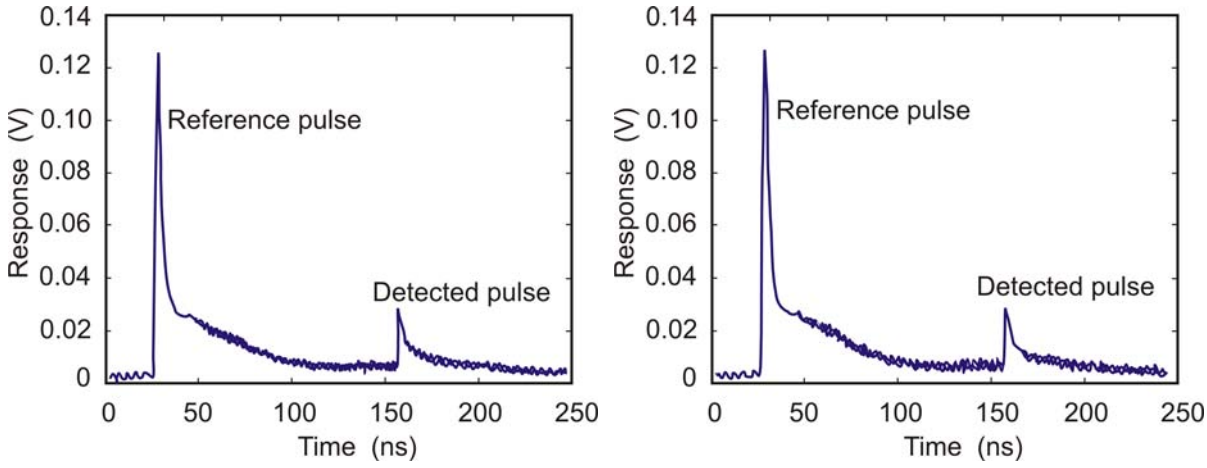

(a) (b)

Figure 4.29 Photodetector responses for a wooden block as reflector at 20 m ahead of the laser radar: (a) the response of APD 1, and (b) the response of APD 2.

The normalized received signal responses of both detectors are presented in Figure 4.30. In Figure 4.30, it can also be recognized the shadow effect by mirrors on the photodetectors for close target distance. It is realized for the target distances of 0 to 20 cm, the attenuation of detected responses are decreased. The reason is that the reflected signals from target are mostly redirected by mirrors at near distance. This

range can be considered as near field. After 20 cm distance, the received signal is decreased with the increase of target distance. For the target distance of 20 cm to 150 cm the decreases of the detected signal is most significant. Again, from target distance of 150 cm to 350 cm and for further distance the detectors responses are decreased but not significant compared to the distance of up to 150 cm. After 20 cm, the ranging can be considered as far field. At far field, the radiation term only exists due to the classical photons [120]. In the far field, the normalized response relatively decreases with the increase of target distance at the rate of $1/r^2$, see Figure 4.30. Therefore, at the far field the normalized response can be presented as proportional to $1/r^2$ of the target distance.

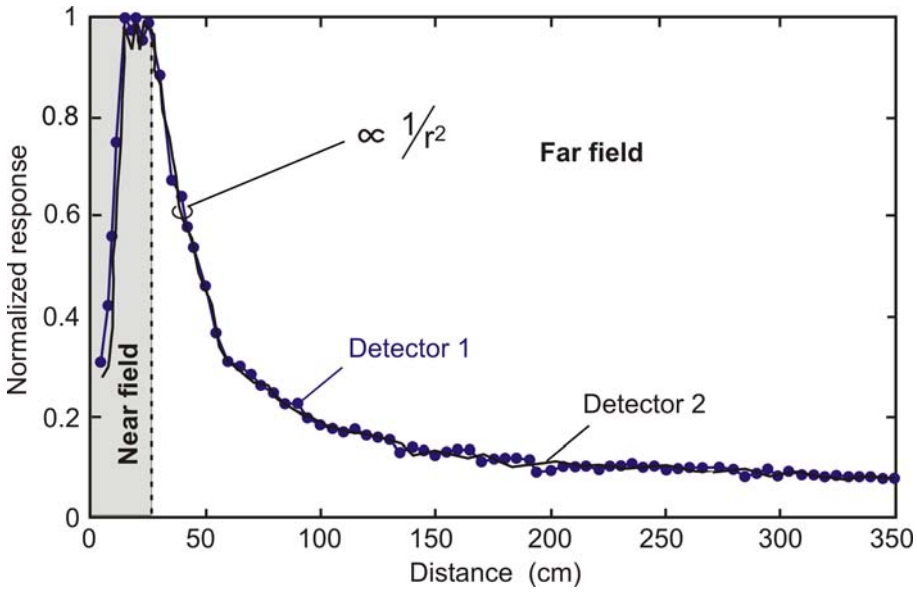

Figure 4.30 Normalized received responses of both photodetectors.

4.7.1 Optimisation of Signal Detection System

The laser radar is calibrated first to achieve the highest performance out of the developed systems. At velocity measurement, several error sources interfere with the measured signals. Errors on measured data are reported already in Chapter 2. Moreover, it is very important to optimize, calibrate, and evaluate the laser radar system before applying it in the measurement system. In this laser radar, the elimination of laser beam interference and reference pulse synchronization are considered as major factors influencing the accuracy of velocity measurement.

***Elimination of Laser Beam Interference*:** The optical reception system of the laser radar is designed to receive only the reflected signal by target from its

corresponding laser beam, see Section 4.5. If in any case, the APD 1 detects the target signal from laser beam 2 or APD 2 from laser beam 1 then it will produce the detection interruption. The interrupted received signal from the targets is the cause of the laser beam interference. Therefore, if there is any interfered signal from the other laser beam, the measurement result will introduce an error to the system. It will be the reason for the failure of velocity measurement. To make clear the effects of signal interference, the measurement has been performed for up to the target distance of 25m. The 25m is the distance from where there are no signals received by the photodetectors. The wood, plastic (brown), and aluminum blocks are used as reflectors and targets. The different reflectors are used also to examine the variation of reflectivity. The measurement has been performed for every 50 cm step distances. The signal interferences for the target angular rotation of 0 to 80 degree of vertical plane with respect to the radar system has also been analyzed. From all planes of the measurement, no interference signal has been observed. The reason is that the signal reflections from all the targets are only detectable when they are on the same axis with the given photodetector. During the photodetection system development, the focus plane of each optical reception system and the active area of corresponding APD are intensively calibrated to achieve the same axis between them. The calibration of the laser system (transmitter and receiver) is performed by using lab instruments (from Photon Control Inc., Cambridge, UK).

***Synchronization of Reference Pulse*:** The laser reference pulses to each photodetector are taken via optical fibers from the transmitter. In the velocity measurement system, the distance of the target is measured, and the processor unit stores the corresponding time of scanning. For a homogenous medium, the distance of the point target is a function of the characteristics of reference pulses. Now, if the characteristic parameters of both reference pulses are different then the measurement of scanning time per point target will also be different. As a result, it will introduce error to the target (vehicle) contour measurement system. It will also introduce the nonlinear error to the velocity measurement system. Moreover, if both reference pulses are synchronized in order to achieve the same characteristics, then such error will be discarded from the contour and velocity measurement system. Therefore, the development of the optical fiber connection from the LD-62 laser diode to APDs has introduced another major point of concern for pulse synchronization.

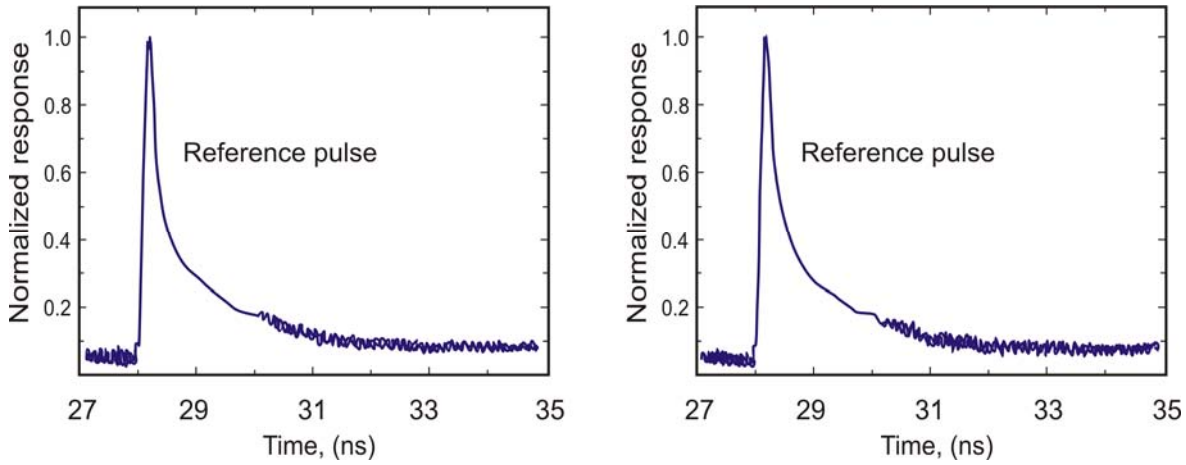

Figure 4.31 Synchronized reference pulses: (a) first photodetector, and (b) second photodetector.

The SIGMA-2000 optical software is used for the design of the optical system. The calibration is performed by the lab instruments (from Photon Control Inc., Cambridge, UK) to produce the synchronized reference pulses. The measurement results of synchronized reference pulses are represented in Figure 4.31. Both reference pulses are measured at a time delay of 28.2 ns (10% pulse) with the rise time of 110.2 ps. Normalized peak responses of both reference pulses have realized the same characteristics. The 50 GHz sampling scope HP5214 is used to measure the synchronized reference pulses. From the measurement, it is observed that the noise level of photodetector 2 is 0.5% more than of photodetector 1 as shown in Figure 4.31. This is because of the differences in the photodetectors circuit system. It is found that 20 mV is the noise level of photodetector 1.

The detection of moving targets by laser radar (with TOF principle) has a great issue on the measurement time of detected pulses. The error may be raised because of ambiguity on the expected measurement time. For example, changes of the time significant points due to the amplitude variation of detected pulses. The preliminary ranging errors of the laser radar are reported in [106, 109, 121]. The errors due to photodetector response delay are reported on [77, 122]. Fundamentally, it depends on the properties of the target surface. For instance, the detected signal pulse amplitude is very much uncertain for a mirror-like surface as it has specular reflection. But in the case of strongly defused type surfaces, the detected signal has lower amplitude because of the scattered reflection.

Therefore, to evaluate higher measurement accuracy, it is indeed necessary to correct the shifting of time significant points. Since, the time significant points from detected pulses are used to detect the target such as velocity.

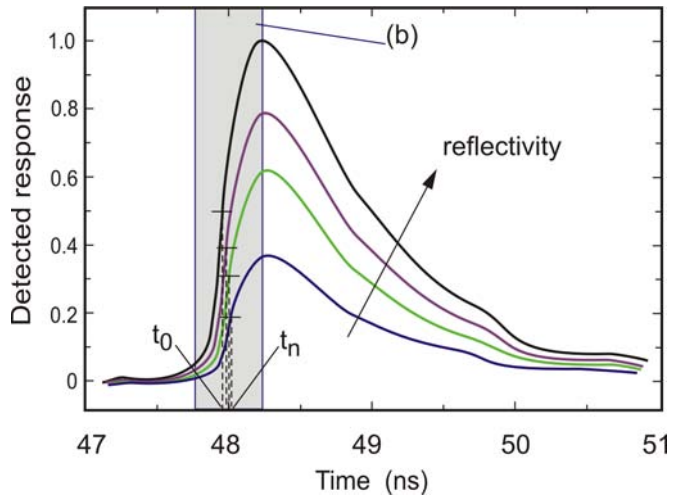

(a)

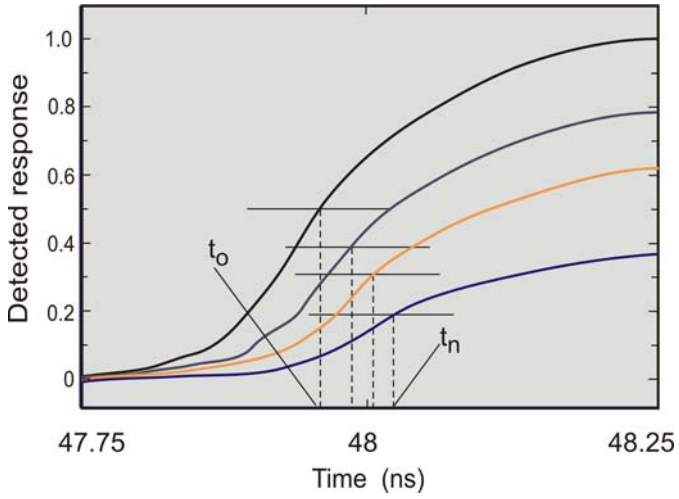

(b)

Figure 4.32 Variation of detected photodetector pulse responses: (a) variation of detected with target reflectivity, and (b) expanded area.

***Variation of Detected Pulse Amplitude*:** The detected signal amplitude variations for the variation of target surface properties and geometries are presented in Figure 4.32. The average of 64 samples is used to measure the received signals. The targets are placed 3m ahead from the laser radar. The targets are aluminium, wood, and plastic (brown) blocks. The highest peak pulse is obtained from the aluminium block. The variation of the photodetector responses due to the variation of the target reflectivity is shown in Figure 4.32(a). The expanded area of the detected responses is shown in Figure 4.32(b). The detected pulse responses can be normalized, and they

can be extended to have the same pulse amplitudes as shown in Figure 4.32(a). Therefore, the time significant point of t_0 for the pulse response with highest peak, and the time significant point of t_n for the pulse response with lowest peak are becoming very closer; see Figure 4.32(b). The measurement time error can be presented as $\Delta t_{err} = (t_0 - t_n)$. From the measurement result, it is evaluated that the maximum velocity error can be $D_r / \Delta t_{err}$ on start-stop system due to the shifting of time significant point, see Section 3.2. For example, if the first detected signal time by APD 1 is t_0 and the first detected signal time of APD 2 is t_n then the detected error velocity will be $D_r / \Delta t_{err}$.

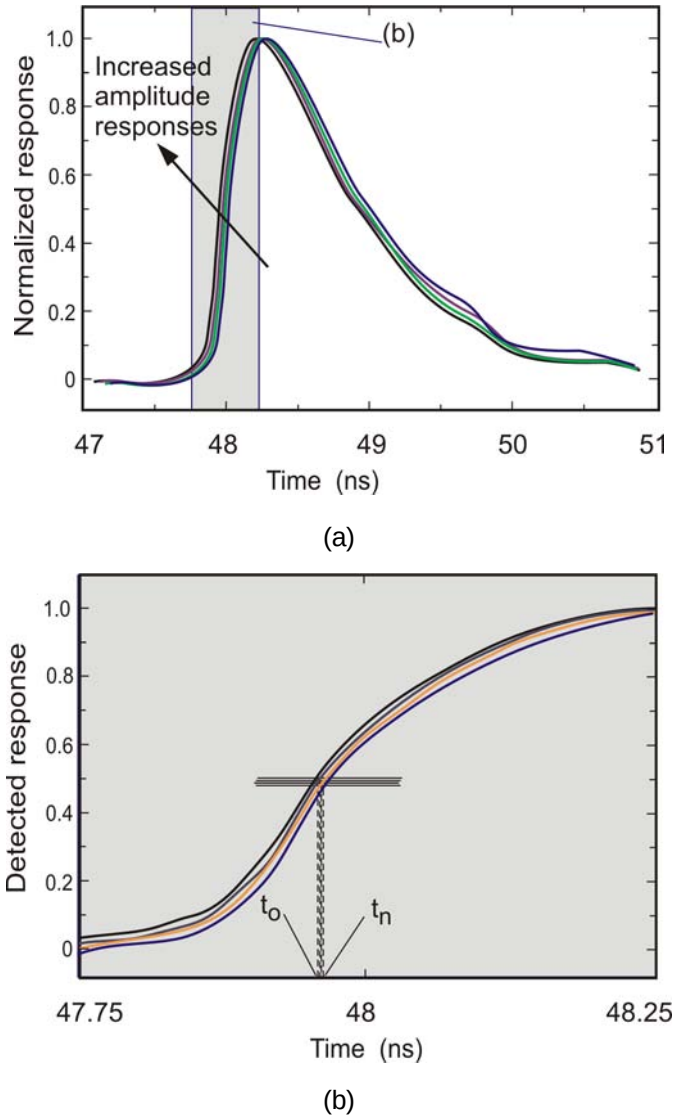

Figure 4.33 (a) Normalization of the amplitude of detected pulse responses, and (b) expanded area.

***Normalization of the Pulse Amplitude Response*:** The errors due to the time shifting of significant point detection can be reduced by increasing the number of

measurement points of each measurement data. But, it will decrease the scanning speed. As a result, it will also limit the velocity measurement range. Therefore, for higher velocity detection it is not applicable. The normalization of the detected target pulses is evaluated to reduce the measurement error. In this case, the amplitudes of the detected responses from targets are equalized, as shown in Figure 4.33. The normalized photodetector responses are shown in Figure 4.33(a). The expanded area of the normalized detected responses is shown in Figure 4.33(b). Therefore, the rise time of all normalized pulses has not changed more than 5% since the detected time difference $\Delta t_{err} = (t_0 - t_n)$ is negligible compared to Figure 4.32. Finally, the slope of the detected pulses are approximated as equal. As the slope of detected pulse responses becomes unchanged, the time differences of the points of measurement are drastically reduced.

4.7.2 System Analysis and Distance Measurement

The accuracy of the modified laser radar system is analysed in this section. First, it is carried out by performing the measurement of distance for a single target. Second, it is carried out by measuring the differences of ranging-distance. The diffused target (wood block) is placed at a distance range between 50 cm and 10m. Moreover, for the velocity measurement of the vehicle, the preliminary distance is considered up to 10m. This range is selected to avoid most of all other peripheral signal interferences on the precise distance detection. At the single target measurement, the target is placed 100% perpendicular to the laser beams. The target is also placed at the same distance but with different angular directions to evaluate the distance differences (ranging-distance) measurement. The angular variation is considered from 0 degree to 80 degrees. The reason for single target distance measurement is to execute the accuracy level of distance measurement and to evaluate the roughness of the target surface profile. The reason for ranging-distance difference measurement is to evaluate the accuracy level of vehicle velocity at the curve of a street.

***Measurement of Distance Uncertainty*:** The distance measurement uncertainty is presented in Figure 4.34 for the target ranging distance of 3.5 m. Each point of distance is measured by using the measurement of 2 sample averages. Two samples per measurement are taken to increase measurement speed. The distance measurement uncertainty is obtained as 0.35 cm for both photodetectors. It is much less than the requirement of the intended application of vehicle velocity measurement

from vehicle (moving target) contours. From the measurement of the distance uncertainty for different distances between 50 cm and 10m, it has been evaluated that the measurement uncertainty has not varied within the selected range.

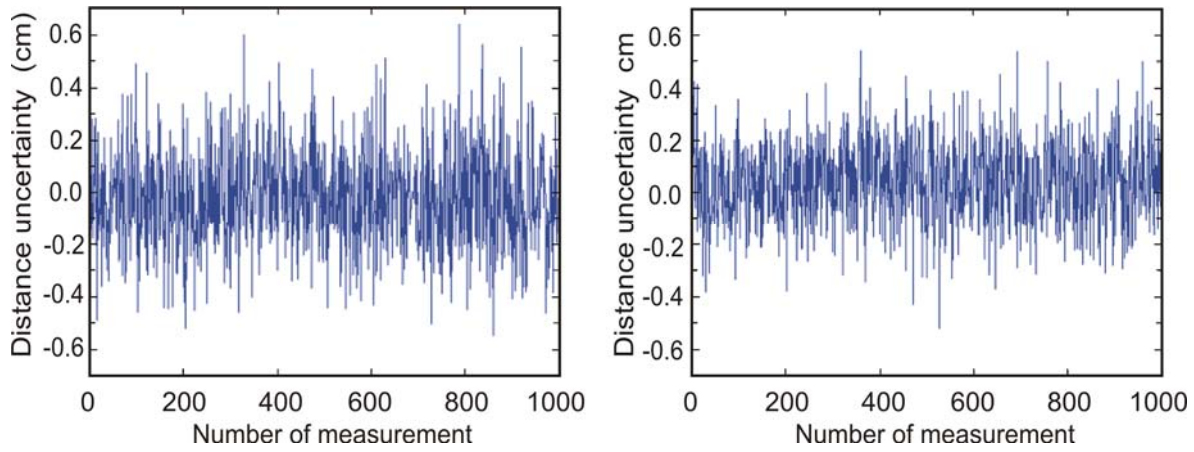

(a) (b)

Figure 4.34 Distance measurement uncertainty using average of 2 samples: (a) photodetector 1, and (b) photodetector 2.

From the measurement, it is evaluated that the distance measurement up to 2 cm has no significant effect on the measurement accuracy of target velocity, according to (3.18) and (3.21). Since, the correlation signal from both detected contours will be used to measure the velocity of the target in a correlation approach, see Section 3.3. The detection time differences of both contours are used to measure the velocity in a start-stop approach, see Section 3.2. Therefore, the used distance uncertainty of 0.35 cm is well satisfying to detect the contours of moving targets such as moving vehicles.

***Extraction of Angular Distance Difference*:** The accurate distance and the extraction of distance differences of detected targets are very important to evaluate the angular direction of the detected target. The accuracy of vehicle velocity for angular directions is directly dependent on the angle of measurement. The angular direction β to the perpendicular position of laser beam can be presented from the distance variation as

$$\beta = \tan^{-1}\left(D_d / D_r\right) \tag{4.7}$$

where the distance variation D_d is the difference of detected target distances between the two photodetectors. For the distance measurement uncertainty of each photodetector ΔD_d, the approximation of point target distance variation for n number of measurements can be approximated as

$$D_d = \frac{1}{n}\sum_{n=1}^{n}\left[\left|r_2(n) - r_1(n)\right| \pm \frac{1}{2}\Delta D_d(n)\right] \tag{4.8}$$

where r_1 is the target distance measured by photodetector 1. The distance r_2 is measured by photodetector 2 for a single target point at any angular direction of β, as shown in Figure 4.35.

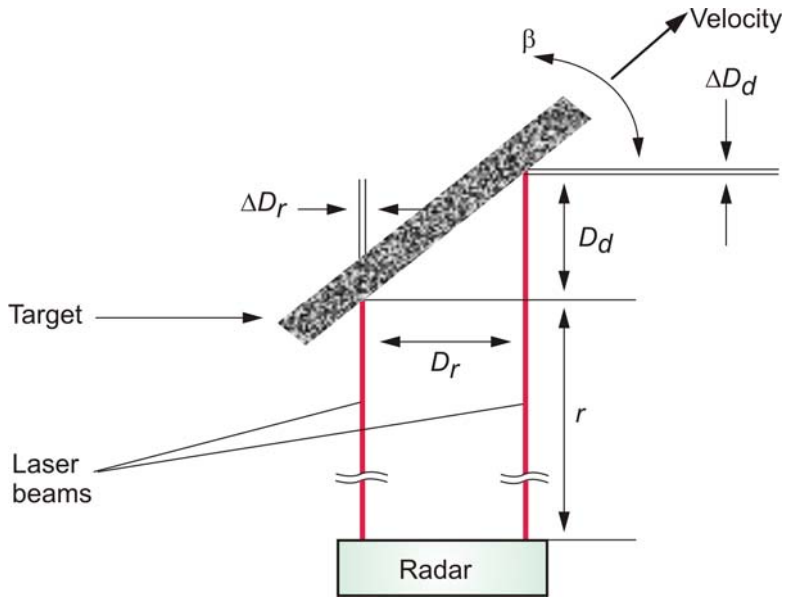

Figure 4.35 Differences of distance due to angular direction. (The target has only angular movement from a fixed place).

The measurement uncertainty of beam distance ΔD_r is occurred due to the variation of beam spot size and beam resolution. The exact beam separation distance can also be approximated for the *n* number of measurement as

$$D_r = \frac{1}{n}\sum_{n=1}^{n}\left[D_{r,real} \pm \frac{1}{2}\Delta D_d(n)\right] \tag{4.9}$$

where $D_{r,real}$ is the expected base separation distance between the two laser beams.

The measurement of angular direction is approximated by using (4.7), (4.8), and (4.9). 100 measurements are taken for each angular position (from 0 degree to 80 degrees) with a wooden block to evaluate the angular variation. It is found that the distance measurement accuracy of angular direction is approximately 99%. It is described that this approximation method will solve the error velocity due to the angular direction of the vehicle for the developed laser radar with two parallel laser beams. As a result, it can be demonstrated that the developed laser radar velocity measurement system can also be used in the curvature of streets.

Chapter 5

Methodology of Precise Velocity and Contour Representation

In this chapter, the data processing techniques of precise velocity measurement using the developed laser radar system are presented. The reproduction technique of the target contour is also reported. By interpreting the received signals, the contour of the target is obtained. The extraction of the developed software is also reported for coding the sampled data for precisely representing the target contour and velocity. Based on TOF principle, two methods of velocity analyses are demonstrated. They are referred to the start-stop system and the correlation system. Both methods are also used to realize the single tracking and the multi-tracking of targets velocity and identification system.

5.1 Data Processing Approach

The received pulses from both detectors are finally processed to obtain the range, contour and velocity of targets. The calibration of the receiving pulses, data selection criterion, reduction of noise level, influences of external and internal factors are considered for further processing of detected signals.

The schematic block diagram of the data processing approach is presented in Figure 5.1. At the beginning of the radar signal processing, the received signals are calibrated to reduce the noises and to obtain the detection of threshold. After calibrating, a time-counter clock signal turns on for the measurement. The measured data are stored up to t_n in a temporary memory. The clock signal t_{reset} is used to reset the clock counter. After resetting the counter, it gets ready to start another measurement from time t_o. The temporarily saved data are coded for further velocity analyses by self developed software codes. There are two possibilities to represent the precise velocity. First, it can be coded within the temporarily saved data. Second, the point targets distance can be

tracked and, by correlation of mapping contours, the velocity can be analysed. Finally, the measured velocities are computed by using the computer.

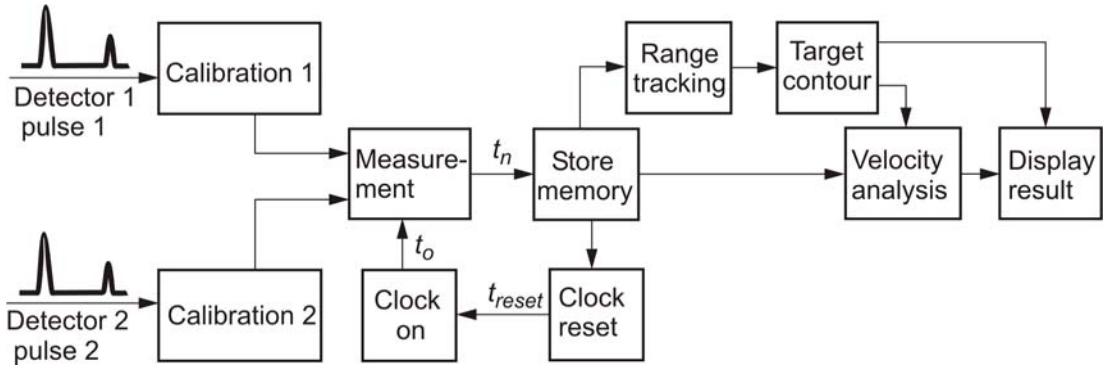

Figure 5.1 Block diagram of the data processing approach.

5.1.1 Calibration of Radar Signals

Before measuring the radar reception signals, a threshold of decisions have been selected. In this case, if the peaks of received pulses are higher than the threshold of decision, then the pulse signals are considered for further signal processing. In the mean time, it is decided that the target is inside the detection range. On the contrary, if the reception signals pulse peak is less than the threshold of decision, then it is supposed that no target is detected. To make assure the level of threshold of decision, a precise calibration is preformed. It has aimed that the radar system is designed to be used in different environmental conditions. The signal detection by the laser system also varies with the variation of external noise factors. The threshold of decision is adjusted avoid the noises on the measurement proceeding. To calibrate the radar system, the peak pulses are measured from each detector in absence of a target with different background conditions. Finally, the threshold of decision is taken for each detector. It is measured that the threshold of decision is a bit different (approximately less than 1 mV difference) in both detectors. The reason is due to the use of two different photodetectors and two separate optical reception systems. In order to optimise the false alarm and detection probabilities, several tests have been conducted. It has been found that 20 mV is the optimum threshold of decision (it is also found that noise level is 15 mV). For further reduction of noises, it has also added more 1 mV to 10 mV with the threshold of decisions, and this is done depending on the background environment of measurement place. Finally, the threshold of decision for detector 1 is denoted as V_{t1}, and the threshold of decision for detector 2 is denoted as V_{t2} for the continuation of measurement.

5.1.2 Measurement of Detected Signals

The block diagram of the radar signal measurement procedure is presented in Figure 5.2. The signals received by the laser system are first filtered by the two detectors. The peak of computed amplifying electrical signals are compared with the threshold value of decision (V_{t1} and V_{t2} respectively).

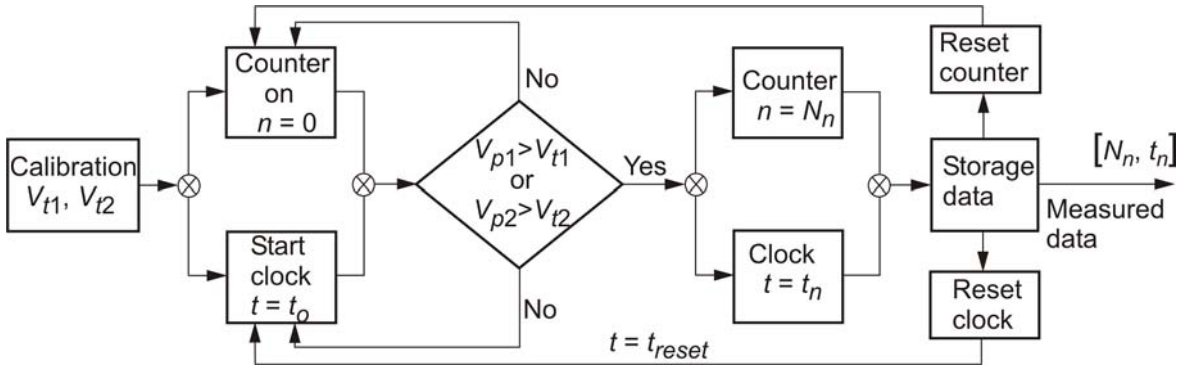

Figure 5.2 Block diagram of the measurement procedure of radar signals.

Before beginning of the measurements, the counter is set to zero, i.e. the number of measurement is zero ($n = 0$). The time clock signal is also zero, i.e. the measurement of clock time is zero ($t = t_o$). The counter and the clock are turned on if any of the received peak signal pulse is more than its corresponding threshold of decision. As a result, the measurement is continued up to the last signal reception from the detectors. The received peak pulse of the detectors 1 and 2 are V_{p1} and V_{p2}, respectively. Now, if detector 1 has detected the reception signal pulse first which is greater than the threshold of decision, i.e. $V_{p1} > V_{t1}$, then the measurement is started. It has also sent a signal to turn on the counter and the clock. Both the counter and the clock have performed the measurement up to the last signal obtained of detector 2 for all $V_{p2} > V_{t2}$. The number of total measurement of n by counter is presented by N_n. The time of total measurement is presented by t_n. The number of measurement N_n consists of the number of pulse detections, the number of pulse detections from each target and the number of error signal detections. The measurement time t_n consists of total scanning time, elapse time per measurement, scanning time per target and time difference between the reference pulse and the detected pulses for each point target. The laser radar system is designed to detect precisely the bi-directional target velocity. Therefore, if the first detected reception signal pulse is detected by detector 2, and which is greater then the threshold of

decision V_{t2}, i.e. $V_{p2} > V_{t2}$, then it has also started the measurement correspondently. The measurement continues up to the last laser signal detection from detector 1 with $V_{p1} > V_{t1}$. After n number of measurements, the number of detection N_{1d1} and its corresponding time of detection t_{1d1} are presented for first detected target from the detector 1. Similarly, the number of detection N_{1d2} and its corresponding time of detection t_{1d2} are presented for first detected target from the detector 2. Therefore, for m number of targets, the detection matrix can be presented as

$$\begin{aligned}[N_n,\ t_n] &= f\left[(N_{d1},\ t_{d1}),(N_{d2},\ t_{d2})\right] \\ &= f\left[\left\{(N_{1d1},....,N_{md1}),(t_{1d1},....,t_{md1})\right\},\left\{(N_{1d2},....,N_{md2}),(t_{1d2},....,t_{md2})\right\}\right] \end{aligned} \quad (5.1)$$

where the total number of measurements and corresponding time data are N_{d1} and t_{d1}, respectively, from the detector 1. The total number of measurement and corresponding time data are N_{d2} and t_{d2}, respectively, for the detector 2. The number of measurements by the detector 1 for m-th target is N_{md1}, and its corresponding time is t_{md1}. The number of detection by the detector 2 for m-th number of target is N_{md2}, and its corresponding time is t_{md2}. Moreover, the measurement is performed to evaluate the target contour. The distance of the target is determined from the time difference of the detected pulse and the reference pulse. Now, for m-th target, the detection parameter for the detector 1 of N_{md1} and t_{md1} can be presented as

$$N_{md1} = f_{d1}\left(N_{md1,\,m},\ \Delta N_{md1,\,err}\right) \quad (5.2)$$

and

$$t_{md1} = f_{d1}\left(t_{md1,\,m},\ t_{md1,\,s},\ t_{md1,\,d},\ \Delta t_{md1,\,err}\right) \quad (5.3)$$

where (5.2) and (5.3) are functions of the detector 1 for m-th target. The number of received measurement and the number of error measurement are $N_{md1,\,m}$ and $\Delta N_{md1,\,err}$, respectively. The detected scanning real time of m-th target is $t_{md1,\,m}$. The time of each scanning is $t_{md1,\,s}$. The time differences (the time differences of reference pulse to received pulse) of laser pulse for each point target is $t_{md1,\,d}$. The scanning error time is $\Delta t_{md1,\,err}$.

Similarly, for *m*-th target the detection parameters for the detector 2 of N_{md2} and t_{md2} can be presented as

$$N_{md2} = f_{d2}\left(N_{md2,\,m},\ \Delta N_{md2,\,err}\right) \tag{5.4}$$

and

$$t_{md2} = f_{d2}\left(t_{md2,\,m},\ t_{md2,\,s},\ t_{md2,\,d},\ \Delta t_{md2,\,err}\right) \tag{5.5}$$

where (5.4) and (5.5) are the functions of the detector 2 for *m*-th target. The number of received measurement is $N_{md2,\,m}$ and the number of error detections is $\Delta N_{md2,\,err}$. The detected scanning real time of *m*-th target is $t_{md2,\,m}$. The time of each measurement is $t_{md2,\,s}$. The time differences of the laser pulse for each point target is $t_{md2,\,d}$ and the scanning error time is $\Delta t_{md2,\,err}$.

After performing the measurement, the detection signal is saved in the temporary memory, and it contains of $[N_n,\ t_n]$ matrix for further data processing. Meanwhile, clock signal t_{reset} has reset all clock timers for the next measurement.

5.1.3 Velocity Analysis for Start-Stop System

The fundaments of start-stop approach for velocity measurement are already presented in Section 3.2. The start-stop is functioning based on the sensing of target. If a target is sensed by any detector then it will continue to scan till it is also sensed by the other detector. However, the temporary saved data from the measurement phase are taken to analyze the target velocity. The matrix $[N_n,\ t_n]$ is taken for every measurement, and it is further decoded for achieving the precise velocity. Since the fixed number of measurements (N_n) are performed, the velocity analysis is followed from the matrix of (5.1). Moreover, if only one target is detected then the further decoding is done for single target. If more than one targets are detected then it is considered as multi-target decoding process. For every target the velocity is evaluated from the detected signal from the detectors and from the pulse detection from counter 1.

***Detection of Single Target and its Velocity*:** The simplest detection technique is single target detection and it is shown in Figure 5.3. From (5.1), it can be demonstrated for a single target that the number of measurement and its corresponding time N_{1d1} and t_{1d1} are detected by the detector 1. The number of

measurement and its corresponding time N_{1d2} and t_{1d2} are detected by the detector 2. Number of detections N_{1d1} and N_{1d2} are controlled by counter 1. If a target is first detected by the detector 1 then the counter 1 sends clock signal to start the detection of [N_{1d1}, t_{1d1}] data. The measurement is continued up to the last detection of the detector 2 with $V_{p2} > V_{t2}$, and it presented by [N_{1d2}, t_{1d2}] data, as shown in Figure 5.3. For the opposite direction of a target, counter 1 is controlled in a reverse manner.

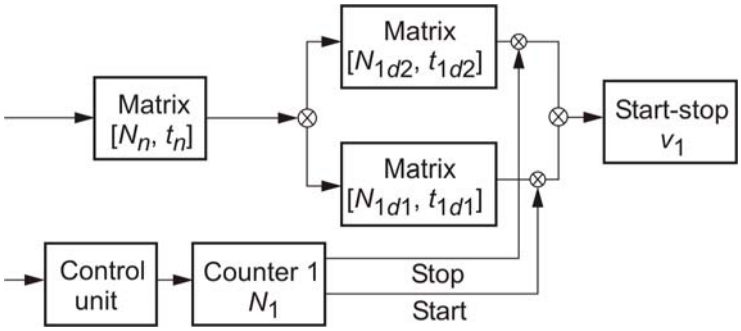

Figure 5.3 Block diagram of the measurement of single-target velocity by start-stop approach.

It is known that the repetition frequency of the laser radar is fixed, and it is controlled by a control unit. For target tracking, if Δs is the distance difference between two scanned pulses, then the detected velocity of point targets can be presented as $v_s = \Delta s \times PRF$. Now, the fixed base distance between two laser beams is D_r. The first detected signal time by the detector 1 and the first detected signal time by the detector 2 are $t_{1d1,\,s}$ and $t_{1d2,\,s}$, respectively. From those detected signals, the measured velocity by start-stop can be presented as

$$v_{ms} = \frac{D_r}{\left| t_{1d2,\,\mathrm{s}} - t_{1d1,\,\mathrm{s}} \right|} \tag{5.6}$$

Alternately, the measured velocity from *n*-th detected signal data can also be written as

$$v_{ms}(n) = \frac{D_r}{\left| t_{1d2,\,\mathrm{s}}(n) - t_{1d1,\,\mathrm{s}}(n) \right|} \tag{5.7}$$

Now, if the n number of scanned data is detected by counter 1 then the actual approximated velocity of a target can be measured as

$$v_m = \frac{D_r PRF}{n} \tag{5.8}$$

***Detection of Multiple Targets and Velocities*:** The block diagram of multiple target tracking by the start-stop approach is presented in Figure 5.4. The measured data of $[N_n, t_n]$ is subdivided into the detector 1 and the detector 2 data as $[N_{d1}, t_{d1}]$ and $[N_{d2}, t_{d2}]$, respectively. By decoding the number of targets, the detected data for each target by each detector has been presented. For the number of detected targets m, the detected signal data for the m-th target is presented as $[N_{md1}, t_{md1}]$ for the detector 1. The detected signal data for the m-th target is presented as $[N_{md2}, t_{md2}]$ for the detector 2, as shown in Figure 5.4.

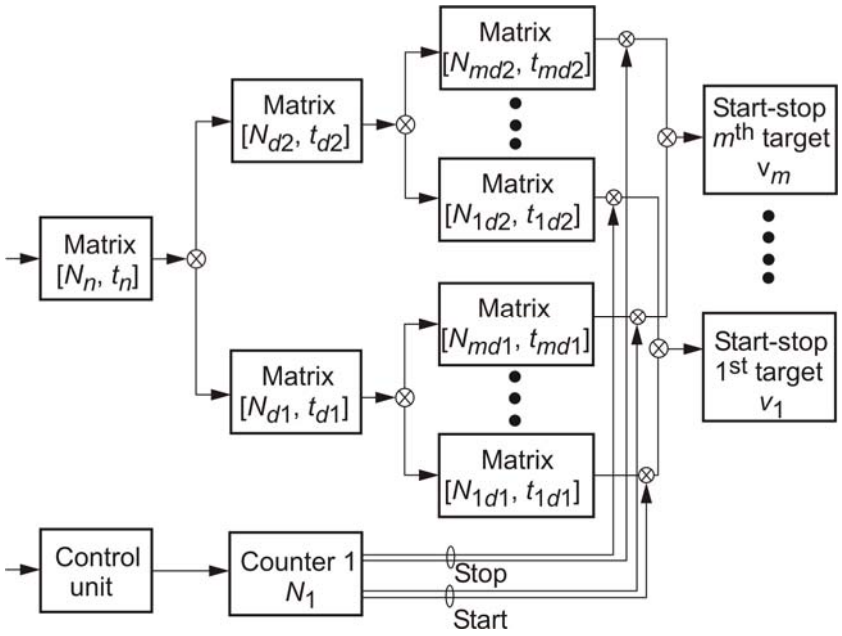

Figure 5.4 Block diagram of the measurement of multiple target velocity by start-stop approach.

The velocity of first target can be presented by (5.6) and (5.7). Since, the multiple targets are detected, therefore the measured velocity from detected data for m-th target can be presented as

$$v_{mm} = \frac{D_r}{\Delta t_m} = \frac{D_r}{\left| t_{md2,\,s} - t_{md1,\,s} \right|} \tag{5.9}$$

The measured velocity from n-th detected signal of m-th target can also be presented as

$$v_{mm}(n) = \frac{D_r}{\left| t_{md2,\,s}(n) - t_{md1,\,s}(n) \right|} \tag{5.10}$$

where for m-th target, the first detected scanning time $t_{md1,\,s}$ has detected by the detector 1 and the first detected scanning time of $t_{md2,\,s}$ has detected by the detector

2, respectively.

The control unit controls the clock signal of start and stop for each target and the counter 1 also counted the detected signal as N_1. If the number of detection by control unit for first target is n_1 and m-th target is n_m then signal detected by counter 1 can be presented as $N_1 = (n_1, \ldots\ldots, n_m)$. The approximated actual measured velocity by counter 1 of m-th target can also be presented as

$$v_m = \frac{D_r PRF}{n_m} \tag{5.11}$$

***Dynamic Measurement of Velocity*:** The measurement of velocity by start-stop approach is presented in Figure 5.5 for any target m without saving the temporary scanning data. The velocity and the corresponding target contour length are measured by the dynamic measurement. It can also evaluate the both directional (toward and backward) targets in dynamic measurement of velocity.

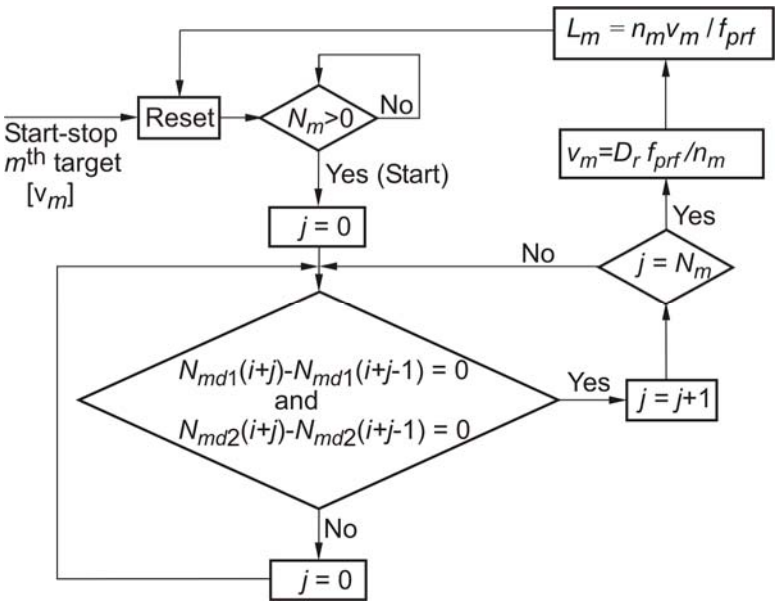

Figure 5.5 Dynamic measurement of velocity by start-stop approach.

For m-th target in any perpendicular direction, if the detected signal is $N_m > 0$ then the clock begins to count and the temporary counter (j) from zero. If no target is detected in a fixed number of scans (for example, $N_m = 1000$), then the radar system decides that there is no target detected by the laser radar system. The counter are reset after N_m, as shown in Figure 5.5. If the target is detected till $j = N_m$ then the velocity is evaluated and displayed. Now, as soon as the m-th target is detected by

the detector 1 it saved the first scanning time of detection as $t_{md1,s}$. The counter 1 has begun to count and it has counted N_m number of data until the detector 2 has detected that target. The detector 2 has saved its first scanning time of detection as $t_{md2,s}$. Counter 1 with N_m number of data has given the velocity, as described in (5.11). The measured velocity from both detectors is presented by (5.9). As the target velocity is measured twice by the radar system, the system accuracy is increased. The final velocity will be computed by the superposition of detected velocities of both detectors.

However, the fundament of length measurement is already presented in Section 3.4. The length of a target can be measured by measuring the detected laser pulses from one of the detectors. But if the target enters at the mid-time of two laser beams due to pulse repetition frequency, then the measuring time will introduce errors. Therefore, the detected scanned data from both detectors is saved on the temporary counter of N_{md1} for the detector 1 and N_{md2} for the detector 2. The approximated number of exact detection $N_{md1,m}$ from N_{md1}, and $N_{md2,m}$ from N_{md2} are considered from the error measurement. Therefore, from (5.2) to (5.6) and from (5.9), the detected target length for *m*-th target can be presented as

$$L_m = \frac{v_{mm}}{2}\left(N_{md1,m}.\, t_{md1,m} + N_{md2,m}.\, t_{md2,m}\right) \tag{5.12}$$

As the detection of counter 1 is n_m for *m*-th target, the length L_{ap} of that target can be approximated as

$$L_{ap} = \frac{n_m v_m}{PRF} \tag{5.13}$$

Finally, by comparing the measured length from (5.12) and (5.13), the accuracy of the length measurement can be evaluated.

5.1.4 Velocity Analysis by Correlation System

The detector 1 received signals are presented by (5.2) and (5.3), and the detector 2 received signal are presented by (5.4) and (5.5). The fundamental background of velocity measurement by correlation of detected target contours is already presented in Section 3.5. The phase of velocity measurement by correlation of target contour is shown in Figure 5.6. In this case, the tracking range of every point target is measured and it gives the target contour. The precise velocity of target is evaluated by using the

correlation of both detected contours. Finally, the result of velocity analyses is displayed in the computer.

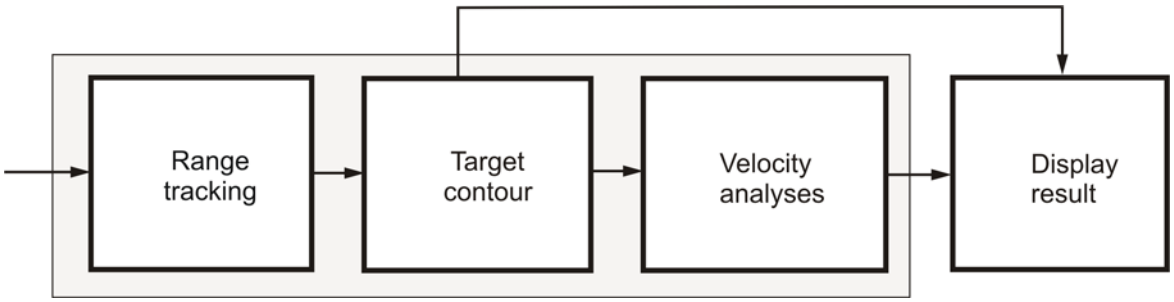

Figure 5.6 Schematic of velocity measurement from target contour.

It is known that the contour of target can be evaluated from horizontal and vertical direction to the target plane, as described in Section 3.5. For any plane of target detection, the surface distance per measurement from the detector 1 for *m*-th target is presented as

$$r_{md1,\,p} = \frac{c_o . t_{md1,\,d}}{2} \tag{5.14}$$

By averaging all of the point target distance from (5.14), the distance of *m*-th target is evaluated. Now, for any minimum time difference signal of $t_{md1,\,\min}$ the minimum surface distance per measurement of *m*-th target from detector 1 is computed as

$$r_{md1,\,p,\,\min} = \frac{c_o . t_{md1,\,d,\,\min}}{2} \tag{5.15}$$

Therefore, the detected contour of the *m*-th target by detector 1 is the envelope of all detected targets distance per measurement, and it is presented as

$$W_{md1} = \sum_{n=0}^{N_n} \left\{ \left[r_{md1,\,p}(1),\, t_{md1,\,s}(1) \right], \ldots\ldots\ldots\ldots, \left[r_{md1,\,p}(n_m),\, t_{md1,\,s}(n_m) \right] \right\} \tag{5.16}$$

where n_m number of point targets are detected from *m*-th target by detector 1 out of N_n number of measurement and the time of each detection is $t_{md1,\,s}$.

Similarly for detector 2 with any plane of target detection, the surface distance per measurement of *m*-th target is presented as

$$r_{md2,\,p} = \frac{c_0 . t_{md2,\,d}}{2} \tag{5.17}$$

Now, for any minimum time difference signal of $t_{md2,\,\min}$ the minimum surface distance per measurement of *m*-th target from detector 2 is computed as

$$r_{md2,\,p,\,\min} = \frac{c_0.t_{md2,\,d,\,\min}}{2} \tag{5.18}$$

For the detection of n_m number of measurement by detector 2, the detected contour of the m-th target is the envelope of the detected all targets distance per measurement, and it is represented as

$$W_{md2} = \sum_{n=0}^{N_n} \left\{ \left[r_{md2,\,p}(1),\, t_{md2,\,s}(1) \right], \ldots\ldots\ldots\ldots, \left[r_{md2,\,p}(n_m),\, t_{md2,\,s}(n_m) \right] \right\} \tag{5.19}$$

where n_m number of target distances are detected from m-th target by detector 2 out of N_n number of measurement and the time of each detection is $t_{md2,\,s}$.

Now, the correlation of both contours W_{md1} and W_{md2} for m-th target is represented as

$$R_{w_{md1},\,w_{md2}}\left(\ell_m\right) = \sum_{n=0}^{N_n} W_{md1}\left[(n-\ell_m).t_{prf} \right] W_{md2}\left(n.t_{prf}\right) \tag{5.20}$$

In (5.20), the maximum $R_{w_{md1},\,w_{md2}}$ is obtained for maximum $\ell_m = \ell_{m,\,\max}$ and it represents the maximum time as $t_{m,\,crr,\,\max} = \ell_{m,\,\max}.t_{prf}$. Finally the precise velocity of the m-th target is represented as

$$V_{m,\,crr} = \frac{D_r}{t_{m,\,crr,\,\max}} = \frac{D_r}{\ell_{m,\,\max}.t_{prf}} \tag{5.21}$$

By using (5.21) for any target m, the precise velocity of that target is evaluated precisely from correlation approach.

5.2 Measurement of Time Significant Point

The target distance per measurement is evauated from the time difference between the detected pulse and the reference pulse. The target contour is measured from all detected target distances per measurement, see Section 5.1. Meanwhile, to evaluate the time difference of the detected pulse and the reference pulse, the time significant points are measured on them (the detected pulse and the reference pulse). Moreover, Section 3.6 has been addressed the correction of time error due to the detected pulse amplitude variations. Therefore, it is very important to consider the detection of time significant point for every detected pulse. The detection of threshold of the detector 1 is V_{t1}, the detector 2 is V_{t2} and they are represented in Section 5.1.1. The detected time

difference of point target for detector 1 is $t_{md1,d}$ and detected time difference of point target for detector 2 is $t_{md2,d}$, as described in Section 5.1.2. The detected time difference $t_{md1,d}$ and $t_{md2,d}$ are the time differences of significant points of reference and detected pulses for the detector 1 and the detector 2, respectively.

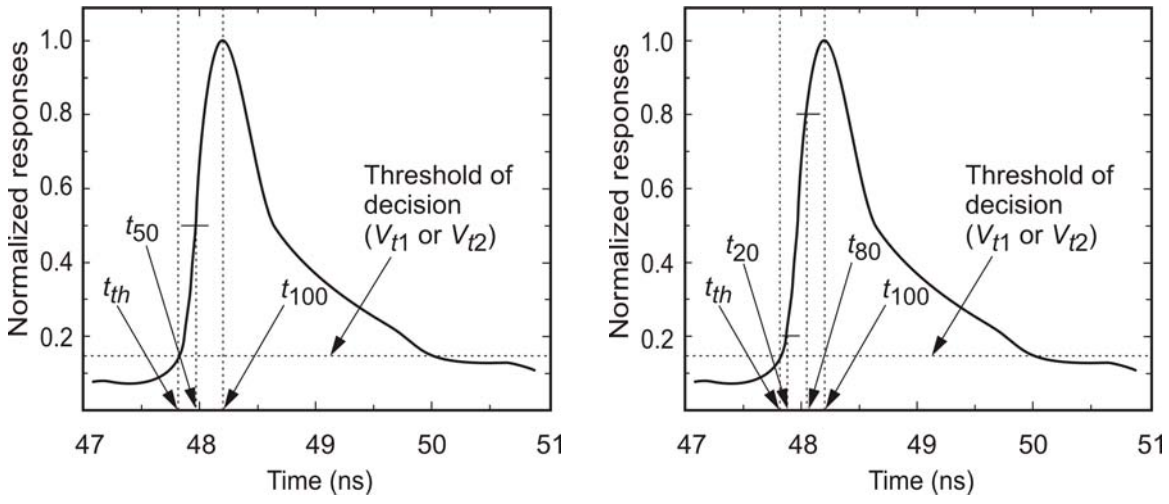

Figure 5.7 Method of detection of time significant point: (a) the 50% method of normalized peak response, and (b) the 20% and 80% method of normalized peak response.

Two different ways of determining the time significant point for pulse detection are illustrated in Figure 5.7. If the sampled time at threshold of decision is t_{th} then it repesents the detected time of laser pulse at threshold of detection. The sampled time of the normalized peak pulse is t_{100}. The first method is the average value of $\{t_{th} + (t_{100} - t_{th})\}/2$ for $t_{th} \le (t_{100})/2$, and it is the nearest sampling time of t_{50}. It is represented as the 50% of peak response. The selection of time significant point of the detected pulse is the time of t_{50}, as shown in Figure 5.7(a). The second method is the detection of time significant point from 20% and 80% of the peak response as shown in Figure 5.7(b), where t_{20} and t_{80} are 20% and 80% of peak responses, respectively. In the 20% and 80% method, the time significant point of t_{20} is the nearest sampling time of $\{t_{th} + (t_{100} - t_{th})\}/5$ for $t_{th} \le (t_{100})/5$. The time significant point of t_{80} is the nearest sampling time of $\{4t_{th} + 4(t_{100} - t_{th})\}/5$ for $t_{th} \le 4(t_{100})/5$, as shown in Figure 5.7(b). From the target range measurement, it has been evaluated that the 20% and 80% method is better than 50% method [57], since it has two sampled data per measurement. The measurement of target contour and velocity is used the time significant point of 20% and 80% method. Therefore, the values of $t_{md1,d}$ and $t_{md2,d}$

are evaluated based on the avaraging of the time significant point of 20% and 80% peaks of the normalized pulses.

5.3 Calibration of Temperature Effect on Measurement System

The target distance is measured by using the TOF principle. The range of targets is measured by using the velocity c_o of light wave as represented in (5.15) and (5.18) for both detectors, respectively. The wave velocity in any medium depends on the material constants and ambient conditions, such as permittivity and temperature. The wave velocity in atmospheric air can be expressed [55, 123] as

$$c_o = \sqrt{\frac{R_{air}\ \mathrm{T}\ \chi}{M}} \tag{5.22}$$

where the air constant $R_{air} = 8.135 \times 10^7$ erg/degree and T (K) is the ambient temperature. The adiabatic coefficient of $\chi = C_p / C_v$ is the gradient of specific heat capacity of the air. The specific heat capacity at constant pressure is C_p, the specific heat capacity at constant volume is C_v and the molecular weight is M.

For the normal atmospheric pressure in air medium (760 torr =1.0332 at.), the wave velocity yields

$$c_o = \left(331.3 + 0.6\mathrm{T}_c\right)\ \text{m/sec} \tag{5.23}$$

where T_c is the ambient atmospheric temperature in °C. Therefore, the wave velocity in air is only temperature dependent as represented in (5.23). It is clear that for temperature variation of $\mathrm{T}_c = \pm 10\ °\mathrm{C}$, the light wave velocity changes as $\Delta c_o = \pm 6\ \mathrm{m/sec}$ (or 1.67 km/h).

The temperature variation from (5.23) is used in (5.14) and in (5.17) for data processing to achieve the precise velocity measurement system.

5.4 Measurement of Contour and Velocity

By using the reported data conversion techniques, contour and velocity of different moving targets are measured and evaluated in this section. The aim is to evaluate the characteristic parameters of the developed laser radar system for the measurement of the contour and precise velocity of vehicles.

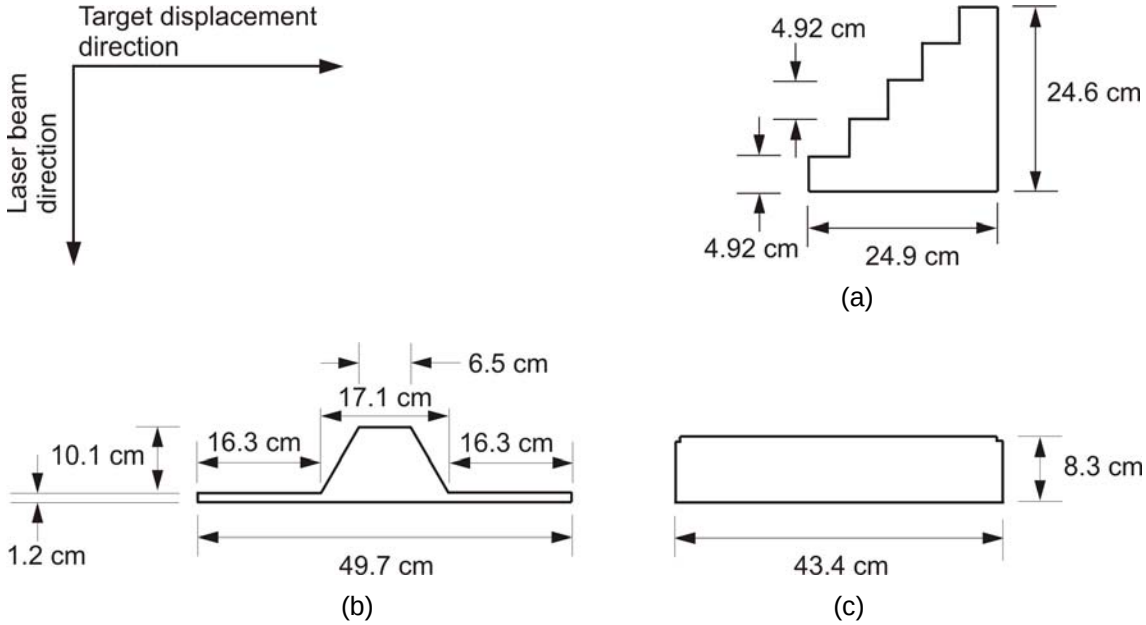

Figure 5.8 Block diagram of test targets: (a) step wooden block, (b) ramp wooden block, and (c) rectangular plastic block.

At the beginning of the measurements, the threshold of decision is taken 20 mV (V_{t1} and V_{t2}), as described in Section 4.1.1. The time significant points of detected laser pulses are taken according to Section 4.2. The targets were fixed on a rolling board, and it has smoothly manually moved from left to right direction as shown in Figure 5.8. Therefore, the contours are measured from the upper surface of the targets. During the measurement the ambient temperature was 22°C. For every target, the measured data ($[N_n, t_n]$ data, see Section 4.1.2) are saved on temporary memory of the computer. The measurements are repeated four times for each target to make sure the reliability of the measured result. Finally, the velocity, contour and length are analyzed according to data processing from Section 5.1.3 and Section 5.1.4.

Several types of target have been taken, which are made of wooden and plastic blocks. Three types of targets are represented as shown in Figure 5.8. The step wooden block of 24.6 cm length and 24.9 cm height is shown in Figure 5.8(a). The ramp wooden block of 49.7 cm length is shown in Figure 5.8(b). The rectangular plastic block of 43.4 cm length and 8.3 cm height is shown in Figure 5.8(c). The contour and velocity of the respective test targets are measured as a single target ($m = 1$) on each measurement. Target displacement and laser beam directions are given according to the shown Figure 5.8.

The two-dimensional contour measurement of the wooden step type target is shown in Figure 5.9. The detected contour of the detector 1 is shown in Figure 5.9(a) and

the detected contour of the detector 2 is shown in Figure 5.9(b). They have slightly different ranging distance detection uncertainty shown in Figure 5.9, and it is due to the difference of circuit systems on both detectors. The differences of velocity measurement by both detectors are reported in Table 5.1. The measured velocity in the start-stop system is 49.955 cm/sec according to (5.6). The measured velocity in correlation from both detected contour is 49.960 cm/sec according to (5.21). The velocity measurement error of start-stop with respect to correlation velocity is 0.01%. The detected target velocity by correlation is more accurate then the start-stop system. The reasons are that it does not have error due the counters and timer delays; moreover, superposition of every measurement is counted for velocity measurement. The detected length of this target is 24.892 cm, but the given length is 24.9 cm, see Figure 5.8(a). The length measurement error is 0.032% for the approximated detected target velocity of 49.96 cm/sec. The measured higher and lower distances are 503.50 cm and 483.58 cm from the laser radar, respectively. The measured height of the step block is (503.20-483.55) cm = 19.65 cm. The step height to be measured for this target is (24.6-4.92) cm = 19.68 cm because of symmetry, see Figure 5.8(a). Therefore, the range measurement error is 0.1%. The error of the range measurement system can be increased by increasing the number of averages per measurement, but it will slow down the scanning speed. Two samples per measurement are taken to make compromise between target contour and velocity measurement system.

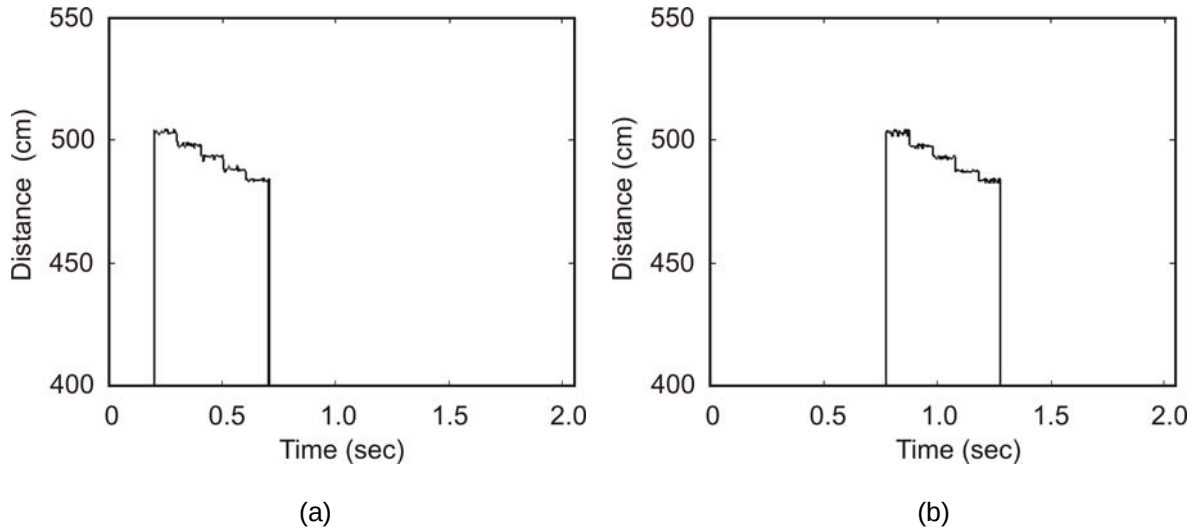

Figure 5.9 Measured contours of wooden step target: (a) detected contour of detector 1, and (b) detected contour of detector 2. Ranging uncertainty of detector 1 and detector 2 are 0.95 cm and 0.97 cm, respectively.

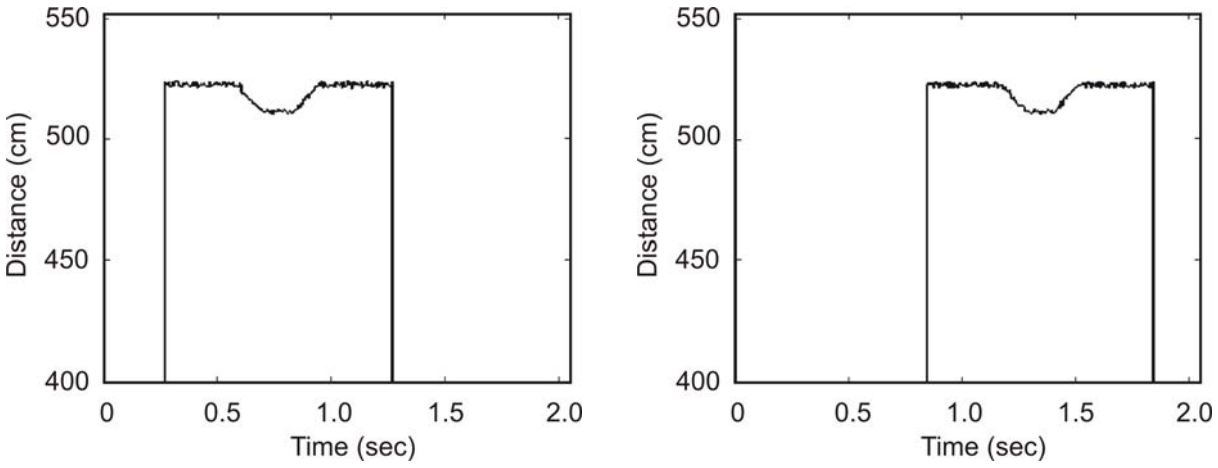

Figure 5.10 Measured contours of wooden ramp-shaped target: (a) detected contour of detector 1, and (b) detected contour of detector 2. Ranging uncertainty of detector 1 and detector 2 are 0.94 cm and 0.95 cm, respectively.

The two-dimensional contour measurement of the wooden ramp shaped target is shown in Figure 5.10. The detected contour of the detector 1 is shown in Figure 5.10(a) and the detected contour of the detector 2 is shown in Figure 5.10(b). Both detectors have different ranging distance uncertainty shown in Figure 5.10, and it is due to the difference of circuit systems. The differences of velocity measurement by both detectors are reported in Table 4.2. The measured velocity by start-stop system is 50.252 cm/sec according to (5.6). The measured velocity by correlation of both detected contour is 50.255 cm/sec according to (5.21). The velocity measurement error of start-stop with respect to correlation velocity is 0.0059%. The detected length of this target is 49.684 cm and the given length is 49.7 cm, see Figure 5.8(b). The length measurement error is 0.03% for the approximated detected target velocity of 50.255 cm/sec. The measured higher distance to the ramp block is 522.42 cm and lower distance is 512.30 cm. The measured height of the ramp wooden block is 10.08 cm, but the given height to be measured of the step block is 10.10 cm, see Figure 5.8(c). Therefore, the range measurement error is 0.19%.

The contour measurement of the rectangular type plastic (light brown, polyvinyl chloride) target is shown in Figure 5.11. The detected contour of the detector 1 is shown in Figure 5.11(a) and the detected contour of the detector 2 is shown in Figure 5.11(b). Both detectors have less ranging distance uncertainties than the wooden targets shown in Figure 5.11, and it is because the plastic surface is smoother than the wood surface. The differences of velocity measurement by both detectors are reported in Table 4.2. The measured velocity in the start-stop system is 50.80 cm/sec

and the measured velocity in the correlation of both detected contours is 50.82 cm/sec. The velocity measurement error of start-stop with respect to correlation velocity is 0.039%. The detected length of this target is 43.37 cm and the given length is 43.40 cm, see Figure 5.8(c). The length measurement error is 0.069% for the detected target velocity of 50.82 cm/sec. The measured ranging distance of the rectangular surface is 529.65 cm. The detected distance measurement uncertainty is 0.85 cm of the detector 1 and 0.845 cm of the detector 2, respectively. The variation of target ranging uncertainty between both detectors is 0.005 cm. It is because of the difference of both detectors circuit systems and differences of connecting wires and passive elements.

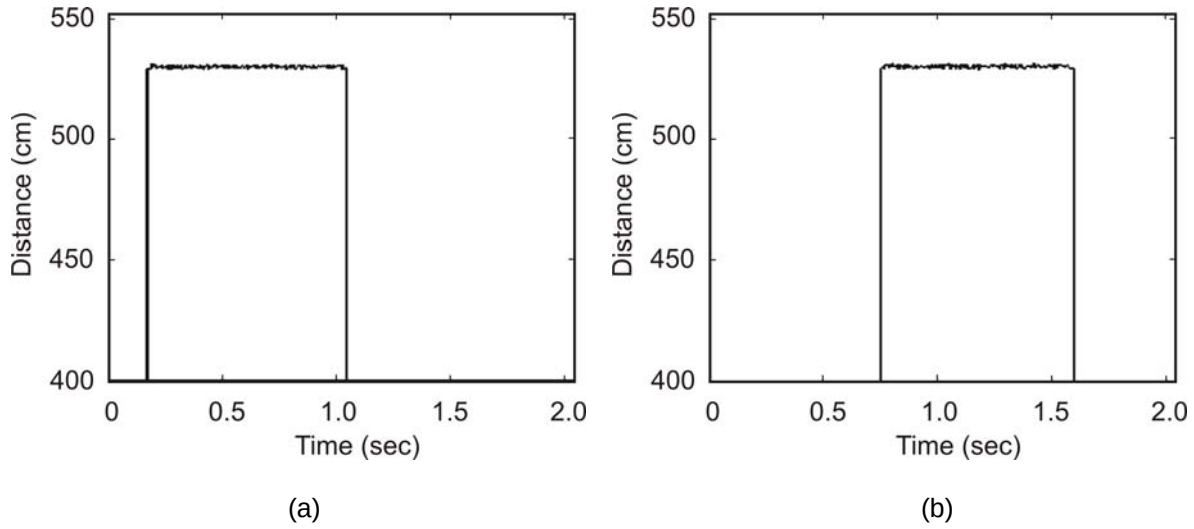

Figure 5.11 Measured contours of plastic rectangle bar target: (a) detected contour of first detector, and (b) detected contour of second detector. Ranging uncertainty of detector 1 and detector 2 are 0.85 cm and 0.845 cm, respectively.

***Measurement of Multiple Targets Contour and Velocity*:** The measurements of multiple targets contour and velocity detection are represented in Figure 5.12. In this case two different targets ($m = 2$) are taken into consideration. The first target is a wooden step block as reported in Figure 5.8(a), and the second target is a wooden ramp block as reported in Figure 5.8(b). The detected contour by the detector 1 is shown in Figure 5.12(a), and by the detector 2 is shown in Figure 5.12(b). The reason of multiple target measurement is taken to evaluate the velocity measurement technique in high traffic congestion.

In this measurement, both wooden block targets are fixed on separate rolling boards. Both targets have moved perpendicular to the laser radar at a time during the measurement. In this case of multi-targets detection, there is a time difference or

range difference between two consecutive detected targets. The ranging distances of detected contour have an abrupt change for different ranges of detected targets. In Figure 5.12(a), the detected range of the first target is 610 cm. After the detection of the first target, in between 0.5832 sec to 0.8082 sec no target is detected. Therefore, the ranging distance becomes zero at this time interval, where no target is detected. Further, at 0.8082 sec the first detector has detected the second target. The detected range of the second target is 539 cm. It is measured that the detected targets have different contour distances and detection time interval, see Figure 5.12. The different time intervals of target contours are used to identify the number of targets. In start-stop approach, the velocity of each target is measured based on the first detected pulse time from that target. In correlation approach, the contour profiles of each target are separately considered to measure the velocity. The method of velocity and contour measurement of multiple targets are presented in Section 5.1.3 and Section 5.1.4.

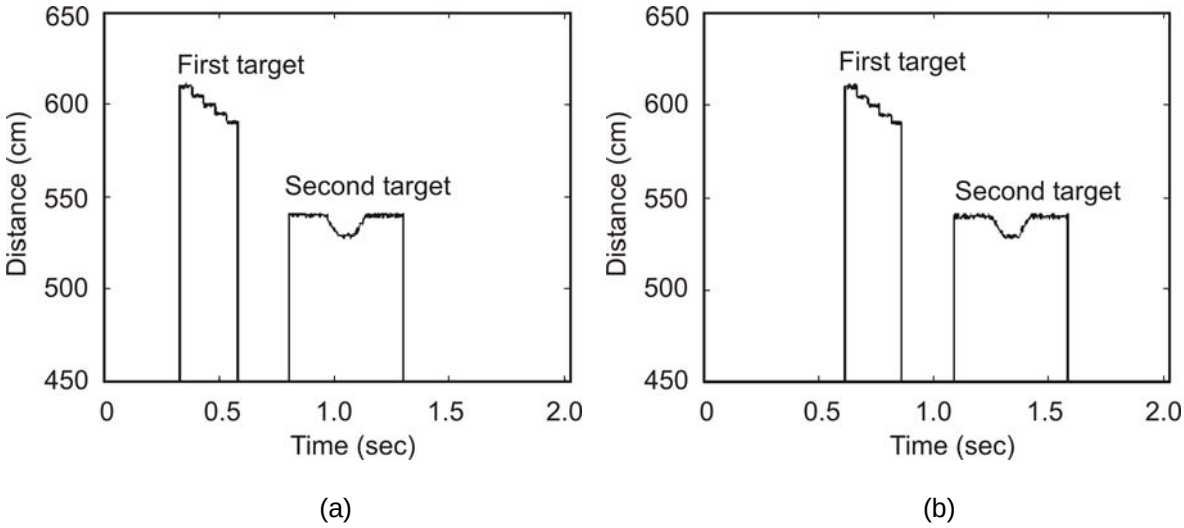

Figure 5.12 Measured contours of multiple targets: (a) detected contour of detector 1, and (b) detected contour of detector 2.

By the start-stop approach, the measured velocity of the first target is 65.50 cm/sec and second target is 70.21 cm/sec, and the velocities are measured according to (5.9). By correlation of contours from both detectors, the measured velocity of first target is 65.52 cm/sec, and the measured velocity of second target is 70.22 cm/sec. From the measured velocity by correlation approach, it is found that the accuracy of detected velocity is increased if the surface length of the target is increased. For example, the first target surface length is 24.9 cm and the detected error velocity is 0.02 cm/sec for the approximated velocity of 65.52 cm/sec. The second target surface length is 49.7 cm and the difference of detected velocity is 0.01 cm/sec for

the velocity of 70.22 cm/sec. It is because the number of detected laser pulses is higher from a larger target surface area, and it reduces measurement error at correlation approach.

5.4.1 Characteristics of Measured Contour and Velocity

To perform the characteristic parameter evaluations, the measurement of target velocity and contour for different ranging distances are represented. The comparison of velocity measurement by start-stop and by correlation is also demonstrated to investigate the reliability of both measurement approaches.

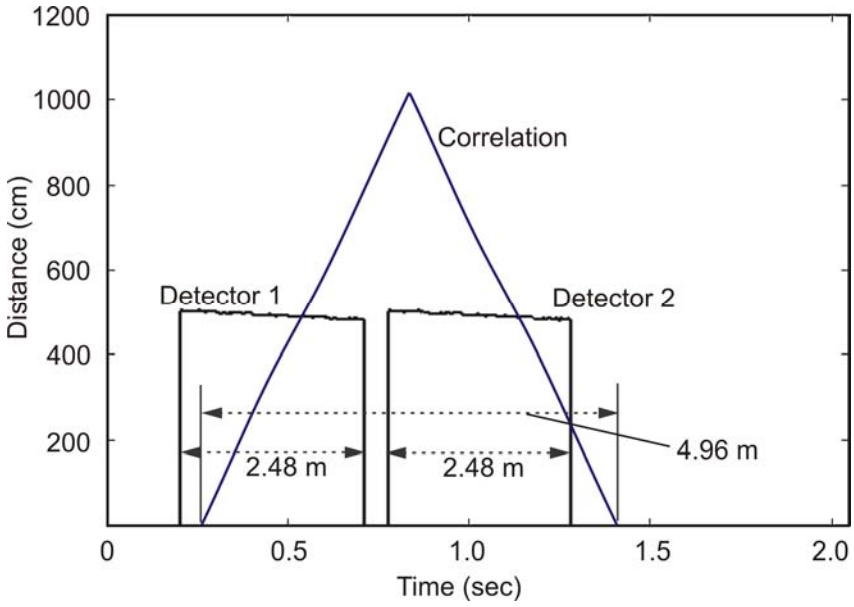

Figure 5.13 Contour and velocity measurement of wooden step target. Detected velocity by start-stop is 55.50 cm/sec, velocity by correlation is 55.51 cm/sec and measured error velocity of 0.001%.

The measurements of velocity by correlation of both detected contours are illustrated in Figure 5.13 for the wooden step block. The dimension of the wooden step block is given in Figure 5.8(a). From Figure 5.13, it is found that the detected velocity from correlation of both contours is 55.51 cm/sec and the velocity by start-stop approach is 55.50 cm/sec. The start-stop velocity measurement error is 0.018% with respect to the correlation velocity of 55.51 cm/sec. The contour length measurement error is 0.016% for the measured velocity. The measurement errors occur due to the internal circuit system delay of the signal processing unit, the time delay of the used counters and the detection time delay due to pulse repetition frequency.

Moreover, the measured velocities of the three different targets are summarized in Table 5.1. Measured two dimensional surface contour length and velocity of test

targets are reported with different ranging distances. The reason for performing this measurement is to evaluate the measurement accuracy for ranging distance, target surface shape, target surface length and different velocities. It is proved that the accuracy of the measurement velocity is higher at slower moving target. This is an advantage over the Doppler radar system. Therefore, the measurement accuracy of the laser radar has predominately shown that its application in vehicle velocity measurement system is highly demanding.

Table 5.1 Detected target and velocity

Target	Distance (m)	Velocity by start-stop (m/s)	Velocity by correlat-ion (m/s)	Error velocity (%)	Detected length by		Velocity by	
					First detector (cm)	Second detector (cm)	First detector (m/s)	Second detector (m/s)
Wooden step shape	2.5	1.200	1.202	0.16	24.89	24.88	1.02	1.02
	4.0	1.210	1.211	0.08	24.87	24.88	1.21	1.20
	5.5	1.100	1.101	0.09	24.90	24.89	1.10	1.11
	8.5	1.150	1.153	0.26	24.86	24.87	1.14	1.15
	10.0	1.300	1.305	0.38	24.84	24.85	1.28	1.29
	12.5	1.220	1.232	0.97	24.85	24.82	1.20	1.21
	16.0	1.210	1.228	1.42	24.82	24.81	1.19	1.20
Wooden ramp shape	2.5	1.210	1.211	0.08	49.67	49.66	1.22	1.20
	4.0	1.220	1.221	0.08	49.68	49.69	1.21	1.21
	5.5	1.120	1.121	0.09	49.66	49.67	1.12	1.12
	8.5	1.170	1.173	0.25	49.65	49.64	1.16	1.16
	10.0	1.250	1.254	0.31	49.63	49.65	1.24	1.25
	12.5	1.230	1.240	0.80	49.64	49.61	1.22	1.21
	16.0	1.220	1.231	0.89	49.62	49.63	1.20	1.21
Rectan-gular plastic bar	2.5	1.250	1.251	0.07	43.29	43.28	1.24	1.25
	4.0	1.200	1.201	0.08	43.29	43.29	1.20	1.20
	5.5	1.100	1.101	0.09	43.30	43.29	1.09	1.10
	8.5	1.150	1.153	0.26	43.28	43.27	1.14	1.13
	10.0	1.310	1.315	0.37	43.25	43.23	1.30	1.31
	12.5	1.250	1.261	0.87	43.21	43.22	1.23	1.24
	16.0	1.240	1.252	0.95	43.19	43.20	1.22	1.23

In Table 5.1, it is shown that the velocity measurement error up to the ranging distance of 10m is less than 0.38%. After 12.5m, the velocity error is increased by more than two times with respect to the ranging distance of 10m. At the moving target distance of 5.5m, the velocity measurement error is 0.09%. The less errors of the velocity measurement is found in the target distance of 2.5m to 10m, and the lowest error is measured at the target distance from 2.5m to 5.5m. It is insisted that the laser beam has perfect detection in this range. The noise interferences on the laser beam detection are increasing gradually at higher ranging distances. It influences the measurement accuracy, see Table 5.1. After the target distance of 10m, the measurement error has increased rapidly. For the distance of 16m, the velocity measurement error is increased at least 0.82% more than the range distance less than 10m for any of the three targets.

It is also evaluated that the velocity measurement by using the correlation of detected contours is more accurate than the velocity measurement by using the start-stop approach. The reason is that at the start-stop approach, the velocity is measured from the detected measured time of the significant points of detected pulses. The time is counted and measured by microprocessor counters. The microprocessor counter has its internal delays. Therefore, the counter also introduced error on the measurement of velocity by the start-stop approach. Contrarily, the velocity by correlation of detected contours is measured considering all points of detection. Therefore, the time of correlation signal ($t_{m,\,crr,\,\max}$, see Section 5.1.4) is achieved, and it has negligible dependence on the first detection time of a target. In Table 5.1, it is shown that the velocity measurement by using the start-stop approach is also varying between both detectors. Since two different detector circuit systems are used the measurement accuracy is also varied.

The velocity measurement accuracy is represented in Figure 5.14(a) and the target surface contour length measurement accuracy is represented in Figure 5.14(b). From Figure 5.14, it is also clear that the ramp shaped target has a maximum accuracy level for both velocity and surface length measurement out of the other two targets. The wooden step target has a lower accuracy level than the other two targets. The main reason is the changing of target surface lengths. At a larger surface length, the measurement time and number of measurements are higher. Therefore, the probability of the measurement time error is low for a target with a larger contour length. The length of the wooden ramp target is 49.7 cm, the rectangular plastic target is 43.4 cm and the wooden step target is 24.9 cm. Since the ramp target has a higher surface

length, the detection probability of the point targets is higher than other targets. So, it can be demonstrated that the detection error becomes less for target with higher surface length.

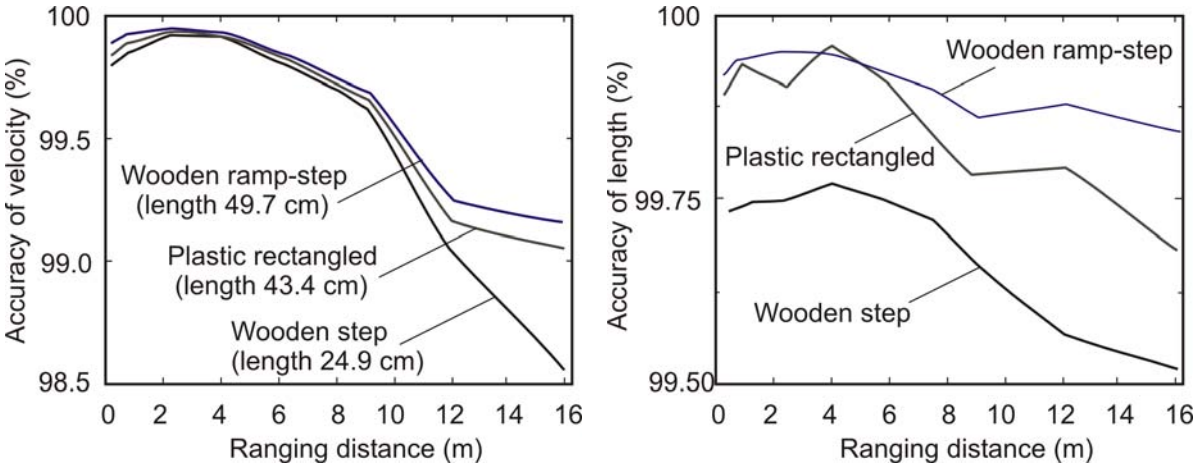

(a) (b)

Figure 5.14 Measured accuracy on velocity and contour length: (a) accuracy of measured velocity, and (b) accuracy of measured target contour length.

It has been evaluated that the accuracy of the velocity measurement is increased with increasing of the length of moving target, see Figure 5.14(a). Moreover, the standard car surface length is between 3.2m to 5m [58, 124]. Therefore, the projected detectable velocity measurement range for car will be from 0 to 150 km/h.

From this developed system, it is possible to detect the wood-block up to 20 m distance without any external signal processing, but for velocity measurement it is suitable up to 16.0 m. The reason of suitable velocity measurement range up to 16.0 m is the signal to noise level interferences that are dominated the threshold of decision V_{t1} and V_{t2} (signal detection is less than 20 mV). The detected reference signal for a target at a distance of 20m is shown in Figure 4.29. From the test measurement, it can also be demonstrated that the system is able to detect the velocity up to 20m distance if an external amplifier with will add after photodetectors in both detectors. Approximated characteristics of the amplifier will be with the bandwidth of 6 GHz (since photodetector rise time is 82 ps), and with gain of 10 dB (since the detection of threshold is 20 mV).

5.4.2 Effect of Angular Variation on System Characteristics

The angular direction of targets to the laser detection beams is analysed in this section. It is performed to characterize the angular directivity of moving targets which can be measured for velocity measurement.

The angular variations on the accuracy level of target velocity and contour are summarized in Table 5.2. To perform this measurement, a wooden target has moved in different angular direction with respect to laser beams. The angular variation of the target moving direction is evaluated for different ranging distances of the targets. In Table 5.2, the ranging distance of a target [wooden ramp shape target has surface length of 49.7 cm, see Figure 5.8(b)] is 8.5m. The ranging distance for angular direction of target is corrected according to Section 4.7 by distance-difference correction. The angular direction (β) is measured by measuring the differences of contour distances according to the background given in Section 4.7. It has also been found that the angular variation on target ranging from 50 cm to 12.5m is almost constant. There are two principle reasons for the constant behaviour of the angular variation of target movement. First, the photodetectors are in an axis with respect to corresponding parallel laser beams, see Section 4.5. Therefore, no target signal from one laser beam to other laser beam is received by the photodetectors. Second, the spot size of the laser beam has varied negligibly with the variation of target distance, see Section 4.5. Therefore, the possibility of laser beam detection from one to other photodetectors is negligible.

Table 5.2 Effect of angular variation on detected velocity and contour

Target	Angular direction of Target (degree)	Velocity by start-stop (m/s)	Velocity by correla-tion (m/s)	Error velocity (%)	Detected length by		Velocity by	
					First detector (cm)	Second detector (cm)	First detector (m/s)	Second detector (m/s)
Ramp shape Wood	0	1.210	1.211	0.09	49.66	49.68	1.22	1.20
	30	1.220	1.221	0.09	49.67	49.69	1.21	1.21
	45	1.150	1.152	0.10	49.67	49.66	1.15	1.14
	50	1.170	1.172	0.11	49.66	49.67	1.18	1.16
	55	1.230	1.252	0.11	49.65	49.64	1.24	1.25
	60	1.220	1.224	0.13	49.64	49.65	1.21	1.23

In Table 5.2, it is shown that the variation of target angular direction has effect on the error level of velocity and contour surface length measurement. However, this variation of error level has no major effect on the accuracy level of the measurement system. For instance, at zero angular degree of target direction, the measured error velocity is 0.09%, but at 60 degrees the error velocity is slightly higher being 0.13%.

The error is also increased on surface contour length measurement. For instance, at the zero angular degree of target direction, the target surface length is measured as 49.68 cm, and the measured error is 0.04%. At the target angular direction of 60 degrees, the measured surface length is 49.65 cm which has the length measurement of 0.10%. The reason is the increase of the laser beam spot size for each measurement of target of detection at the higher angular direction. As a result, the beam scattering is also increased at higher angular direction, and the probability of laser signal detection by photodetector becomes lower. However, the laser radar can also be used at an angle of 60 degrees to the moving targets, see Table 5.2. Therefore, this measurement proved that the laser radar system can be placed in curved streets.

Chapter 6

Experimental Velocity Measurement of Automobile

The practical outdoor measurement of car velocity and contour is presented in this chapter. In both velocity measurement approaches (start-stop approach and correlation approach), the effects of vehicle surface profile variations are also reported. The measurement setup is another factor of system evaluation. The laser system setup of the velocity measurement is also presented for different car contour profiles. The relationship and difference of velocimetry both in indoor and outdoor is reported. The relative variations of the velocity for the variation of laser system for further external factors are also described. Finally, a complete datasheet of the developed pulse laser radar for vehicle velocity measurement is presented.

6.1 Test Car for Outdoor Measurement

The outdoor vehicle velocity and contour for a Mercedes-Benz C180 car with silver coloured surface were measured. It is shown in Figure 6.1.

Figure 6.1 Test car. The solid lines indicate the used scan height.

The measurement was performed by driving this car on a parking place at day time and at ambient temperature of 25 °C. The car has run at different velocities with different distances from the laser radar system. The reason of measuring the car velocity at

different limits is to characterize the laser radar ratings for car as vehicle. The different ranging distances are taken to evaluate the measurement accuracy of distance ranging.

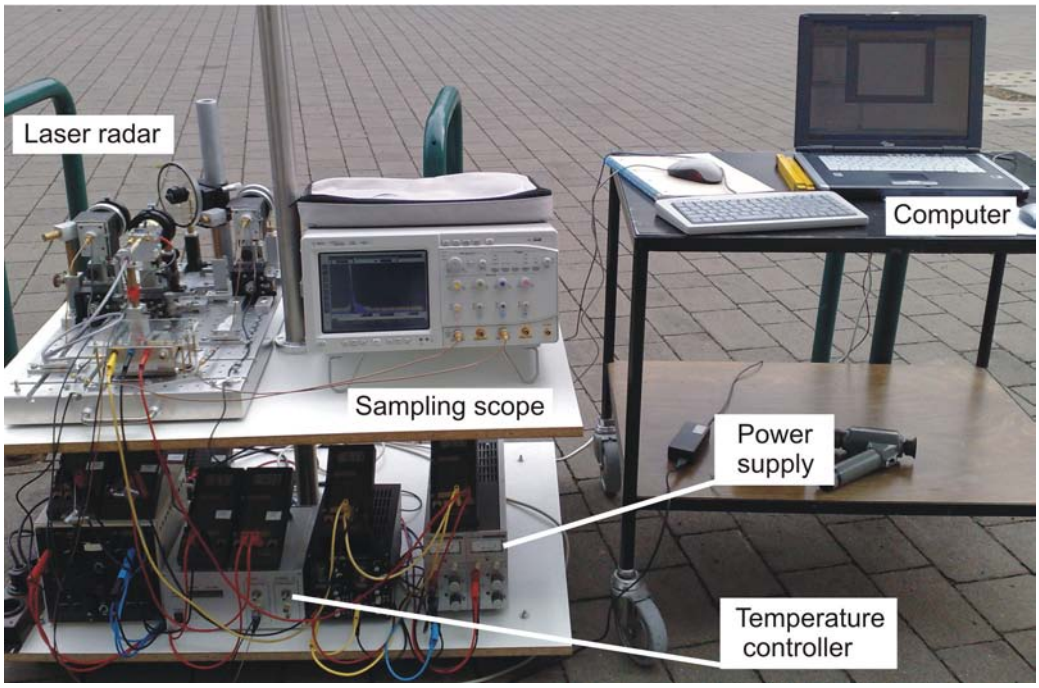

Figure 6.2 Laser radar measurement setup.

However, it is already demonstrated in Chapter 4 that at present the developed laser radar is used to measure the two dimensional contour of the vehicles. Therefore, different scanning lines were also chosen for the measurement of different contour profiles. For example, the vehicle contour is varied from the body to its window frames and also with different scanning lines on the vehicle body. The contour variation with scanning lines happened due to the variation of surface geometry. Three different scanning heights are considered to evaluate the vehicle contour profile measurement, as shown in Figure 6.1. The lowest height of $h_1 = 70$ cm is taken to evaluate the discontinuity of the contour profile due to the presence of tyres on vehicle wheels. The middle height of $h_2 = 80$ cm is taken to evaluate the vehicle full surface profile contour and its accuracy. The upper height of $h_3 = 110$ cm is taken to evaluate the windows frame structure contour of the vehicle.

The laser radar system measurement setup for outdoor environment is shown in Figure 6.2. The radar system is mounted on a movable table as shown in Figure 6.2. The movable table is adjusted at different heights (h_1, h_2, and h_3) and different positions to detect different contour profiles of the car.

6.2 Measurement of Car Contour and Velocity

The measurement of contour and its corresponding velocity are reported in this section for three different scanning heights of h_1, h_2, and h_3. The measured scanning line lengths on the car contour are: The scanning line for h_1 = 422.5 cm, the scanning line for h_2 = 407.2 cm, and the scanning line for h_3 = 200.4 cm, respectively.

6.2.1 Contour and Velocity from Vehicle Body with Wheels

The first measurement is carried out for the car height of $h_1 = 70$ cm. The measured results are shown from Figure 6.3 to Figure 6.8.

In Figure 6.3, two discontinuities (blank contour) on vehicle surface contour are shown. The front side wheel and the back side wheel are the causes of the discontinuities on surface contour. The area of discontinuity from the front side wheel is more than from the back side wheel. The reason is the existing scanning line length variation between both wheels (the scanning line length on front side wheel is longer than on back side wheel), as shown in Figure 6.1. The detected ranging distance of the moving car from both detectors is 510 cm, as shown in Figure 6.3(a) and Figure 6.3(b) for the car driving velocity of $v_r = 8$ km/h. The driving velocity (v_r) is estimated from the tachometer reading of that car. The velocity measured by start-stop approach is evaluated to be $v_{st} = 7.985$ km/h and by correlation approach $v_{crr} = 7.995$ km/h. The velocity measured from detector 1 (v_{d1}) is 7.985 km/h and from detector 2 (v_{d2}) is 7.986 km/h. The scanned contour length was measured as $L_m = 422.49$ cm. The measured velocity error is presented as

$$\text{Velocity error} = \frac{(v_{st} \text{ or } v_{crr}) - v_r}{(v_{st} \text{ or } v_{crr})} \times 100\% \tag{6.1}$$

and by start-stop it is 0.18% and by correlation it is 0.06%. It can be demonstrated that the measured velocity error by start-stop approach is higher than correlation approach. The reason is that at start-stop approach the detected time difference ($\Delta t_m = t_{md2,s} - t_{md2,s}$, according to Section 5.1.3) of both detectors is counted only from time significant points. The measurement time delay of used computer processor and counter are also included on scanning data. Therefore, referring the start-stop approach the error of velocity is higher. On the other hand, regarding the correlation approach, the maximum time difference ($t_{m,crr,\max}$, according to Section 5.1.4) of both

detectors is counted based on the superposition and multiplication of each and every scanned time difference. Therefore, the velocity measurement accuracy by the correlation approach is higher than that by the start-stop approach.

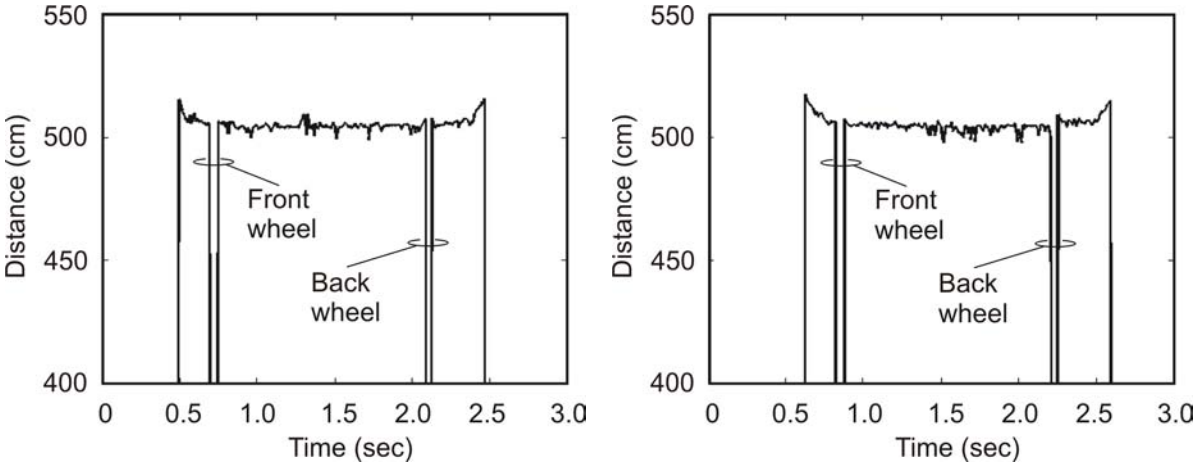

Figure 6.3 Measured car contour at height $h_1 = 70$ cm and velocity $v_r = 8$ km/h: (a) contour detected from detector 1, and (b) contour detected from detector 2. Extracted velocity and car length parameters are: $v_{st} = 7.98$ km/h, $v_{crr} = 7.99$ km/h, $v_{d1} = 7.985$ km/h, $v_{d2} = 7.986$ km/h, and $L_m = 422.49$ cm.

The reason of two major discontinuities (blank contour) on the car contour is the presence of black tyre on the car wheels. The vehicle tyre is one of the highly defused black targets. The light reflectivity from black target is very much less than any other type of target [125–128]. Therefore, the reflected laser signal from a highly diffused black surface (from tyre) is very low to evaluate the tyre contour without any external filter and amplifier. Moreover, the detection of threshold value is chosen to avoid the noise interferences on detected signals (see Chapter 5). As a result, both tyre areas are considered as no target is detected since the detected signal value is less than the threshold of decision. However, to detect the contour of the tyre existence (diffused black target), it is necessary to use external filter to reduce the detected signal noises. Further amplification of the detected signals is also needed. The existence of such discontinuity on vehicle contour has no effect on the measured velocity by the reported method (by start-stop approach and by correlation approach). Therefore, the detection of diffused black target is not included in this dissertation. One of the future extensions of this work can be a work phase to evaluate also the diffused black targets, such as vehicle tyres.

From Figure 6.4 to Figure 6.8, two discontinuities (due to tyres) are also presented on vehicle surface contours. The presence of front side wheel and the back side wheel tyres is assured on scanning line h_1. Moreover in Figure 6.4, the detected ranging distance of the car from both detectors is 495 cm for the car velocity of $v_r = 10$ km/h. The velocity measured by start-stop approach is $v_{st} = 9.98$ km/h and by correlation approach is $v_{crr} = 9.99$ km/h. The velocity measured from detector 1 is $v_{d1} = 9.98$ km/h and from detector 2 it is $v_{d2} = 9.98$ km/h. The detected scanned contour has a length of $L_m = 422.49$ cm. The measured velocity error by start-stop is 0.2% and by correlation is 0.1% according to (6.1).

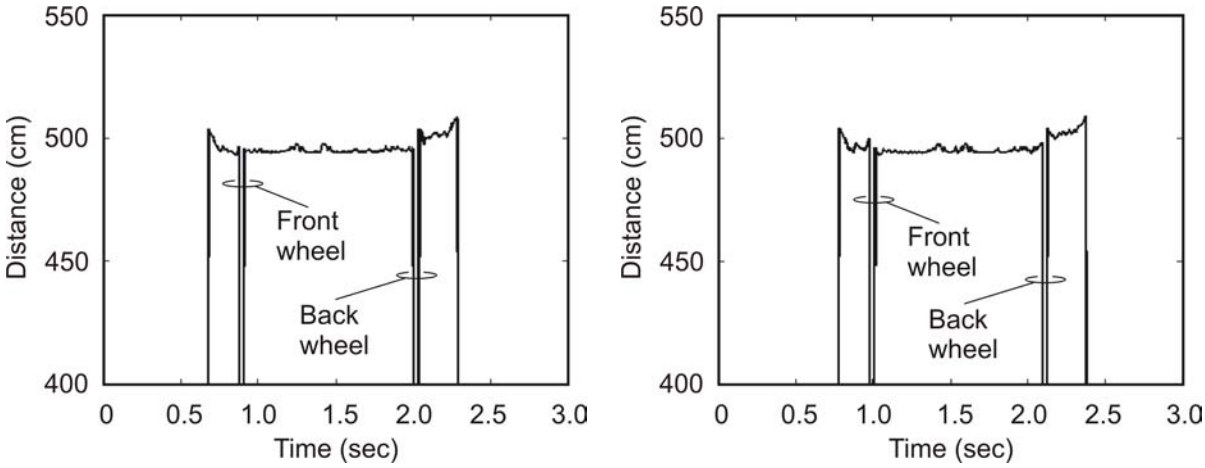

Figure 6.4 Measured car contours at $v_r = 10$ km/h: (a) contour detected from detector 1, and (b) contour detected from detector 2. Extracted velocity and car length parameters are: $v_{st} = 9.98$ km/h, $v_{crr} = 9.99$ km/h, $v_{d1} = 9.98$ km/h, $v_{d2} = 9.98$ km/h, and $L_m = 422.49$ cm.

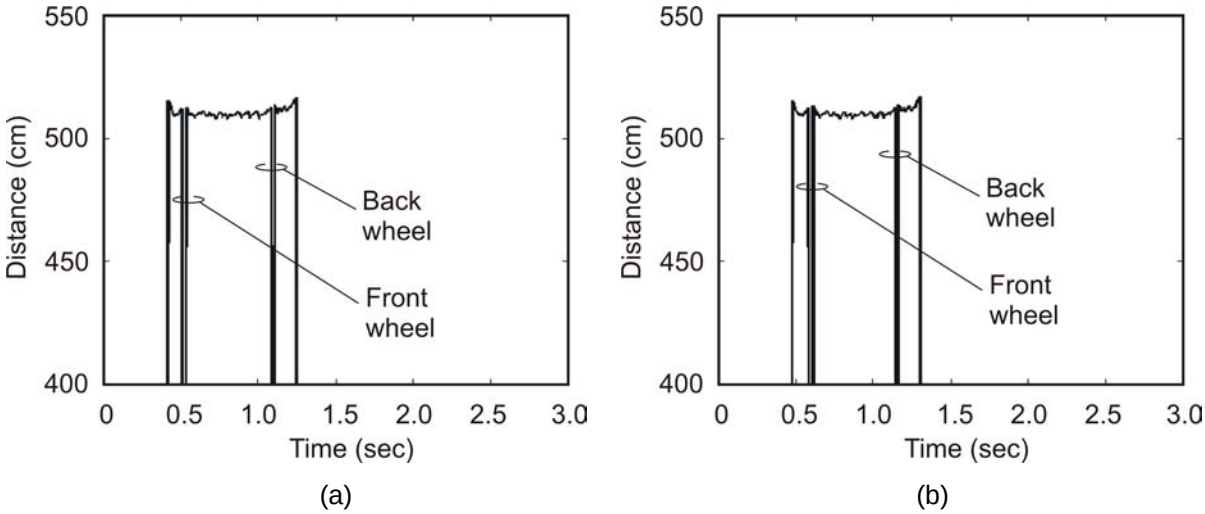

Figure 6.5 Measured of car contours at $v_r = 20$ km/h: (a) contour detected from detector 1, and (b) contour detected from detector 2. Extracted velocity and car length parameters are: $v_{st} = 20.04$ km/h, $v_{crr} = 20.02$ km/h, $v_{d1} = 20.04$ km/h, $v_{d2} = 20.04$ km/h, and $L_m = 422.48$ cm.

In Figure 6.5, the distance to the car detected by both detectors is 520 cm for the car velocity of $v_r = 20$ km/h. The velocity measured by start-stop approach is $v_{st} = 20.04$ km/h and by correlation approach is $v_{crr} = 20.02$ km/h. The velocity measured from detector 1 is $v_{d1} = 20.04$ km/h and from detector 2 it is $v_{d2} = 20.04$ km/h. The detected scanned contour has a length of $L_m = 422.48$ cm. The measured velocity error by start-stop is 0.2% and by correlation is 0.1% according to (6.1).

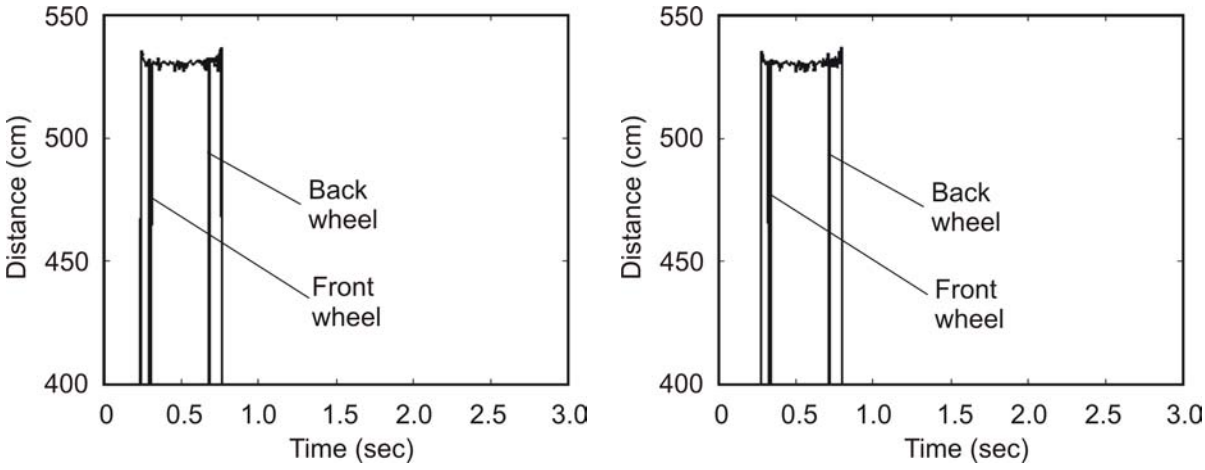

Figure 6.6 Measured car contours at $v_r = 30$ km/h: (a) contour detected from detector 1, and (b) contour detected from detector 2. Extracted velocity and car length parameters are: $v_{st} = 29.93$ km/h, $v_{crr} = 29.97$ km/h, $v_{d1} = 29.93$ km/h, $v_{d2} = 29.93$ km/h, and $L_m = 422.48$ cm.

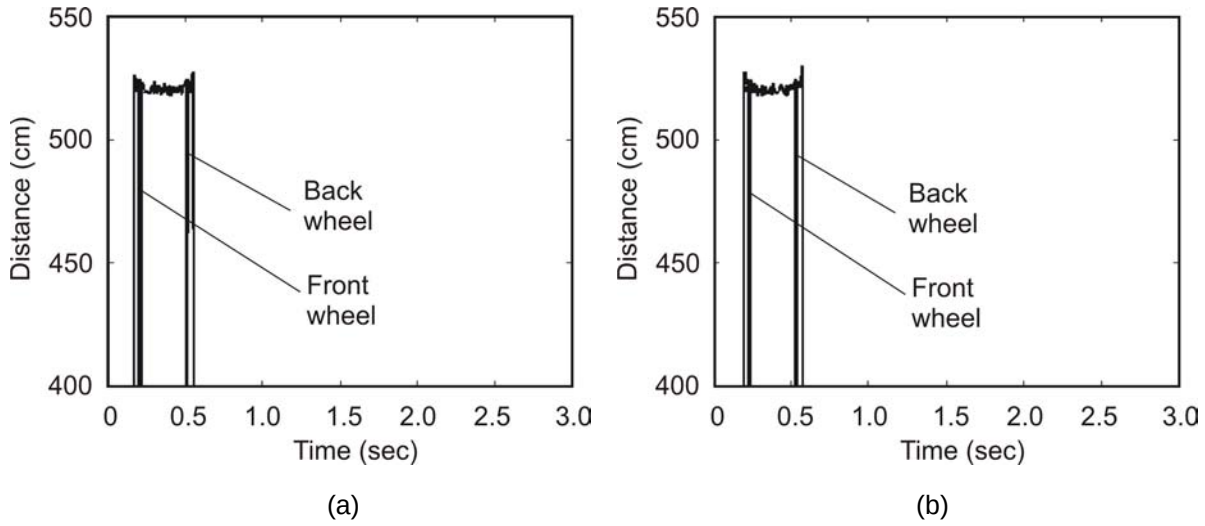

Figure 6.7 Measured car contours at $v_r = 42$ km/h: (a) contour detected from detector 1, and (b) contour detected from detector 2. Extracted velocity and car length parameters are: $v_{st} = 41.90$ km/h, $v_{crr} = 41.95$ km/h, $v_{d1} = 41.90$ km/h, $v_{d2} = 41.90$ km/h, and $L_m = 422.46$ cm.

In Figure 6.6, the distance to the car detected by both detectors is 535 cm for the car velocity of $v_r = 30$ km/h. The velocity measured by start-stop approach of $v_{st} = 29.93$ km/h and by correlation approach of $v_{crr} = 29.97$ km/h. The velocity measured from detector 1 is $v_{d1} = 29.93$ km/h and from detector 2 is $v_{d2} = 29.93$ km/h. The detected scanning contour length is $L_m = 422.48$ cm. The measured error velocity by start-stop is 0.23% and by correlation is 0.1% according to (6.1).

In Figure 6.7, the distance to the car detected by both detectors is 525 cm for the car velocity of $v_r = 42$ km/h. The velocity measured by start-stop approach is $v_{st} = 41.90$ km/h and by correlation approach is $v_{crr} = 41.95$ km/h. The velocity measured from detector 1 is $v_{d1} = 41.90$ km/h and from detector 2 is $v_{d2} = 41.90$ km/h. The detected scanned contour length is $L_m = 422.46$ cm. The measured velocity error by start-stop is 0.23% and by correlation is 0.12% according to (6.1).

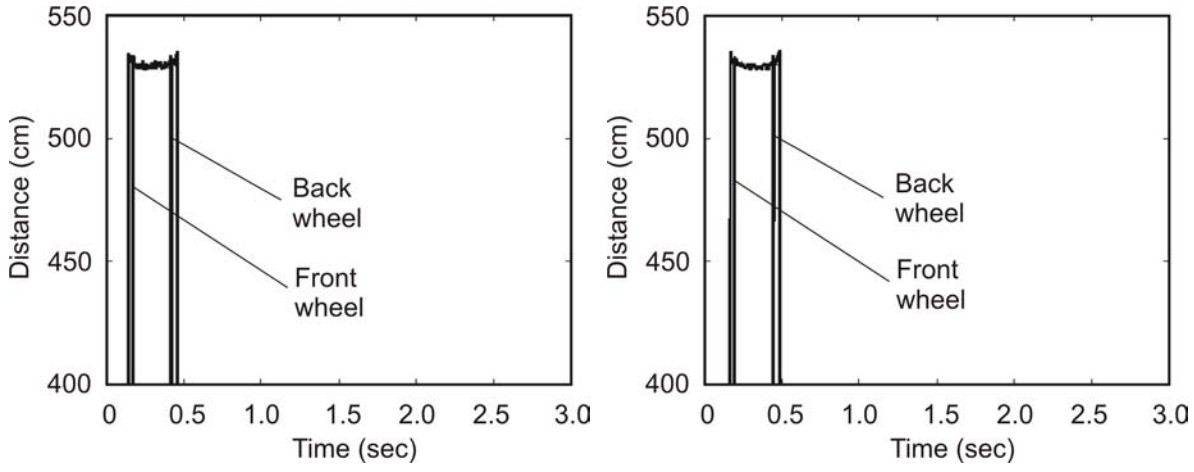

Figure 6.8 Measured car contours at $v_r = 50$ km/h: (a) contour detected from detector 1, and (b) contour detected from detector 2. Extracted velocity and car length parameters are: $v_{st} = 49.88$ km/h, $v_{crr} = 49.93$ km/h, $v_{d1} = 49.87$ km/h, $v_{d2} = 49.89$ km/h, and $L_m = 422.44$ cm.

In Figure 6.8, the distance to the car detected by both detectors is 535 cm for the car velocity of $v_r = 50$ km/h. The velocity measured by start-stop approach is $v_{st} = 49.88$ km/h and by correlation approach is $v_{crr} = 49.93$ km/h. The velocity measured from detector 1 is $v_{d1} = 49.88$ km/h and from detector 2 is $v_{d2} = 49.88$ km/h. The detected scanned contour length is $L_m = 422.44$ cm. The measured error velocity by start-stop is 0.24% and by correlation is 0.14% according to (6.1).

The measurement of vehicle contour and velocity for the scanning line h_1 height of 70 cm is taken for ranging distance up to 10m. The discussed Figures 6.3 to 6.8 show the result within a range interval of 5m to 6m to present and idealize the car velocity measurement parameters for a certain ranging distance. The other reason is to visualize the variation of measurement accuracy for the certain ranging distance. If the measurement accuracy for several distance intervals are known then it can be easily extracted by further signal processing. However, from the measurement result it has been evaluated that the ranging distance up to 12.5m has no effect on the velocity. After 12.5m the detected car contour was not errorless. It is because of the low signal level of detection after 12.5m distance. The analysis of measurement velocity and the effect of scanning line variations are presented in Section 6.3.

6.2.2 Contour and Velocity of Vehicle Body

The following measurements have been carried out at the scanning line height of $h_2 = 80$ cm. In Figure 6.1, it is shown that at this height the car surface is only the metal body. Therefore, there is no diffused area (such as a black body) existing along this scanning line.

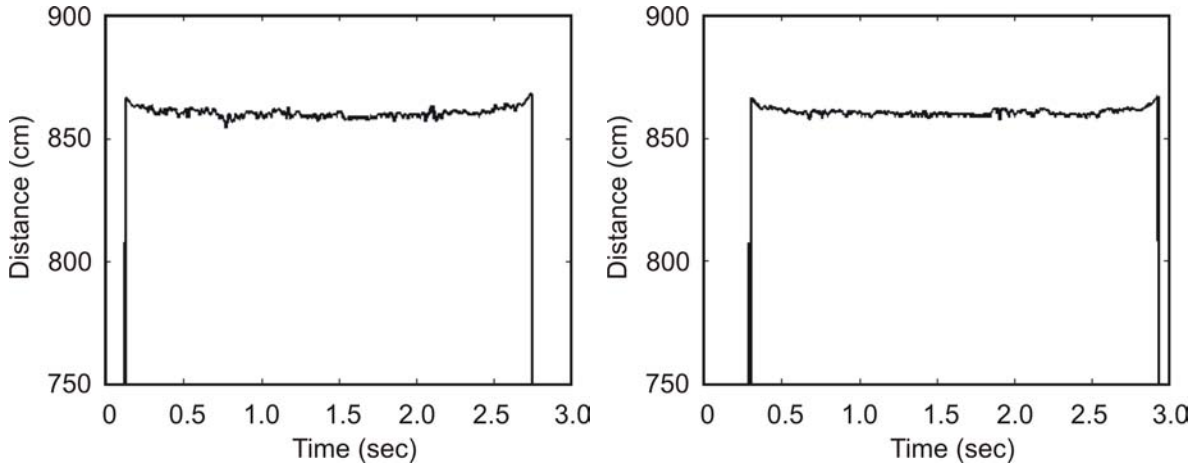

Figure 6.9 Car body contours at height $h_2 = 80$ cm and velocity $v_r = 6$ km/h. Measured by (a) detector 1, and (b) detector 2. Extracted velocity and car length parameters are: $v_{st} = 5.99$ km/h, $v_{crr} = 6.0$ km/h, $v_{d1} = 5.99$ km/h, $v_{d2} = 5.99$ km/h, and $L_m = 407.19$ cm.

In Figure 6.9, the distance to the car detected by both detectors is 865 cm for the car velocity of $v_r = 6$ km/h. The measured velocity by start-stop approach is $v_{st} = 5.99$ km/h and by correlation approach is $v_{crr} = 6.0$ km/h. The measured velocity from

detector 1 is $v_{d1} = 5.99$ km/h and from detector 2 is $v_{d2} = 5.99$ km/h. The detected scanned contour length is $L_m = 407.19$ cm. The measured velocity error by start-stop is 0.16% and by correlation is 0% according to (6.1).

In Figure 6.10, the distance to the car detected by both detectors is 750 cm for the car velocity of $v_r = 10$ km/h. The measured velocity by start-stop approach is $v_{st} = 9.98$ km/h and by correlation approach of $v_{crr} = 9.99$ km/h. The velocity measured from detector 1 is $v_{d1} = 9.98$ km/h and from detector 2 is $v_{d2} = 9.98$ km/h. The detected scanned contour length is $L_m = 407.17$ cm. The measured velocity error by start-stop is 0.2% and by correlation is 0.1% according to (6.1).

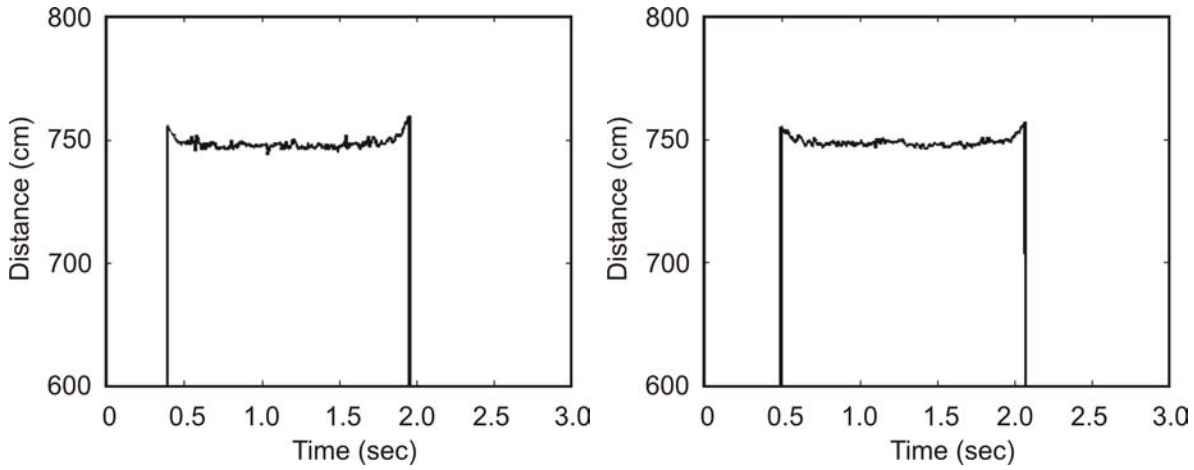

Figure 6.10 Car body contours at height $h_2 = 80$ cm and velocity $v_r = 10$ km/h. Measured by (a) detector 1, and (b) detector 2. Extracted velocity and car length parameters are: $v_{st} = 9.98$ km/h, $v_{crr} = 9.99$ km/h, $v_{d1} = 9.98$ km/h, $v_{d2} = 9.98$ km/h, and $L_m = 407.17$ cm.

In Figure 6.11, the distance to the car detected by both detectors is 740 cm for the car velocity of $v_r = 20$ km/h. The velocity measured by start-stop approach is $v_{st} = 19.95$ km/h and by correlation approach is $v_{crr} = 19.98$ km/h. The velocity measured from detector 1 is $v_{d1} = 19.95$ km/h and from detector 2 is $v_{d2} = 19.95$ km/h. The detected scanned contour length is $L_m = 407.16$ cm. The measured velocity error by start-stop is 0.25% and by correlation is 0.1% according to (6.1).

In Figure 6.12, the distance to the car detected by both detectors is 750 cm for the car velocity of $v_r = 30$ km/h. The measured velocity by start-stop approach is $v_{st} = 29.93$ km/h and by correlation approach is $v_{crr} = 29.98$ km/h. The measured velocity from

detector 1 is $v_{d1} = 29.93$ km/h and from detector 2 is $v_{d2} = 29.92$ km/h. The detected scanned contour length is $L_m = 407.15$ cm. The measured error velocity by start-stop is 0.23% and by correlation is 0.07% according to (6.1).

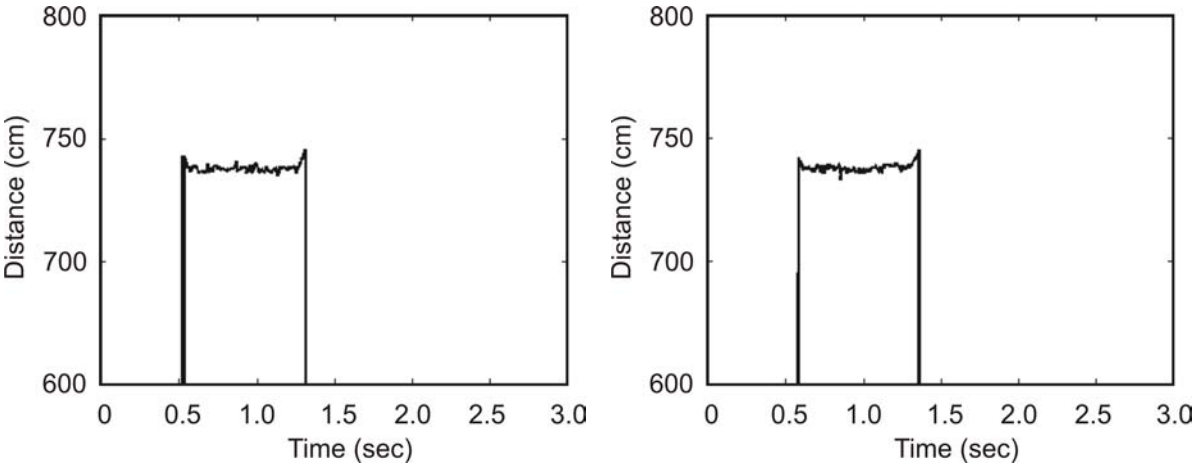

(a) (b)

Figure 6.11 Car body contours at height $h_2 = 80$ cm and velocity $v_r = 20$ km/h. Measured by (a) detector 1, and (b) detector 2. Extracted velocity and car length parameters are: $v_{st} = 19.95$ km/h, $v_{crr} = 19.98$ km/h, $v_{d1} = 19.95$ km/h, $v_{d2} = 19.95$ km/h, and $L_m = 407.16$ cm.

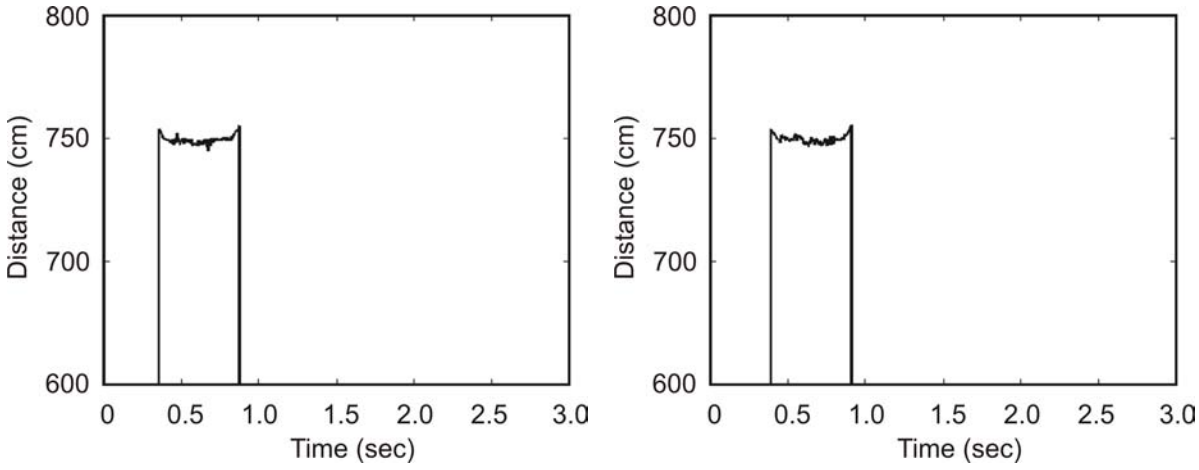

(a) (b)

Figure 6.12 Car body contours at height $h_2 = 80$ cm and velocity $v_r = 30$ km/h. Measured by (a) detector 1, and (b) detector 2. Extracted velocity and car length parameters are: $v_{st} = 29.93$ km/h, $v_{crr} = 29.98$ km/h, $v_{d1} = 29.93$ km/h, $v_{d2} = 29.92$ km/h, and $L_m = 407.15$ cm.

In Figure 6.13, the distance to the car detected by both detectors is 775 cm for the car velocity of $v_r = 38$ km/h. The measured velocity by start-stop approach is $v_{st} = 37.91$ km/h and by correlation approach is $v_{crr} = 37.96$ km/h. The measured velocity from

detector 1 is $v_{d1} = 37.91$ km/h and from detector 2 is $v_{d2} = 37.91$ km/h. The detected scanned contour length is $L_m = 407.16$ cm. The measured velocity error by start-stop is 0.24% and by correlation is 0.1%.

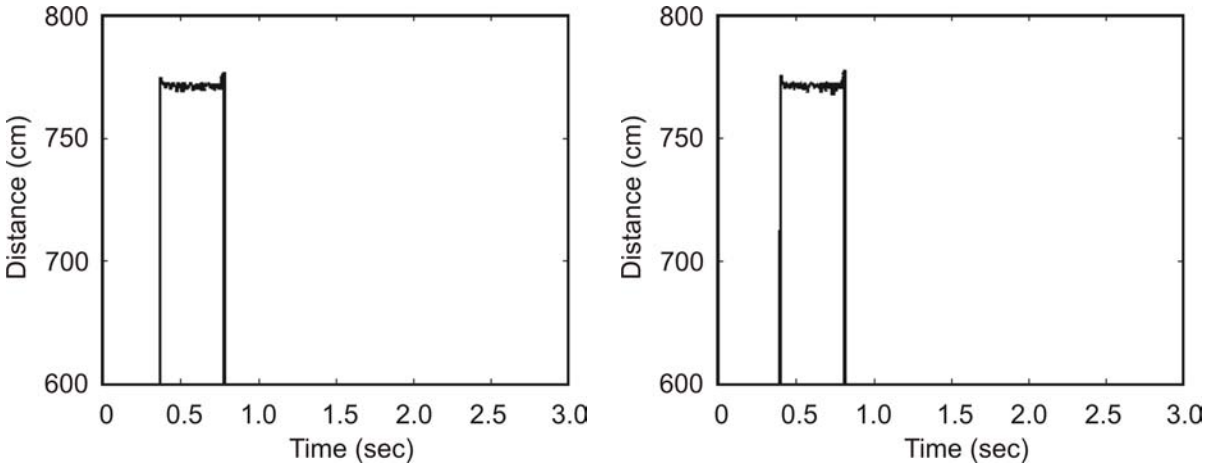

Figure 6.13 Car body contours at height $h_2 = 80$ cm and velocity $v_r = 38$ km/h. Measured by (a) detector 1, and (b) detector 2. Extracted velocity and car length parameters are: $v_{st} = 37.91$ km/h, $v_{crr} = 37.96$ km/h, $v_{d1} = 37.92$ km/h, $v_{d2} = 37.90$ km/h, and $L_m = 407.16$ cm.

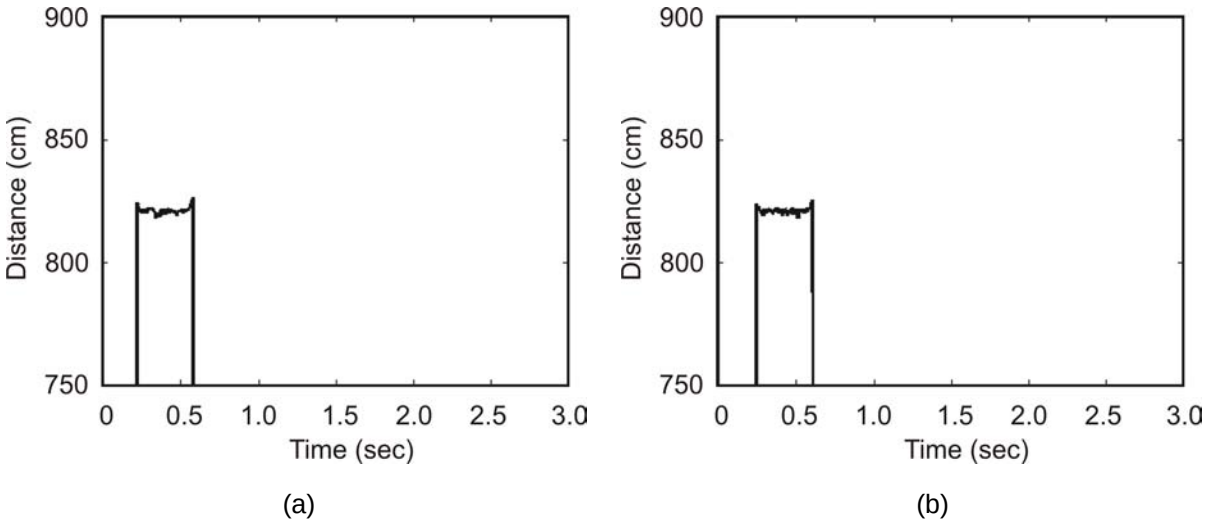

Figure 6.14 Car body contours at height $h_2 = 80$ cm and velocity $v_r = 50$ km/h. Measured by (a) detector 1, and (b) detector 2. Extracted velocity and car length parameters are: $v_{st} = 49.87$ km/h, $v_{crr} = 49.94$ km/h, $v_{d1} = 49.87$ km/h, $v_{d2} = 49.87$ km/h, and $L_m = 407.14$ cm.

In Figure 6.14, the distance to the car detected by both detectors is 830 cm for the car velocity of $v_r = 50$ km/h. The measured velocity by start-stop approach is $v_{st} = 49.87$ km/h and by correlation approach is $v_{crr} = 49.94$ km/h. The measured velocity from detector 1 is $v_{d1} = 49.87$ km/h and from detector 2 is $v_{d2} = 49.87$ km/h. The detected

scanned contour length is $L_m = 407.14$ cm. The measured velocity error by start-stop is 0.26% and by correlation is 0.12%.

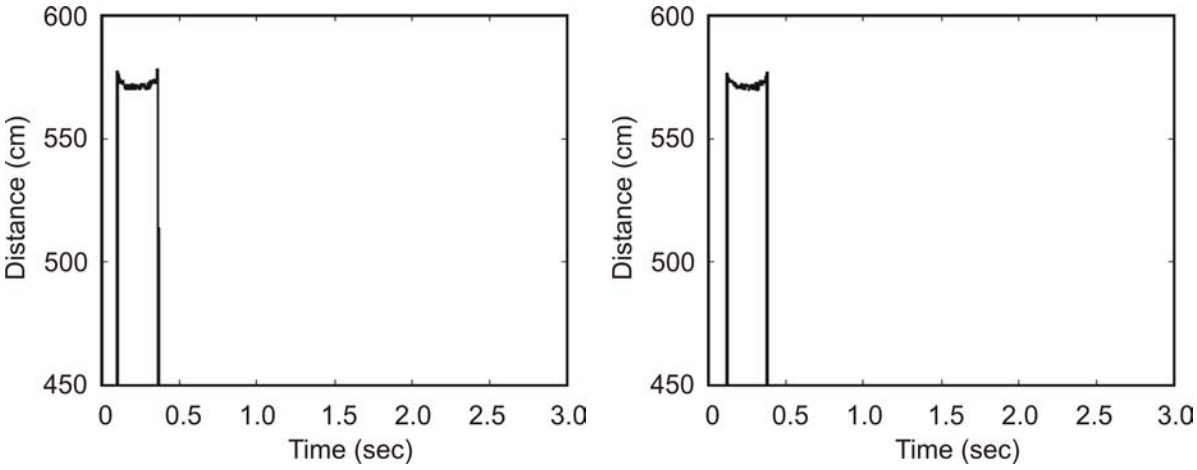

Figure 6.15 Car body contours at height $h_2 = 80$ cm and velocity $v_r = 60$ km/h. Measured by (a) detector 1, and (b) detector 2. Extracted velocity and car length parameters are: $v_{st} = 59.84$ km/h, $v_{crr} = 59.93$ km/h, $v_{d1} = 59.85$ km/h, $v_{d2} = 59.83$ km/h, and $L_m = 407.11$ cm.

In Figure 6.15, the distance to the car detected by both detectors is 580 cm for the car velocity of $v_r = 60$ km/h. The measured velocity by start-stop approach is $v_{st} = 59.84$ km/h and by correlation approach is $v_{crr} = 59.93$ km/h. The measured velocity from detector 1 is $v_{d1} = 59.85$ km/h and from detector 2 is $v_{d2} = 59.83$ km/h. The detected scanned contour length is $L_m = 407.11$ cm. The measured error velocity by start-stop is 0.27% and by correlation is 0.11% according to (6.1).

From the measurement of 2D contour from Figures 6.9 to 6.15, it is also shown that there is no major discontinuity on the detected contours of the car body. As it is approximated, the vehicle metal body has highest signal reflection compared to other parts of the vehicle body. Therefore, the detected signals also have almost no errors. It can be demonstrated that most of all number of measurement from of vehicle metal body in scanning line h_2 are detected by the laser radar system. Further vehicle analysis regarding scanning lines on car body is reported in Section 6.3.

6.2.3 Contour and Velocity from Car Windows Frame

This measurement was carried out on the scanning line height of $h_3 = 110$ cm. In Figure 6.1, it is shown that at this scanning line the car surface has two metal frames around glass windows. It is also shown in Figure 6.1 that two pure black bars also exist in this scanning line.

The measured contours from the car windows frames are presented in Figures 6.16 to 6.20. The measurement velocities are also reported with figure captions. In those measurements, the detected contour length L_m is the length from front side frame to back side frame in the scanning line h_3, rest of the parameters are as before.

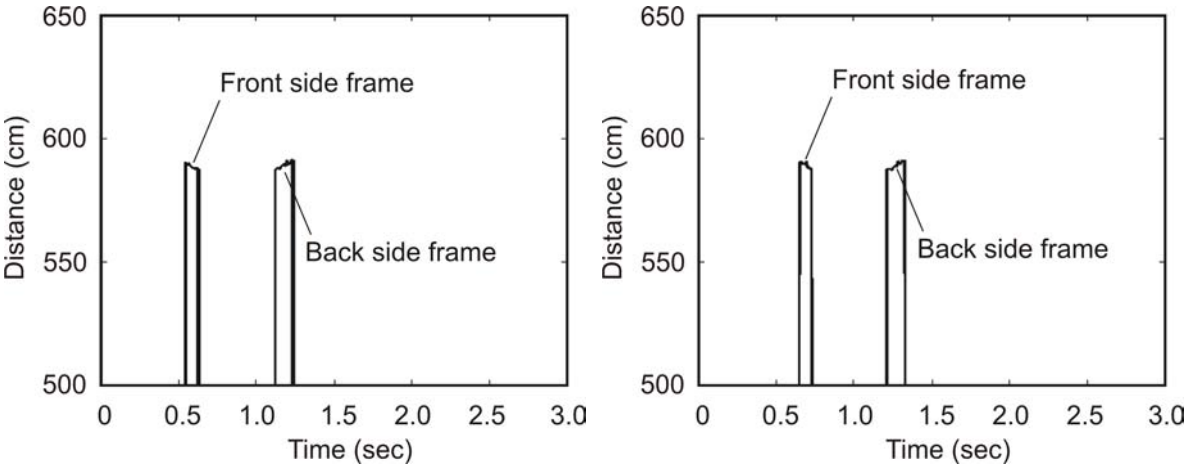

Figure 6.16 Car windows frame contours at velocity $v_r = 10$ km/h. Measured by (a) detector 1, and (b) detector 2. Extracted velocity and windows length parameters are: $v_{st} = 9.96$ km/h, $v_{crr} = 9.98$ km/h, $v_{d1} = 9.96$ km/h, $v_{d2} = 9.96$ km/h, $L_m = 200.25$ cm, velocity error by start-stop = 0.40%, and velocity error by correlation = 0.20%.

From the measured contours, the front side metal frame and the back side metal frame are only detected by the laser radar system. The reason is the selection of the level of threshold decision. Moreover, the detected signals by detectors from the reflected signal from the pure black bars and window glasses are less than the level of threshold detection. Therefore, those areas are considered as no target of detection. However, the target with pure black surface and transparent glass are not included with this work. A future extension of this work can be to evaluate the detection criteria of different diffused materials. Moreover, it is also illustrated in

Figure 6.16 to Figure 6.20 that the back side frame is wider than the front side frame. It is practically symmetrical to the test car windows frames, shown in Figure 6.1.

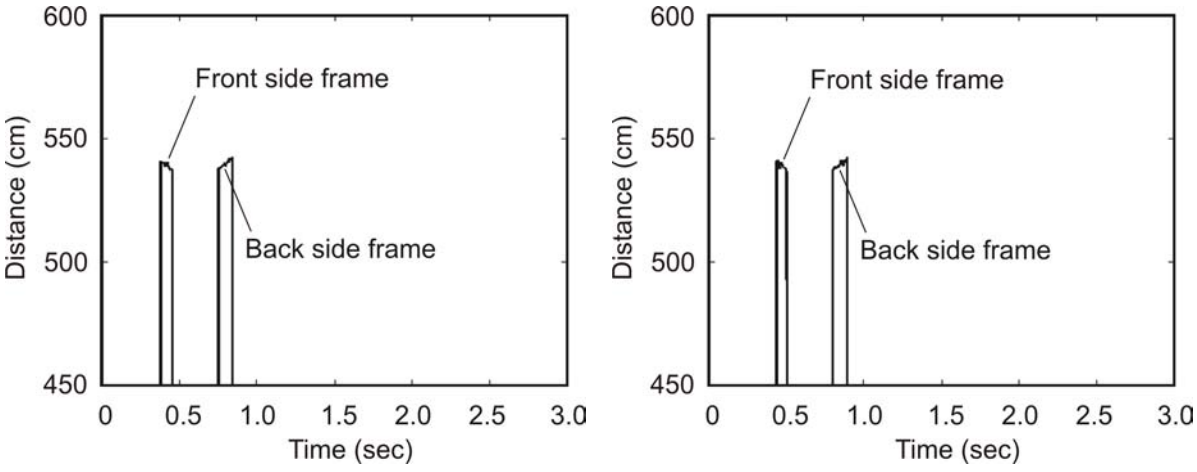

Figure 6.17 Car windows frame contours at velocity $v_r = 20$ km/h. Measured by (a) detector 1, and (b) detector 2. Extracted velocity and windows length parameters are: $v_{st} = 9.96$ km/h, $v_{crr} = 9.98$ km/h, $v_{d1} = 9.96$ km/h, $v_{d2} = 9.96$ km/h, $L_m = 200.22$ cm, velocity error by start-stop = 0.40%, and velocity error by correlation = 0.20%.

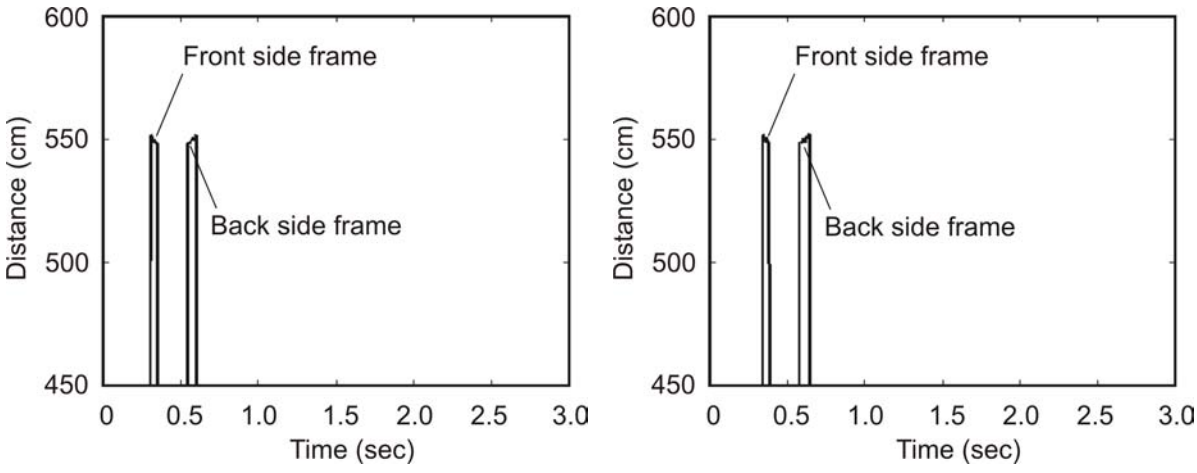

Figure 6.18 Car windows frame contours at velocity $v_r = 30$ km/h. Measured by (a) detector 1, and (b) detector 2. Extracted velocity and windows length parameters are: $v_{st} = 29.87$ km/h, $v_{crr} = 29.93$ km/h, $v_{d1} = 29.87$ km/h, $v_{d2} = 29.87$ km/h, $L_m = 200.21$ cm, velocity error by start-stop = 0.43%, and velocity error by correlation = 0.23%.

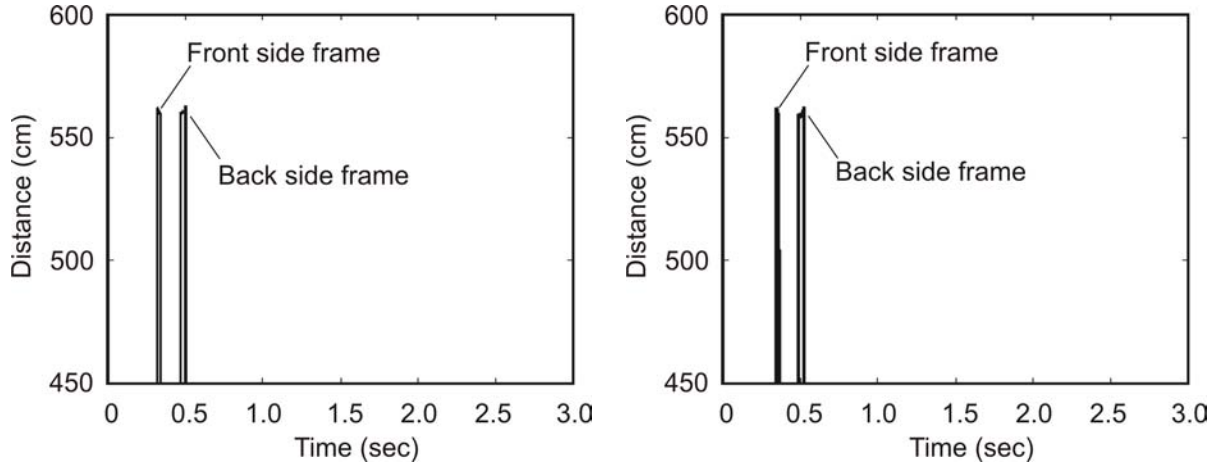

Figure 6.19 Car windows frame contours at velocity $v_r = 40$ km/h. Measured by (a) detector 1, and (b) detector 2. Extracted velocity and windows length parameters are: $v_{st} = 39.82$ km/h, $v_{crr} = 39.91$ km/h, $v_{d1} = 39.83$ km/h, $v_{d2} = 39.81$ km/h, $L_m = 200.10$ cm, velocity error by start-stop = 0.45%, and velocity error by correlation = 0.21%.

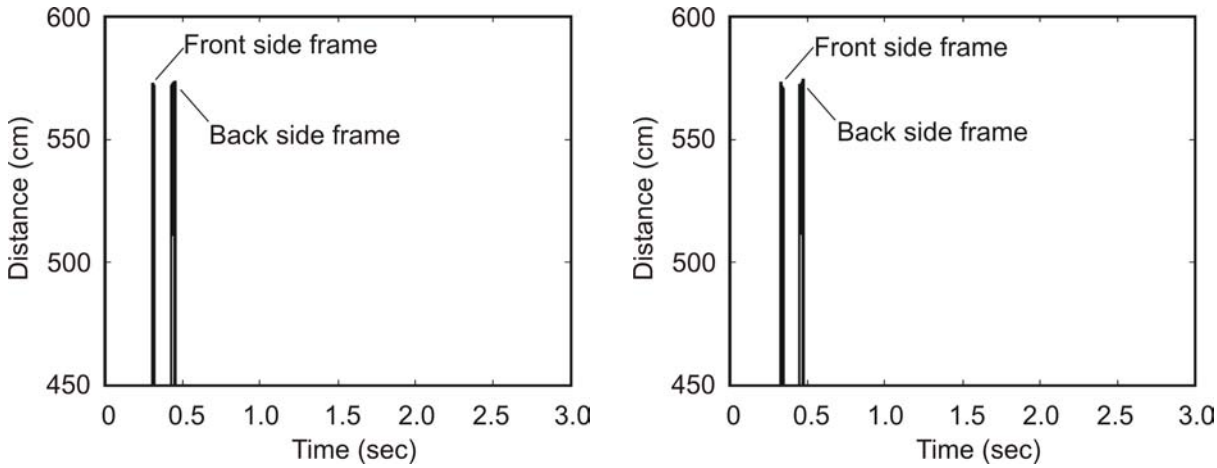

Figure 6.20 Car windows frame contours at velocity $v_r = 50$ km/h. Measured by (a) detector 1, and (b) detector 2. Extracted velocity and windows length parameters are: $v_{st} = 49.75$ km/h, $v_{crr} = 49.84$ km/h, $v_{d1} = 49.74$ km/h, $v_{d2} = 49.76$ km/h, $L_m = 200.04$ cm, velocity error by start-stop = 0. 50%, and velocity error by correlation = 0.32%.

6.3 Vehicle Velocity Analysis

The accuracy level of the measured velocities for the test car is demonstrated in this section. As three different scanning lines are taken to evaluate the car contour and velocity, therefore, the measurement accuracy of different scanning line are also evaluated in this section. The measured accuracy of velocity is presented as

$$\text{Accuracy of velocity} = \frac{(v_{st} \text{ or } v_{crr})}{v_r} \times 100\% \qquad \text{for} \quad (v_{st} \text{ or } v_{crr}) < v_r$$

$$= \frac{v_r}{(v_{st} \text{ or } v_{crr})} \times 100\% \qquad \text{for} \quad (v_{st} \text{ or } v_{crr}) > v_r \tag{6.2}$$

The accuracy level of car velocity measurement is reported in Figure 6.21 for vehicle distance to 8m, according to (6.2). Moreover, it is already reported that parallel laser beams with the same characteristics (synchronized, same optical properties) are used for tracking the targets. Therefore, the ranging distance variations have no effect on the measurement system. Moreover, it is also described that the measurement of the velocity is evaluated for the start-stop approach and for the precision correlation approach. The measured accuracy variations of the test car velocity for both approaches are also reported in Figure 6.21. The level of accuracy illustrations of three scanning lines are followed in Figure 6.21(a) for scanning line h_1, Figure 6.21(b) for scanning line h_2, and Figure 6.21(c) for scanning line h_3. Relative variations of car velocity measurement accuracy for three different scanning lines can be easily demonstrated from Figure 6.21.

In Figure 6.21, it is also proven that the velocity measurement based on correlation of both detected contours is the best approach. The achieved velocity measurement accuracy by correlation approach is more than 99.75% for the car velocity up to 60 km/h. For instance at the velocity 60 km/h, the measured accuracy of velocity by correlation approach is 1.5 times more than start-stop approach. Moreover, in simple start-stop approach, the error occurs from the used radar circuit system and also from used pulse repletion frequency. The error signals which are detected by photodetectors are also the reason for lower accuracy measured by the start-stop approach. Therefore, it is hardly possible to achieve the measurement accuracy by the start-stop approach as high as by the correlation approach. However, the measurement accuracy of car velocity by the start-stop approach is also achieved more than quite satisfaction according to the German norm [56], see Section 2.3. The reasons are the use of short pulse (rise time 28 ps) laser in the transmitter with pulse repetition frequency of 37.5 kHz and high sensitive (rise time 82 ps and 50 A/W) photodetectors in the receiver of the laser radar system.

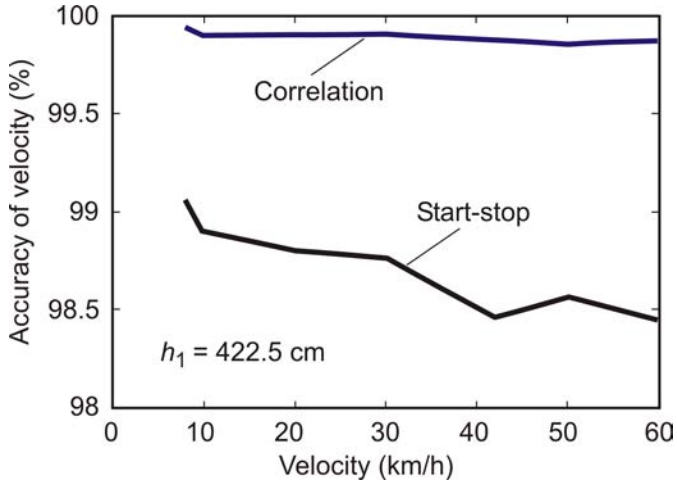

(a)

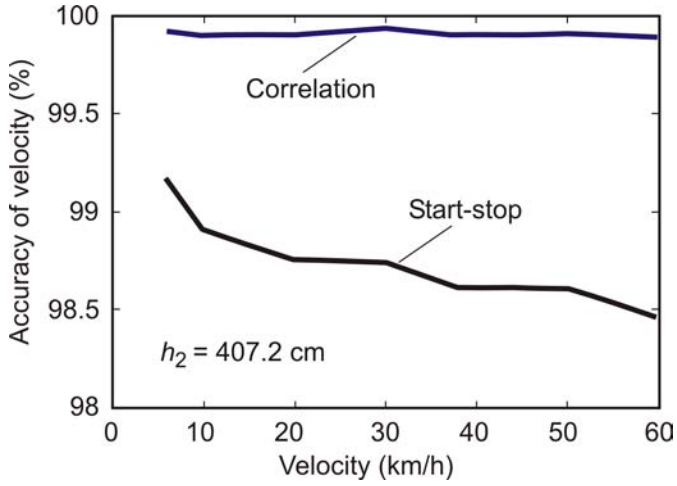

(b)

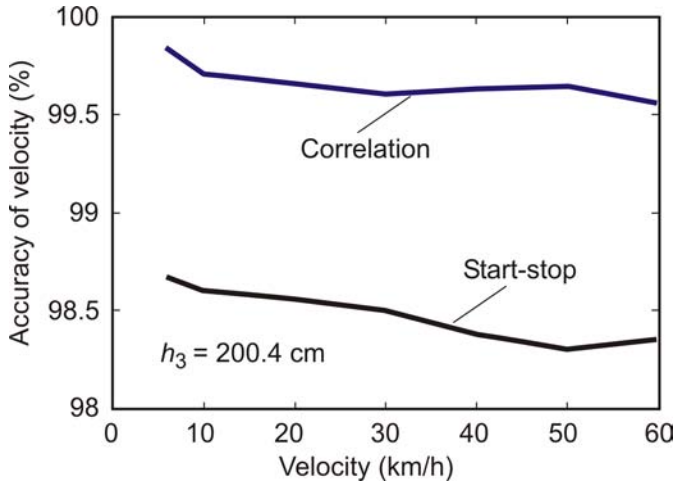

(c)

Figure 6.21 The accuracy level of measured velocities. Differences of measured accuracy of start-stop and correlation approaches for (a) scanning line of h_1, (b) scanning line of h_2, and (c) scanning line of h_3.

It is also demonstrated that in case of the correlation approach, the superposition of both contour signals is considered. The time differences of every measurement from both contours are evaluated to achieve the maximum value of elapsed time to cross through parallel laser beams by moving target. Therefore, the accuracy of correlation approach is highest for velocity measurement. As every measurement of detected target surfaces is considered in the correlation approach, therefore, the accuracy of correlation approach is varied with the variation of target contour length. It is also evaluated that at a higher contour length the accuracy of the correlation approach is also higher. In Figure 6.21, it is proven that at the scanning line of h_2 the accuracy is higher compared to h_1 and h_3; it is 99.85%. The reason is that the car contours length on h_2 is the longest (422.5 cm). At the scanning line h_3 the accuracy level is lower (99.5%) compared to h_1 and h_2, because the car contour scanning length is the shortest (200.4 cm) in h_3.

The velocity analyses from Figure 6.21 demonstrate that the highest accuracy of velocity measurement is achieved from the scanning on vehicle body.

***Evaluation of Vehicle Length Measurement*:** The achieved car contour length measurement accuracy is represented in Figure 6.22 for the discussed scanning lines. The length measurement accuracy is 99.5% achieved for the scanning line (for h_1) length of 422.5 cm. The fundaments of length measurement errors are described in Section 3.4. Furthermore, the used computer delay, counter delay and sampling scope delay are the causes of lower accuracy than the given length of the moving target. The length measurement accuracy for scanning lines of h_2 is approximately more than scanning line of h_1, as shown in Figure 6.22. It is to notify that the scanning line lengths of h_1 and h_2 are 422.5 and 407.2 cm respectively. Therefore, the measurement accuracy for h_1 have to be higher than for h_2 because the scanning length of h_1 is longer than h_2. The existence of two contour discontinuity on h_1 due to wheel tyres has reduced the number of point targets on it compared to h_2. As a result, measurement accuracy for h_2 is highest with compared to h_1 and h_3. Again, the scanning line h_3 has lowest accuracy of 99.8% up to 60 km/h. The reason of the scanning line length on h_3 is 200.4 cm with contour discontinuity due to windows. However, the car length measurement is

achieved more than 99.5% for the velocity up to 60 km/h by the developed laser radar system.

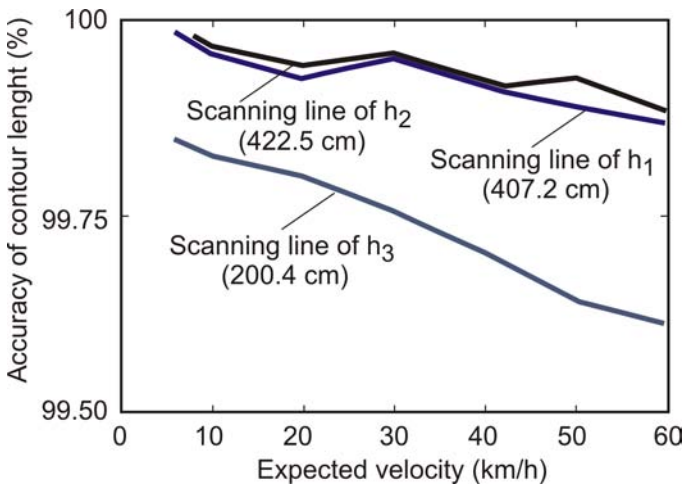

Figure 6.22 The measured accuracy of car contour length of three different scanning lines.

6.4 Laser Radar Datasheet

The characteristic specifications data of the developed laser radar are summarized in this section for the measurement of contour and precise velocity.

Control unit

Trigger pulse:	PRF	37.5 kHz
	Pulse width	20 ns
	Peak pulse	5V

Laser transmitter

Current pulse generator:	Switching device	avalanche BJT transistor
	Rise time	2.26 ns
	Pulse width	4 ns
	Peak pulse	40A
Laser pulse generator:	Laser diode	GaAs SH LD-62
	Laser class	Class 1
	Optical wavelength	904 nm (IR)
	Optical impulse	375 Watts
	Average radiation	510 μW @ PRF 37.5 kHz

	Rise time	28 ps
	Pulse width (FWHM)	32 ps
	Emitting area	152 μm ×2.02 μm
	Laser radiation angle	16°
Laser beam:	System	two parallel beams
	Spot size	0.65 cm at 2m distance
	Average laser radiation	140 μW
	Maximum peak pulse	98 Watts
	Laser class	Class-1, eye-safe

Photodetector

Photodiode:	Device	Si avalanche photodiode
	Chip type	APD-230
	Wavelength	400 nm to 1100 nm
	Maximum response	50 A/W @ λ = 800 nm
	Rise time	82 ps
	Pulse width (FWHM)	180 ps
	Active area	0.042 mm^2 (diameter: 230 μm)
	Dark current	0.6 nA (typically for M = 100)
	Operating temperature	-20 °C to 70 °C
Detector Bias Network:	Bandwidth	DC to 13.5 GHz
	Transmission loss	0.5 dB
	Reflection loss	20 dB
	Operating range	DC to 300V

Laser radar system

Radar:	Laser class	Class-1
Measuring beams:	Two parallel laser beams	
	Beam separation	28.8 cm
	Spot size	0.65 cm
	Average radiation	140 μW
	Maximum peak impulse	98 Watts
Measuring range:	Ranging distance	20 cm to 15.5m

	Distance uncertainty	0.75 cm
Length Measurement:	Estimated accuracy	98.4% for target length 25 cm, and velocity 1.2 m/s
		99.5% for car with velocity 60km/h
Velocity Measurement:	Estimated accuracy	97.5% for target length 25 cm, and velocity 1.2 m/s
		98.5% for car with velocity 60km/h.
	Technique	Correlation, in Figure 6.23
		Simple start-stop, in Figure 6.23.

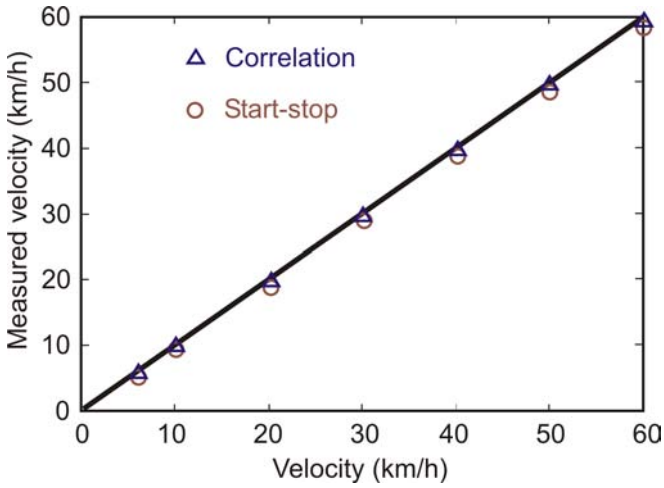

Figure 6.23 Relative variation of the measurement velocity with respect to the estimated velocity.

Chapter 7

Conclusion and Future Work

In this thesis, a near-field pulse laser radar system has been developed for precise vehicle velocity measurement, along with contour profiling and ranging distance. For precise velocity measurement, the elapsed time of moving vehicles to cross parallel laser beams in known distance is used. The parallel laser beams are synchronized and calibrated to achieve a fixed distance in base distance. Two methods are used to measure the precise elapsed time of moving vehicles. These are simple start-stop and correlation approaches. The TOF principle is used to detect the vehicle contour profile and ranging. The eye safe class-1 laser system with very short laser pulses (rise time 28 ps and pulse width 32 ps), based on TOF principle is used to detect the targets with a pulse repetition frequency of 37.5 kHz. Two highly sensitive (50 A/W) avalanche type photodetectors are used to detect the reflected signals from the targets. To reduce the nonlinearity of photodetection techniques, the broadband biasing networks are developed. These high voltage bias networks operate from DC to 13.5 GHz and up to the supply voltage of 300V with transmission loss of 0.8 dB. The parasitic effects of the photodetectors are reduced by incorporating gold wire bonding (2 mm long and 25 μm diameter) of APD230 chip with a 50Ω SMA female connector. The achieved rise time is of 82 ps at the developed photodetector circuits.

The laboratory and real-life tests presented in this thesis prove that the pulse laser radar sensor system using two parallel laser beams is capable of detecting the precise vehicle velocity, contour, length and ranging for multiple-targets in bi-directions. Therefore, such pulse laser radar is suitable for tracking the velocity of the vehicles in highly congested traffic and even in curvy road conditions. The velocity measurements from the correlation of both detected contours are of great demand in applications of parallel beam laser radar system for vehicle velocity measurement. As a result, the achieved accuracy at the velocity measurement is up to 99.5% using the

correlation approach for a car travelling at 60 km/h. It is experimentally proved that the accuracy of the length measurement is 99.75% for a target having the length of 2m. Moreover, the uncertainty of the ranging distance measurement is 0.75 cm. Achieved accuracy of the measurement results signifies the importance of the developed pulse laser radar in velocimetry applications.

The detection of threshold is used to determine the target's contour and velocity. Therefore, the number of sample detections is compromised for having a faster scanning. However, the smaller number of samples per measurement causes the higher uncertainty of distance ranging. The achieved distance ranging uncertainty is 0.75 cm with two samples per measurement, and correspondingly, the accuracy of the measurement of car velocity is 99%, achieved at 60 km/h. The photodetectors and the detector scanning technique are capable of obtaining the highest accuracy for the detection of moving targets. The investigation and the generation of very fast photodetection, for instance, increasing the sensitivity of photodetectors (rise time less then 80 ps), are of great importance in future applications for detecting high speedy moving targets.

The laser radar system is developed for tracking of moving targets from 20 cm to 12.5m. This tracking range can be extended by adding amplifier (bandwidth 6 GHz, gain 10 dB) with high sensitive detectors (M>150). Moreover, the development of high gain detectors will also be helpful to detect the contour of highly diffused targets, such as tyres of wheels and glass windows.

The developed laser radar system needs to be mounted at a fixed place for the detection of the moving targets. The development of the signal processing for the mobile operation of this radar system would be of great importance in future at the velocimetry application.

An efficient data acquisition technique is essential to achieve the fast data processing. In this work, the 40 Gsa/sec oscilloscope DSO81204B is used as a sampler. The development and implementation of compact sampler, based on extended sampling technique, can be used in this radar system for better performance. The synchronization of the sampling unit should be performed by using the reference signal from control unit. Furthermore, the investigation and improvement of data conversion rate at the compact sampler unit will also be performed as a future extension of this work.

The compactness of the sensor system is a fundamental issue for the industrial application. The realized base distance between both the laser beams is 28.8 cm. Another future goal is to decrease the base distance from 28.8 cm. For instance, if the base distance will be 10 cm, then the sensor system will be more compact than present laser radar system.

The energy consumption of a sensor system is an important concern for commercial applications. Different supply voltages are applied for different system modules of the developed pulse radar system. Future research work can be concentrated on the development and implementation of a compact DC supply voltage generator so that the sensor system becomes autonomous and ready for use in real-life dynamic applications.

References

[1] International Electrotechnical Commission: Safety of laser products, Part-1: Equipment classification, requirements and user's guide. *IEC 60825-1 (2001-2008)*, consolidated ed. 1.2, IEC, Geneva, 2001.

[2] Kompa, G., "Extended time sampling for accurate optical pulse reflection measurement in level control," *IEEE Trans. Instrum. Meas.*," IM-33, No. 2, June 1984, pp. 97–100.

[3] Biernat, A., and G. Kompa, "A laser radar for precise 2D and 3D-object imaging," *Topical Meeting 'Optoelectronic Distance/Displacement Measurements and Applications',* Ecole des Mines de Nantes, France, July 1997, pp. 601-604.

[4] Kompa, G., "Pulsed laser radar for 3D-quality assurance of hot workpieces," *OPTO 96 Kongressband, ,Optical Sensor Technology, Measuring Techniques, Electronics,* Germany, September 25 - 27, 1996, pp. 93-98.

[5] Kamucha, G. N., "*A non-invasive registration technique in hip-joint replacement surgery using laser-radar imaging*," Dissertation, Department of High Frequency Engineering, University of Kassel, December 2003.

[6] Kohn, J., and J. J. Clawson, "Police radar/laser detector with integral vehicle parameter display," *US Patent 6587068*, July 2003.

[7] Nöding, M., and M. -C. Amann, "FMCW-lidar with widely tunable laser diodes: influence of the tuning behaviour on the distance measurement," *Journal of optics*, Vol. 29, June 1998, pp. 212-215.

[8] Dieckmann, A., and M. -C. Amann, "FMCW-lidar with tunable twin-guide laser diode," *Trends in Optical Fibre Metrology and Standards, NATO ASI series E: Applied Science, ed O. D. D. Soares,* Vol. 285, 1995, pp. 791-801.

[9] Amann, M. –C., T. M. Bosch, M. Lescure, R. A. Myllylae, and M. Rioux, "Laser ranging: a critical review of usual techniques for distance measurement," *Opt. Eng., SPIE*, Vol. 40, No. 1, 2001, pp. 10-19.

[10] Melngailis, I., W. E. Keicher, C. Freed, S. Marcus, B. E. Edwards, A. Sanchez, T. Y. Fan, and D. L. Spears, "Laser radar component technology," *Proceedings of the IEEE*, Vol. 84, February 1996, pp. 227–267.

[11] Nagasaku, T., H. Kondoh, and H. Shinoda, "Radar sensor," *United States Patent US6717544B2*, April 6, 2004.

[12] Breed, D. S., and M. Beach, "Vehicle position determining system and method," *United States Patent US20080040029A1*, February 14, 2008.

[13] Olson, R. A., R. L. Gustavson, R. J. Wangler, and R. E. McConnell, "Active near-field object sensor and method employing object classification techniques," *United States Patent US5321490*, June 14, 1994.

[14] Handerson et al., "Eyesafe coherent laser radar for velocity and position measurement," *United States Patent*, No. 5237331, August 17, 1993.

[15] Finger, A., and S. Zeisberg, “Ultra wideband technique,“ *IEEE-MTT/AP German Newsletter,* Vol. 8, No. 1, June 2004.

[16] Rollmann, G., P. Knoll, M. Mekhaiel, V. Schmid, and H. –L. Bloecher, “Short range radar (SRR) – system for automotive applications,” *IEEE-MTT/AP German Newsletter,* Vol. 8, No. 1, June 2004.

[17] Yarouyoy, A. G., and L. P. Ligthart, “UWB radars: recent technological advantages and applications,” *IEEE Radar Conference 2007*, April 17 – 20, 2007, pp. 43–48.

[18] Nagasaku, T., H. Kondoh, and H. Shinoda, “Velocity sensor and ground vehicle velocity sensor using the same,” *United States patent, US7310061*, December 18, 2007.

[19] Rahimi, A. R., A. R. Holt, G. J. G. Upton, and S. Krämer, “Attenuation Calibration of an X-Band Weather Radar Using a Microwave Link,” *Journal of Atmospheric and Oceanic Technology*; Vol. 23, No. 3, March 1, 2006, pp. 395-405.

[20] Babbitt, W. R., ”Microwave signal processing with spatial-spectral holography,” *IEEE 18th Annual meeting on Laser and Electro-Optics Society*,October 22 – 28, 2005, pp. 837-838.

[21] Thompson, S. D., ”A microwave radar for vehicular applications,” *IEEE 1996 Microwave and Millimeter-Wave Monolithic Circuits Symposium*, June 16 – 18, 1996, pp. 7-9.

[22] Sawicki, D. S., *Traffic radar handbook, A comprehensive guide to speed measuring systems*, Lightning Source Inc*,* ISBN-13: 978-0759688339, 2002.

[23] Suzuki, T., and T. Kanada, “Measurement of vehicle motion and orientation using optical flow,” *IEEE/IEEJ/JSAI International Conference Proceedings on Intelligent Transportation Systems*, 1999, pp. 25-30.

[24] Tamiya, N., H. Mandai, and T. Fukae, “Optical speed spectrum radar for lateral detection in vehicles,” *IEEE 4th International Symposium on Spread Spectrum Techniques and Applications Proceedings*, Vol. 1, September 22 – 25, 1996, pp. 195-198.

[25] Winkler, V., “Range Doppler detection for automotive FMCW radars,” *IEEE Proceeding of the 37th European Microwave Conference, EURAD 2007,* October 10 - 12, 2007, pp. 166-169.

[26] Mazzci, J. A., and A. F. Major, *Lasers: A new challenge for the military communicator*. Signal, July 1975, pp..25-28.

[27] Woodward, P. M., *Probability and information theory with application to radar*, Pergamon Press, New York, 1953.

[28] Wiener, N., *Extrapolation interpolation and smoothing of stationary time series*, Wiley, New York, 1957.

[29] Jung H. G., Y. H. Cho, P. J. Yoon, and J. Kim, “Scanning laser radar-based target position designation for parking aid system,” *IEEE Conference Proceeding on Intelligent Transportation Systems*, Vol. 10, No. 4, October 2008, pp. 406-424.

[30] Schaudel, D., “Prozess-Sensoren schaffen und erhalten Werte in der Prozessindustrie,“ *Vortrag auf der NAMUR HS 2007*, Lahnstein, 2007.

[31] Schaudel, D. ,“Prozess-Sensoren schaffen und erhalten Werte in der Prozessindustrie,“ Prozess Sensorik, *atp*, February 2008.

[32] Jelalian, A. V., *Laser radar systems*, Artech House, Boston, 1992.

[33] Barton, D. K. *The radar equation*, Radar, Vol. 2, Artech House, Boston, 1974.

[34] Samson, V., F. Champagnat, and J. –F. Giovannelli, "Point target detection and subpixel position estimation in optical imagery," *Appl. Opt.* Vol. 43, 2004, pp. 257-263.

[35] Ingham, D. R., "A Hybrid Method Based on Reciprocity for the Computation of Diffraction by Trailing Edges," *IEEE Trans. Antennas Propagat.*, Vol. 43, No. 11, November 1995, pp. 1173–1182.

[36] Yee, K., D. Ingham, and K. Shlager, "Time-Domain Extrapolation to the Far Field Based on FDTD Calculations," *IEEE Trans. Antennas Propagat.*, Vol. 39, No. 3, March 1991, pp. 410–413.

[37] Balanis, C. A. *Advanced Engineering Electromagnetics*, ISBN 0-471-62194-3, Wiley, 1989.

[38] Wang, J., and J. Chun, "Extended target detection and tracking using the simultaneous attitude estimation," *IEEE Conference Proceeding of the American Control Conference*, June 2000, pp. 4341-4342.

[39] Priebe, C. E., D. J. Marchette, Y. Park, and R. R. Muise, "Application of integrated sensing and processing decision trees for target detection and localization on digital mirror array imagery," *Appl. Opt.*, Vol. 45, 2006, pp. 3022-3030.

[40] Eismann, M. T., "Strategies for hyperspectral target detection in complex background environments," *IEEE AC*, December 2005, pp. 1-10.

[41] Curran, P. J., *Principles of remote sensing*, Longman Group Lim., London and New York, 1985.

[42] Wang, J., and M. Sugisaka, "Study on robust target detection technique, *IEEE Conf. of SICE 2004*, Vol. 1, August 2 – 4, 2004, pp. 772-775.

[43] Oselto, O., *Principles of lasers*, 4th ed., Springer, Berlin-New York, 1998.

[44] Chambers. B., and A. Tennent, "Reflection of radar signals from multiple phase-modulated surfaces," *IET Radar Sonar Navig.*, Vol. 1, No. 2, 2007, pp. 158-163.

[45] Grantham, J. W., and E. C. Meidunas, "Laser radar in adverse weather," *SPIE proceedings series on Laser radar technology and applications*, Vol. 3380, April 14 - 16, 1998, pp. 303-314.

[46] Amoroso J. S., R. W. Conklin, "Automatic adaptive sensitivity time control for a ground mapping radar," *United Sates Patent, US4509050*, April 2, 1985.

[47] Yamada, Y., S. Tokoro, and Y. Fujita, "Development of a 60 GHz radar for rear-end collision avoidance," *IEEE Proceedings of the Intelligent Vehicles '94 Symposium*, October 24 - 26, 1994, pp. 207-212.

[48] Shina, T., and K. Ikeda, "Measurement of slant visual range in laser radar operation considering the spread of transmitted laser beam caused by small particles in the atmosphere," *Journal of Light & Visual Environment*, Vol. 23, No. 1, 1999, pp. 50-58.

[49] Kawata, H., H. Endo, and Y. Eto, "A study of laser radar, Nissan Motor Co. Ltd, " *The 10th International Technical Conference on Experimental Safety Vehicles*, July 1-4, 1985.

[50] International Electrotechnical Commission: IEC 825-1 Safety of laser products-Part 1: Equipment classification, requirements and user's guide. *IEC*, Geneva, 1984.

[51] DIN EN 60825-1 (VDE 0837 Teil 1): 1997-03 Sicherheit von Laser-Einrichtungen-Teil 1: Klassifizierung von Anlagen, Anforderungen und Benutzer-Richtlinien; Deutsche Fassung EN 60825-1:1994 + A11:1996.

[52] EN 60825-1: Safety of Laser Products - Part 1: Equipment, Classification, Requirements and User's Guide, Bureau Central de la Commission Electrotechnique Internationale, Geneva, 1993.

[53] International Electrotechnical Commission: IEC 60825-1:2007: Safety of laser products - Part 1: Equipment classification and requirements. German Version EN 60825-1:2007, *IEC*, 2007.

[54] Sutter, E., *Stutz vor optischer Strahlung: Laserstrahlung, inkohärente Strahlung, Sonnenstrahlung*, Normenreihe DIN EN 60825, VDE 0837, ISBN 978-3-8007-3072-8, Berlin, 2008.

[55] Träger, F., *Springer handbook of lasers and optics*, Springer, New York, 2007.

[56] Eichordnung, *Messgeräte in Straßenverkehr*, Deutscher Eichverlag, 1988.

[57] Casanovas, R. S., *Genaue Geschwindigkeitmessung mit Hilfe eines Laserimpuls radarsystem*, Diplomarbeit, Department of High Frequency Engineering, University of Kassel, Germany, 1994.

[58] Hobson, G. S., H. Roe, and J. P. Hawley, "Microwave classification of road vehicles," *Proc. 20th European Microwave conference*, Vol. 2, 1991, pp. 996-1001.

[59] Kompa, G., and W. Drevenstedt, "Optimization of high power semiconductor laser pulses for radartype sensors," *Proc. of 5th Conference on Microwaves and Optronics (MIOP)*, Paper 3A.1, April 24 - 26, 1990, pp.193–198.

[60] Volpe, F. P., A. Stolze, V. Gorfinkel, and G. Kompa, "Energiereiche Pikosekundenimpulse von Halbleiterlasern im gütegeschalteten Betriebszustand für radarsensorische Anwendungen," *Konferenz für Mikrowelle und Optronik (MIOP)*, May 25 - 27, 1993, pp.276–280.

[61] Volpe, F. P., A. Stolze, V. Gorfinkel, and G. Kompa, "Generation of picosecond single optical pulses of high peak power for laser sensor application," *Conference on Lasers and Electro-Optics (CLEO'93)*, Vol. 11, Paper CMA4, May 2 – 7, 1993, pp. 19-22.

[62] Gorfinkel, V. B., G. Kompa, J. Sola, and F. P. Volpe, "Generation of powerful picosecond optical pulses from semiconductor lasers with modal gain controlled by pumping current (simulation and experiment)," *Symposium Handbook of 21st International Symposium on Compound Semiconductors (ISCS'94)*, September 18 - 22, 1994,

[63] Biernat, A., and G. Kompa, "Powerful picosecond laser pulses enabling high resolution pulses laser radar," *Special Issue of Journal of Optics on Optoelectronic Distance / Displacement Measurements and Applications*, IOP Publishing, Vol. 29, No. 3, Vol. 29, 1998, pp. 225-228.

[64] Biernat, A., and G. Kompa, "Generation of high-power picosecond laser pulses," *Conf. Proc. of GaAs'98 held in the frame of the European Microwave Week '98*, Amsterdam, Netherlands, October 5 - 9, 1998, pp. 510-514.

[65] Gorfinkel, V. B., G. Kompa, S. A. Gurevich, G. E. Shtengel, and I. E. Chebunina, "High-frequency modulation of a QW diode laser by dual modal gain and pumping current control," *Proc. of 20th Int. Symposium on Gallium Arsenide and Related Compounds*, Paper TuA8, 1993.

[66] Gorfinkel, V., G. Kompa, J. Sola, and F. P. Volpe, “New Technique for generating powerful picosecond optical pulses from semiconductor lasers for high-resolution pulsed radar systems,” *European Conference on Lasers and Electro-Optics (ECLEO'94)*, August 28 – September 2, Paper CMD2, 1994.

[67] Gorfinkel, V. B., G. Kompa, M. Novotny, A. Stolze, S. A. Gurevich, G. E. Shtengel, and I. E. Chebunina, “1/f Modulation Response of AlGaAs/GaAs SQW Laser with Dual Modal Gain and Pumping Current Control,“ *Proceedings CLEO/PACIFIC RIM*, Paper F13, 1994, pp.190-191.

[68] Kompa, G., V. Gorfinkel, J. Sola, A. Stolze, W. Vogt, and F. Volpe, “Powerful picosecond-pulsed laser radar with micrometer ranging resolution,” *26th European Microwave Conf. Proc.*, September 9 - 12, 1996, pp.147-152.

[69] Biernat, A., G. Ridino, and G. Kompa, “Numerical transient simulation of SH laser diodes under strong and highly dynamic carrier injection,” *Int. IEEE Workshop on 'Experimentally based FET device modelling & related nonlinear circuit design'*, July 17 - 18, 1997, pp. 43.1-7.

[70] Biernat, A., “*Erzeugung und Anwendung von ultrakurzen Laserradarimpulsen mit hoher Leistung*,” Dissertation, Department of High Frequency Engineering, University of Kassel, 1999.

[71] Kersten, B., “*Untersuchungen zur Stromansteuerung von Pulslaser dioden*,” Projektarbeit III, Department of High Frequency Engineering, University of Kassel, 1988.

[72] Volpe, F. P., “*Erzeugung von optischen Pikosekundenimpulsen hoher Leistung mit Halbleiterlasern zur Nahberiechs-Entfernungs messung mit submillimetermeßgenauigkeit*,” Dissertation, Department of High Frequency Engineering, University of Kassel, November 1994.

[73] Casey, H. C., and M. B. Panish, *Heterostructure lasers, Part-A: Fundamental principles*, ISBN: 0-12-163101-X, Academic press, first edition, 1978.

[74] Vasil’ev, P., *Ultrafast diode lasers, fundamentals and applications*, ISBN: 0-89006-736-8, Artech House Inc., 1995.

[75] Silfvast, W. T., *Laser fundamentals*, *ISBN: 0-521-55617-1,* Cambridge University Press, 1996.

[76] Singh, J., *Semiconductor devices: Basic principles*, ISBN: 0-471-36245.X, John Wiley & Sons Inc., 2001.

[77] Pulsed laser diode, LD62, *Technical Datasheet*, Laser Diode, Inc., USA, 1998.

[78] Biernat, A., and G. Kompa, “A laser radar for precise 2D and 3D-object imaging,” *Topical Meeting 'Optoelectronic Distance/Displacement Measurements and Applications'*, France, July 1997.

[79] Kompa, G., “Optical short-range radar for level control measurement,” *Proceedings of the IEEE*, Vol. 131, No. 3, June 1984, pp. 159-164.

[80] Kompa, G., A. Stolze, W. Vogt, and F. P. Volpe, “Pikosekunden-Laserradar und faseroptisches Abtastsystem zur dynamischen on-line Konturvermessung, “*Broschüre zur Abschlußpräsentation des vom BMBF geförderten Verbundprojektes "3D-Objektvermessung auf größere Entfernungen"* am 21. und 22.06.1995 auf der Laser '95, 1995.

[81] New Focus user’s manual: Fiber-coupled, Ultrahigh-speed Photodetector Modules. *Model series 100X and 101X,* New Focus Int., 2002.

[82] Harth, W., and H. Grothe, *Sende- und Empfangs dioden für die Optische Nachrichtentechnik*, B. G. Teubner, Stuttgart. Leipzig, May 1998.

[83] Kellner, W., and H. Kniepkamp, *GaAs Feldeffekt transistoren*, Springer-Verlag, Berlin. Heidelberg. New York. Tokyo, 1984.

[84] Thompson, G. H. B., *Physics of Semiconductor Laser Device*, John Wiley & Sons, New York, 1980.

[85] 74HCT4040, 12 stage binary ripple counter, *Technical Datasheet*, Philips Semiconductors, 2007.

[86] 74HC4T4017, Johnson decade counter with 10 decoded ouputs, *Technical Datasheet*, Philips Semiconductors, 2007.

[87] 74HC4049, Hex inverting high-to-low level shifter, *Technical Datasheet*, Philips Semiconductors, 2007.

[88] 74ACT245, Octal bi-directional tranceiver, *Technical Datasheet*, Philips Semiconductors, 2007.

[89] NE521, High-speed dual-differential comparator/sense amp, *Technical Datasheet*, Philips Semiconductors, 2007.

[90] Okhrawi, M., "*Entwurf und Aufbau einer Samplingbrücke zur Zeittransformation von ps-Bereich in den μs-Bereich*," Master-Thesis, Department of High Frequency Engineering, University of Kassel, September 1991.

[91] Avalanche photodiodes, series APD230-9, *Technical Datasheet*, Silicon sensor GmhH, Germany, 2008.

[92] Djebari, M., "*Photoempfänger für Pikosekunden-Laserimpulseradar*," Dissertation, Department of High Frequency Engineering, University of Kassel, June 2000.

[93] Portnoi, E. L., E. B. Venus, A. A. Khazan, V. B. Gorfinkel, G. Kompa, J. H. Marsh, E. A. Avrutin, I. Thayne, and D. A. Barrow, "Monolithically integrated optoelectronic downconverter," *14th IEEE Int. Semiconductor Laser Conference*, Sept. 19 - 23, Paper M4.3, 1994, pp. 304-319.

[94] Stolze, A., and G. Kompa, "Nonlinear modelling of dispersive photodiodes based on frequency- and time-domain measurements," *26th European Microwave Conf. Proc.*, September 9 - 12, 1996, pp. 379-382.

[95] Biernat, A., M. Djebari, J. Weide, and G. Kompa, "Modelling, simulation and optimization of ultrafast semiconductor lasers and nonlinear photodetectors for laser radar sensors with micrometer accuracy," *Int. IEEE Workshop on 'Experimentally based FET device modelling & related nonlinear circuit design'*, July 17 - 18, 1997, pp. 44.1-6.

[96] Stolze, A., "*Breitbandige meßtechnische Charakterisierung und Modellierung von Sperrschicht-Photodioden für den gezielten rechneer-gestützten Entwurf von optoelektronischen Breitbanddetektoren*," Dissertation, Department of High Frequency Engineering, University of Kassel, July 1995.

[97] Advanced Design System (ADS), *High Frequency Design Software*, Agilent Technologies, USA, 2003.

[98] PTFE materials, *Technical Datasheet*, Taconic Advance Dielectric Division, USA, 2007.

[99] Hybrid Multilayer Printed Circuit Boards for Microwave and RF Applications, TECONIC Resource Center, Advanced Dielectric Division, USA, 2008.

[100] Lee, S. -S., Y. Yoshida, T. Nishino, Y. Suehiro, H. Ohhashi, T. Fukami, M. Kimata, and O. Ispida, "A MEMS-based hybrid circuit having metalized cavity for Ku-band wireless Communication," *IEEE l2th International Conference on Solid Slate Sensors, Actuators and Microsystems*, June 8 – 12, 2003, pp. 1792-1795.

[101] Abuasaker, S., and G. Kompa, "A high sensitive receiver for baseband pulse microwave radar sensor using hybrid technology," *IEEE Radar Conference 2002*, April 22-25, 2002.

[102] Wasige, E., G. Kompa, F. van Raay, I. Schmale, I. W. Rangelow, W. Scholz, F. Shi, R. Kassing, R. Meyer, M. -C. Amann, and P. Hudek, "Air bridge based planar hybrid technology for microwave and millimeterwave applications," *27th European Microwave Conf. Proc.*, Jerusalem, Israel, September 8 - 12, 1997, pp. 375-378.

[103] Mohammadi, F. A. l., M. C. E. Yagoub, and K. Raahemifar, "Time-domain 3D electromagnetic model for hybrid and monolithic microwave and optoelectronic integrated circuits," *Microwave and Optical Technology Lett.*, Vol. 43, No 4, November 2004, pp. 276-280.

[104] Yu, R., "*Millimeter-wave on wafer and network measurement using active probes*," Dissertation, University of California Santa Barbara, Santa Barbara 1994.

[105] Devabhaktuni, V. K., B. Chattaraj, M. C. E. Yagoub, and Q. J. Zhang, "Advanced microwave modeling framework exploiting automatic model generation, knowledge neural networks and space mapping," *IEEE Trans. Microwave Theory Tech.*, Vol. 51, No. 7, July 2003, pp. 1822-1833.

[106] Ghose, A., "*Pulsed measurement based nonlinear characterization of avalanche photodiode for the time error correction of 3D pulsed laser radar*," Dissertation, Department of High Frequency Engineering, University of Kassel, July 2005.

[107] Paul J. B., "Active, Optical Range Imaging Sensors," Machine Vision and Applications (1988), *1988 Springer-Verlag*, New York Inc., Vol. 1, No. 2, June 1988, pp.127-152.

[108] Kompa, G., M. Djebari, and A. Stolze, "A new concept for the correction of ranging errors originating in the nonlinearities of photoreceivers," *EOS 14th Topical Meeting on Optoelectronic Distance/Displacement Measurements and Applications, Topical Meetings Digests Series*, Vol. 14, July 8 - 10, 1997.

[109] Amann, M. -C., T. Bosch, M. Lescure, R. Myllylä, and M. Rioux, "Laser ranging: A critical review of usual techniques for distance measurement," *SPIE Optical Engg.*, Vol. 40, No.1, January 2001, pp. 10-19.

[110] Ghose, A., B. Bunz, J. Weide, and G. Kompa, "Large signal modelling of avalanche photodiode for correction of optical power dependent nonlinearity," *IEEE Proc. of 34th European Microwave conference,* October 3 - 7, 2005, pp. 357–360.

[111] SIGMA 2000*, Optical design software*, Kidger Optics Ass., Canada, 2000.

[112] Hwang, F. –K., *Thin Lens combinations*, NTNUJAVA Virtual Physics Laboratory, (www.phy.ntnu.edu.tw), Taiwan, 2008.

[113] NIR antireflection-coated lenses, BK-7 series with AR.16, *Technical Datasheet*, Newport Corporation, USA. 2007.

[114] Silver coating with ER.2 and RAGV NIR broadband SiO_2 mirrors, *Technical Datasheet*, *Linos Photonics Ltd.*, Germany, 2007.

[115] Circular Linear Variable ND Filters, 100FS04DV.4, UV grade fused silica, *Technical Datasheet*, Newport Corporation, USA. 2007.

[116] NIR prism with UV silver coating, *Technical Datasheet*, Linos Photonics Ltd., Germany, 2007.

[117] Das, P., *Lasers and optical engineering*, Springer-Verlag, New York, 1991.

[118] Greivenkamp, J. E. *Field Guide to Geometrical Optics,* SPIE Field Guides vol. FG01. SPIE. ISBN 0-8194-5294-7., 2004.

[119] Hecht, E., *Optics* , 2nd edition, Addison Wesley. ISBN 0-201-11609-X., 1987.

[120] Jackson, J. D., *Classical Electrodynamics*, 3rd edition, Wiley: New York, 1998.

[121] Djebari, M., G. Kompa, and A. Stolze, "Error correction of the response delay due to the nonlinearities of photoreceivers," *Journal of Optics*, Vol. 29, No. 3, 1998, pp. 194-198.

[122] Ghose, A., B. Bunz, J. Weide, and G. Kompa, "A measurement based approach to extract nonlinearity in avalanche photodiode," *Telsiks 2005*, Nis, Serbia and Montenegro, September 28 - 30, 2005, pp. 373-376.

[123] Bergmann, L., "*Der Ultraschall*," Verlag Hirzel, Zürich 1949.

[124] Gajda, J., R. Sroka, M. Stencel, A. Wajda, and T. Zeglen, "A vehicle classification based on inductive loop detectors," *Proc. of 18th IEEE Instrumentation and Measurement Technology Conference, 2001 (IMTC 2001)*, Vol. 1, May 21 - 23, 2001, pp. 460–464.

[125] Korba, L., S. Elgazzar, and T. Welch, "Active Infrared Sensors for Mobile Robots," *IEEE Transaction on Intrumentation and Measurement*, Vol. 43, No. 2, April 1994, pp. 283-287.

[126] Yazici, B., "Estimation of radar target reflectivity in ultra wideband regime," IEEE *ICASSP 2004*, August 30, 2004, pp. 52-56.

[127] Liu, Y., H. L. Pratt, "Variations in target reflectivity at 1.064 and 1.318 micron," *IEEE ICASSP 2004*, August 30, 2004, pp. 52-56.

[128] Levent, S., "Target reflectivity and RCS interactions in integrated maritime Surveillance systems based on Surface-Wave High-Frequency radars," *IEEE antennas & propagation*, Vol. 43, No. 1, February 2001, pp. 36-51.

Sohrab Monsi was born in Brahmanbaria, Bangladesh in 1977. He received his B. Sc. degree in electrical and electronic engineering from the Bangladesh University of Engineering and Technology (BUET), Bangladesh in 2001, and his M. Sc. in communication and information technology from the University of Bremen, Germany, in December 2005. In March 2006, he joined the Department of High Frequency Engineering, at the University of Kassel, Germany, and in April 2009, he received his PhD (Dr.-Ing.) degree in High Frequency Engineering from the University of Kassel: